MECHANISTIC STUDIES ON AZA-NAZAROV REACTIONS AND DEVELOPMENT OF TEMPLATE-DIRECTED PHOTOCHEMICAL [2+2] CYCLOADDITION REACTIONS

THESIS SUBMITTED TO

THE GRADUATE SCHOOL OF ENGINEERING AND SCIENCE

OF BILKENT UNIVERSITY

IN PARTIAL FULFILLMENT OF THE REQUIREMENTS FOR

THE DEGREE OF

MASTER OF SCIENCE

IN CHEMISTRY

By

Bilge Banu YAĞCI

January 2021

MECHANISTIC STUDIES ON AZA-NAZAROV REACTIONS AND DEVELOPMENT OF TEMPLATE-DIRECTED PHOTOCHEMICAL [2+2] CYCLOADDITION REACTIONS

By Bilge Banu YAĞCI

January 2021

We certify that we have read this thesis and that in our opinion it is fully adequate, in scope and in quality, as a thesis for the degree of Master of Science.

Yunus Emre TÜRKMEN (Advisor)

Bilge BAYTEKİN

Ferdi KARADAŞ

Hamdullah KILIÇ

Akın AKDAĞ

Approved for the Graduate School of Engineering and Science:

Ezhan KARAŞAN

Director of the Graduate School

ABSTRACT

MECHANISTIC STUDIES ON AZA-NAZAROV REACTIONS AND DEVELOPMENT OF TEMPLATE-DIRECTED PHOTOCHEMICAL [2+2] CYCLOADDITION REACTIONS

Bilge Banu Yağcı

M.S.c in Chemistry

Advisor: Yunus Emre Türkmen

January 2021

As a sub-class of Nazarov reactions, the aza-Nazarov reactions, which have remarkable importance due to their use in the synthesis of five-ring nitrogen containing structures, are rarely studied. For the first time in the literature, the aza-Nazarov reaction was developed with 3,4-dihydroisoquinoline and α, β-unsaturated acyl chloride compounds operating under catalytic and moderate conditions with high efficiency, but the investigation and development studies of the proposed mechanism for this reaction were not conducted. The complete understanding of the mechanism has great importance for the development of advanced synthesis methods of this reaction and the diversification of its products. In the first part of this thesis, control experiments were conducted to examine the steps of this particular aza-Nazarov reaction mechanism; identification of the side-product, effectiveness of the achiral anion binding catalysts on this reaction, independent aza-Nazarov reactions of the minor and major isomers of the acyl chloride compounds, use of thiophene-based substrate and β-silicon stabilization effect on the mechanism with a different approach were investigated. In the second part of this thesis, a new photochemical [2 + 2] cycloaddition reaction was developed to achieve *regio*- and *stereo*-control by

utilizing the 1,8-diolnaphthalene as a template molecule. With this method, unsymmetrical cyclobutane products were synthesized for the first time as well as symmetrical cyclobutane products using *trans*-cinnamic acid derivatives. The fact that this reaction is carried out in solid state without using solvent and no side-product formation is observed and the recovery of the template molecule accomplished at the end of this reaction greatly contributes to developments in green chemistry.

Keywords: Aza-Nazarov mechanism, photochemical [2+2] cycloaddition reaction, unsymmetrical cyclobutane synthesis

ÖZET

AZA-NAZAROV REAKSİYONU MEKANİSTİK ÇALIŞMALARI VE KALIP MOLEKÜLÜ ARACILIĞI İLE FOTOKİMYASAL [2+2] SİKLOKATILMA REAKSİYONLARININ GELİŞTİRİLMESİ

Bilge Banu Yağcı

Kimya, Yüksek Lisans

Tez Danışmanı: Yunus Emre Türkmen

Ocak 2021

Nazarov tepkimelerinin bir türevi olan aza-Nazarov tepkimeleri, nitrojen içeren beş halkalı yapıların sentezinde kullanılmaları sebebiyle ender çalışılan önemli tepkimelerdir. Literatürde ilk defa katalitik ve ılıman koşullar altında, yüksek verimle çalışan 3,4-dihidroizokinolin ve α,β-doymamış açil klorür bileşikleri ile aza-Nazarov tepkimesi geliştirilmiş fakat bu tepkime için önerilen mekanizmanın inceleme ve geliştirme çalışmaları yapılmamıştır. Mekanizmanın tamamen anlaşılır hale gelmesi, bu reaksiyonun ileri sentez yöntemlerinin geliştirilmesi ve ürünlerinin çeşitlendirilmesi açısından büyük önem taşımaktadır. Bu tez çalışmasının ilk kısmında aza-Nazarov tepkimesine ait mekanizma basamaklarının incelenmesi için yapılan kontrol deneylerinde sırasıyla; tepkime yan ürününün tespiti, akiral anyon bağlanma katalizörlerinin tepkime üzerindeki verimlilikleri, açil klorür bileşiğinin minör-majör izomerlerinin birbirinden bağımsız tepkime basamaklarının incelenmesi, tiyofen bazlı subsrat kullanımı ve farklı bir yaklaşım ile β-silikon kararlılık etkisinin mekanizma üzerindeki etkisi incelenmiştir. Bu tez çalışmasının ikinci kısmında, 1,8-diolnaftalin kalıp molekülü aracılığıyla gerçekleştirilen yeni bir fotokimyasal [2+2] siklokatılma tepkimesi *regio*- ve *stereo-kontrolü* başarmak

üzere geliştirilmiştir. Bu yöntemle, *trans*-sinnamik asit türevleri kullanılarak simetrik siklobütan ürünlerinin yanı sıra ilk defa simetrik olmayan siklobütan ürünü sentezlenmiştir. Bu tepkimenin katı halde, çözücü olmadan gerçekleştirilmesi, yan ürün elde edilmemesi ve tepkime sonunda kalıp molekülünün geri kazanımı yeşil kimya alanındaki gelişmelere büyük katkıda bulunmaktadır.

Anahtar Kelimeler: Aza-Nazarov mekanizması, fotokimyasal [2+2] siklokatılma tepkimesi, simetrik olmayan siklobütan sentezi

ACKNOWLEDGEMENT

First and foremost, I am extremely grateful to my supervisor Asst. Prof. Dr. Yunus Emre Türkmen, who has attitude and substance of a genius, for his continuous support and patience during my studies. His immense knowledge and plentiful experience has enabled me to have such a high quality and valuable thesis today. I believe that what I learned from him would help me a lot in the future and provide me a better opportunities in my academic career. Besides my advisor, I would like to thank my examining committee; Prof. Dr. Hamdullah Kılıç, Prof. Dr. Akın Akdağ, Asst. Prof. Dr., Ferdi Karataş and Asst. Prof. Dr. Bilge Baytekin for all the considerate guidance and helping me to finalize this work. The expeditious assistance provided by our collaborator Dr.Yunus Zorlu was also greatly appreciated. I wish to extent my special thanks to TÜBİTAK for the financial support provided for the first project (Mechanistic Studies on aza-Nazarov Reaction, Project No: 116Z171) during my thesis studies.

I cannot forget my brilliant friends Yeşim Şahin and Dilgam Ahmedli who went through hard times together, cheered me on, and supported each accomplishment.

From the bottom of my heart, my deep and sincere gratitude to my family for their continuous and unparalleled love and support every single day of my life. Nothing motivates me more than feeling my family standing by my side. I could not have done this without support of my unprecedented mother Meral and father İlyas. My sister and best friend forever Süyümbike Betül, there is no such words to describe my love for you. You and your successes are the reason where I am today. I am grateful that you shine like a star in my life. You are "*one in a million*". I also admire Nazlı's (my cat) effort to jump to the computer while I was writing my thesis.

LIST OF ABBREVIATIONS

AgOTf	Silver Trifluoromethanesulfonate
DCM	Dichloromethane
DME	Dimethoxyethane
DMF	Dimethylformamide
dr	Diastereoisomeric ratio
EtOAc	Ethyl acetate
FTIR	Fourier-Transform Infrared
HRMS (TOF)	High Resolution Mass Spectrometry (Time-of-Flight)
MeCN	Acetonitrile
MeOH	Methanol
NBS	*N*-Bromosuccinimide
NMR	Nuclear Magnetic Resonance
R_f	Retention Factor
TMS	Trimethylsilyl
TLC	Thin Layer Chromatograhy
UV	Ultraviolet
ZnOTf	Zinc Trifluoromethanesulfonate

TABLE OF CONTENTS

LIST OF FIGURES

LIST OF SCHEMES

LIST OF TABLES

1. MECHANISTIC STUDIES ON AZA-NAZAROV REACTIONS

1.1. INTRODUCTION

1.1.1. Nazarov Reaction

Named reactions have a special place in synthetic organic chemistry as they often play an important role in key carbon-carbon or carbon-heteroatom bond-forming steps.[1] One such important named reaction, the Nazarov cyclization, was developed by the prominent Russian scientist Ivan Nazarov in 1942.[2] The reaction attracted tremendous attention due to its ability to transform divinyl ketones to cyclopentenone scaffolds and is known as one of the most effective methods for the synthesis of five membered rings. In the conventional mechanism of the Nazarov reaction, a Brønsted or Lewis acid that acts as catalyst or promoter coordinates to the carbonyl group of a divinyl ketone (**1**, Scheme 1). This coordination stimulates the electrocyclization of pentadienyl cation **2**, which then proceeds to form an oxallyl cation (**3**) though a 4π electrocyclization process.[3,4] In terms of conservation of orbital symmetry, the conrotatory closure of the p orbitals leads to construction of a new carbon- carbon bond in the pentadienyl cation **2**, which bring outs new stereocenters on the oxallyl cation **3** resulting in R^2 and R^4 groups having *trans* rearrangement. Elimination of a *β*-hydrogen produces an enolate (**4**) which is still coordinated to the Lewis acid promoter. The subsequent protonation of enolate **4** provides the final cyclopentenone product **5**.

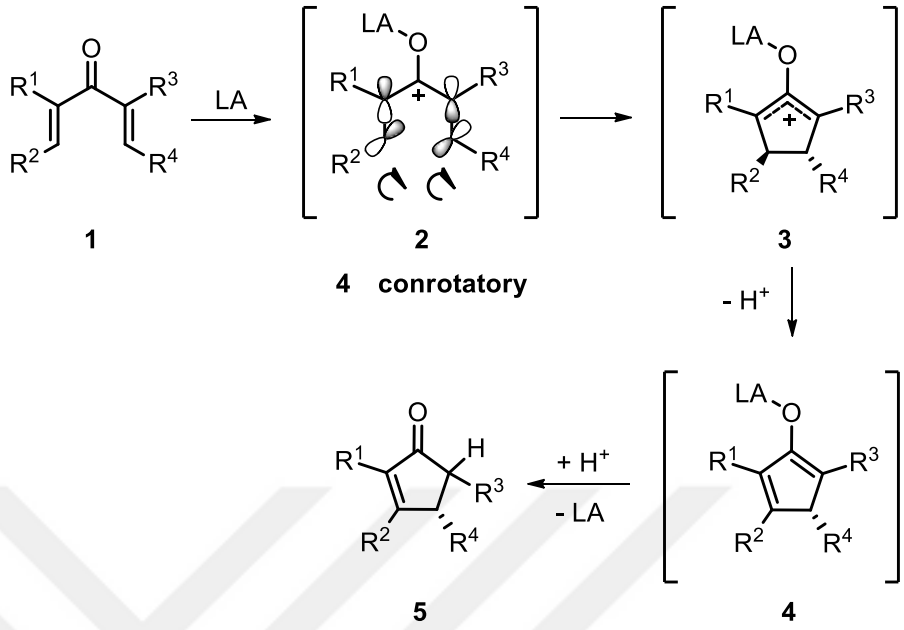

Scheme 1. Mechanism of Nazarov reaction.

The Nazarov reaction is encountered frequently in organic synthesis due to its applications in the synthesis of natural products that especially possess cyclopentanone-based structures.[5] The Nazarov reaction works with various starting dienones, which can be substituted with a variety of different functional groups. This feature of the reaction enables the synthesis of complex and richly functionalized five membered ring moieties that have remarkable significance in obtaining pharmaceuticals and natural products.

1.1.2. Aza-Nazarov Reaction

Aza-Nazarov reaction, a sub-class of the conventional Nazarov reaction, in which the cyclization involves the formation of nitrogen-containing five membered rings, is at the focus of many studies in recent years.[6,7] Generally, the reaction involves an *N*-acyliminium ion intermediate, which is then cyclized to *N*-containing heterocycles in the presence of Brønsted or Lewis acids (Scheme 2).

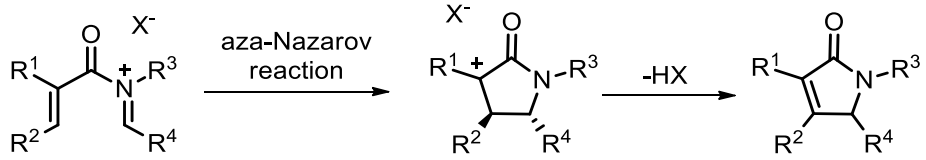

Scheme 2. An example of an aza -Nazarov reaction.

Nitrogen-containing heterocyclic structures constitute the major skeleton of various biologically active alkaloid compounds. Therefore, considering the importance of such heterocycles in the field of medicinal and pharmaceutical chemistry, investigation on the development of aza-Nazarov reaction expected to shed light on the new methods for the synthesis of prominent heterocyclic compounds.

1.1.3. Recent Developments on Aza-Nazarov Reaction

Since the discovery of Nazarov reaction, numerous studies were conducted focusing on the synthesis of all-carbon, five-membered rings. Although nitrogen-containing heterocycles have remarkable significance on natural products chemistry and drug discovery, studies on related aza-Nazarov reactions have been very limited.

Klumpp and co-workers reported a pioneering study in 2007 in which they prepared *N*-acyliminium salts in situ by using a variety of acyl chlorides and substituted imines.[8] The electrocyclization of these *N*-acyliminiums induced in the presence of excess triflic acid (TFOH) afforded aza-Nazarov products in good to high yields (Scheme 3a). Furthermore, in a study reported in 2011, the same research group advanced this method to afford ring-fused isoindolinone derivatives by super-acid promoted aza-Nazarov reaction (Scheme 3b).[9] The use of superstoichiometric (i.e., 5 equivalents) amounts of the highly corrosive and expensive

TfOH is the major drawback of these methodologies. In addition, the use of such superstoichiometric amounts of a Brønsted or Lewis acid promoter necessitates a different conceptual approach for the development of a catalytic enantioselective variant of this reaction.

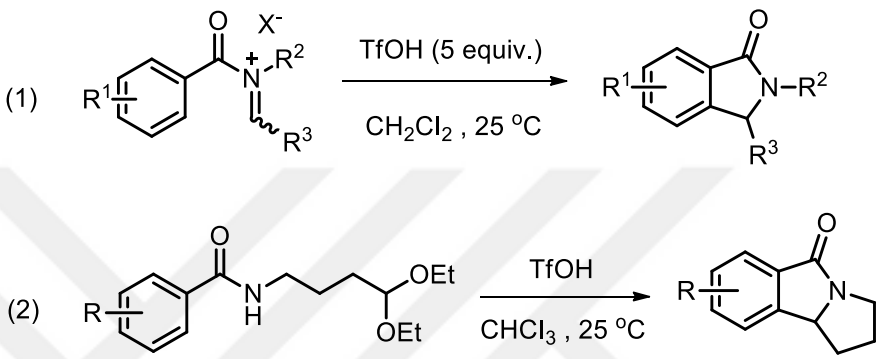

Scheme 3. Studies on aza-Nazarov reaction by Klumpp and co-workers.

Würthwein research group reported synthesis of *N*-substituted pyrroles via a Brønsted acid-promoted aza-Nazarov reaction (Scheme 4).[10] Their study showed that depending on the acid concentration, the reaction follows different pathways. Electrophilic conditions (2 equiv. of TfOH, dilute solution) were found to afford *N*-indolinylpyrrole products, whereas superelectrophilic conditions (7-10 equiv. of TfOH, concentrated solution) resulted in N-N bond cleavage and, gave NH-pyrrole and acetylated indole products.

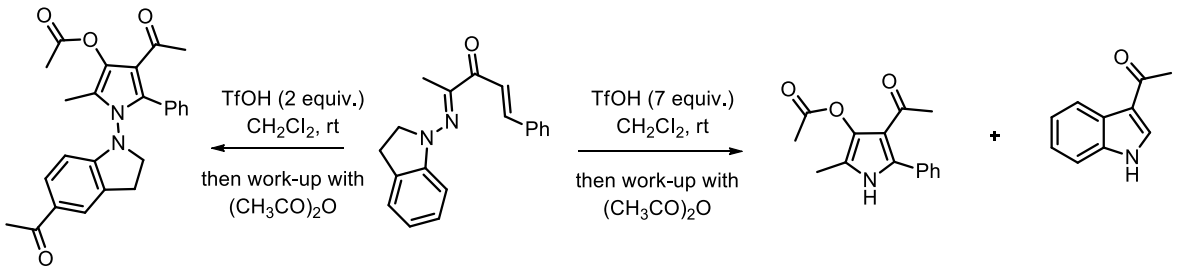

Scheme 4. Aza-Nazarov reactions under conditions of varying acidity.

With the application of a similar strategy, Würthwein and co-workers extended their work on aza-Nazarov reaction to produce substituted *N*-alkoxy- and *N*-amino pyrroles starting from 1-aza-3-hydroxy-penta-1,4-dienes in the presence of superstoichiometric amounts of TfOH (Scheme 5).[11]

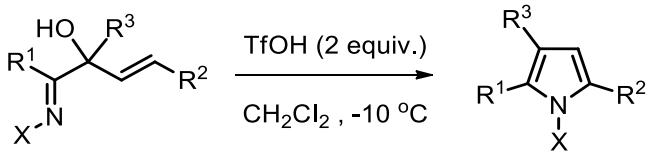

Scheme 5. Synthesis of *N*-alkoxy- and *N*-amino pyrroles by aza-Nazarov cyclization.

Another important contribution in the literature to the field of aza-Nazarov reaction is the work by Tius and co-workers reported in 2010.[12] In this study, racemic keto-azirine **6** undergoes an enantioselective aza-Nazarov reaction in the presence of the chiral organocatalyst **8**, and then undergoes a ring expansion that furnishes the six-membered product **7** with high enantioselectivity as illustrated in Scheme 6. This marks the first example of a catalytic aza-Nazarov reaction as well as the only enantioselective example of this reaction to date. However, it should be noted that it is a rather specialized transformation with a very narrow substrate scope.

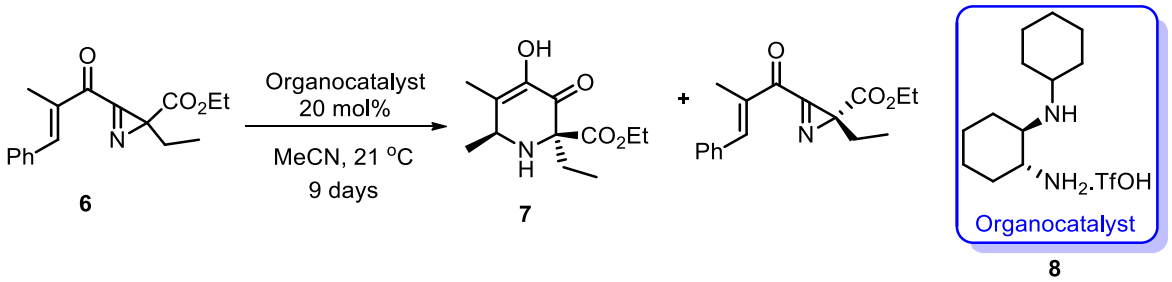

Scheme 6. Catalytic enantioselective aza-Nazarov reaction.

In 2019, Türkmen research group developed a novel aza-Nazarov reaction between 3,4-dihydroisoquinolines and α-β-unsaturated acyl chlorides which operates in the presence

of a catalytic amount of Lewis acid and under mild conditions to afford α-methylene-γ-lactam aza-Nazarov products.[13] The method requires the use of substoichiometric amounts of AgOTf (20 mol%) as an anion exchange reagent. In this work, heterocyclic aza-Nazarov products were obtained in good to high yields (up to 79%) as single diastereomers.

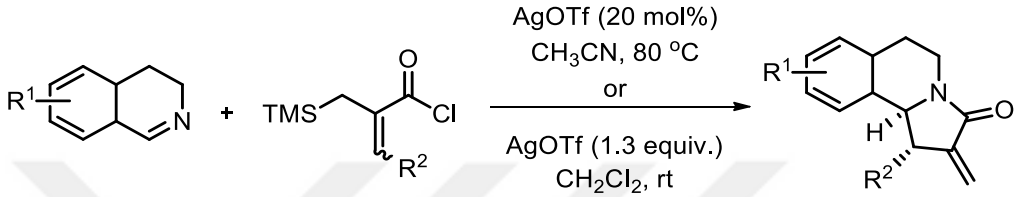

Scheme 7. Aza -Nazarov reactions with anion exchange catalysis.

In addition to these studies, in a recent work reported in 2019, Rasapalli and co-workers employed TfOH-promoted aza-Nazarov reactions of quinazolinonyl enones in order to afford tricyclic quinazolin-dione derivatives, which were further used in the synthesis of C-ring substituted luotonins and vasicinones (Scheme 8).[14]

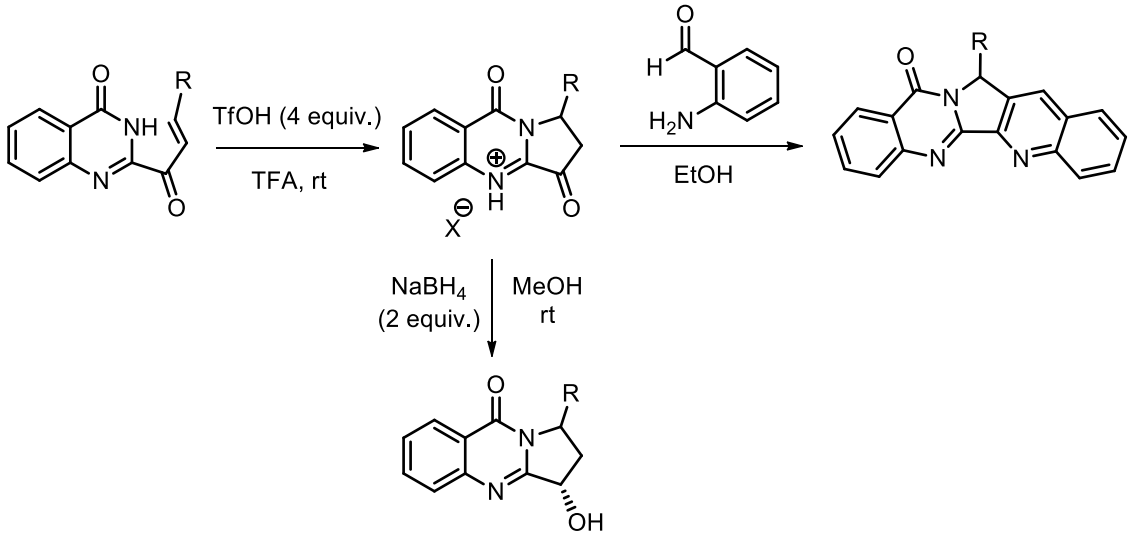

Scheme 8. TfOH-Mediated aza -Nazarov reactions of quinazolinonyl enones.

1.1.4. Aim of This Project

This part of the thesis intended to present detailed studies towards understanding the mechanism of the aza-Nazarov cyclization reaction. These studies included; first, the effect of water on the reaction mechanism and determination of side-product of the reaction, secondly, our efforts on further development of this reaction through the use of achiral anion binding catalysts. In the following, aza-Nazarov reaction will be investigated by conducting mechanistic studies to render the mechanism of this reaction comprehensible. Considering the importance of thiophene-based scaffolds in natural product chemistry, we will perform aza-Nazarov reaction utilizing a thiophene-based imine in order to isolate nitrogen and sulfur containing aza-Nazarov product. In addition to these, our studies to exploit the *β*-silicon stabilization effect in a different context for the development of a related aza-Nazarov reaction will be described.

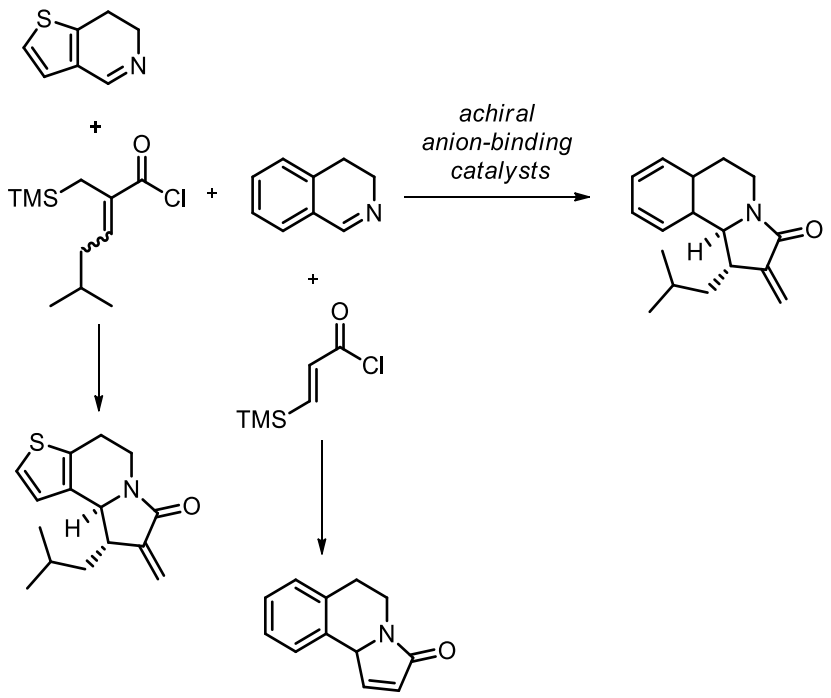

Scheme 9. Studies towards understanding the mechanism of the aza-Nazarov cyclization reaction.

1.2. RESULTS AND DISCUSSION

1.2.1. The Effect of Water on the Reaction Outcome

During the optimization and substrate scope studies on the aza-Nazarov cyclization reaction, an aldehyde signal at around 10 ppm in the ^{1}H-NMR spectra of crude reaction mixtures was frequently encountered. For instance, in the reaction of 3,4-dihydroisoquinoline **10** and acyl chloride **15**, a signal at 10.36 ppm was observed in varying amounts depending on the reaction conditions. It should be noted that this signal almost vanished under the optimized reaction conditions whereas its intensity was larger when a relatively less anhydrous solvent was used or when the reaction was not run under an inert atmosphere. Apparently, this signal does not belong to the reactants **10** and **15** as well as the aza-Nazarov product **24**. It should also be added that the observed side product could be detected in TLC analysis under UV light among the other spots.

Based on these observations, we hypothesized that the presence of adventitious water in reaction mixture could lead to an aldehyde side product formation through the hydrolysis of the *N*-acyliminium intermediate **16** with H_2O. The proposed pathway for this process is shown below in Scheme 10. According to this pathway, the initial reaction between imine **10** and acyl chloride **15** would give the *N*-acyliminium intermediate **16**. In the absence of water and under the optimal reaction conditions, this intermediate could proceed to the regular aza-Nazarov product **24** with no or minimal formation of the aldehyde-containing side product. However, if the aza-Nazarov reaction is slow or when water is present in the medium, then the attack of H_2O on the iminium **16** could give aminal **17**, which would subsequently open to give the final proposed hydrolysis side product **18**.

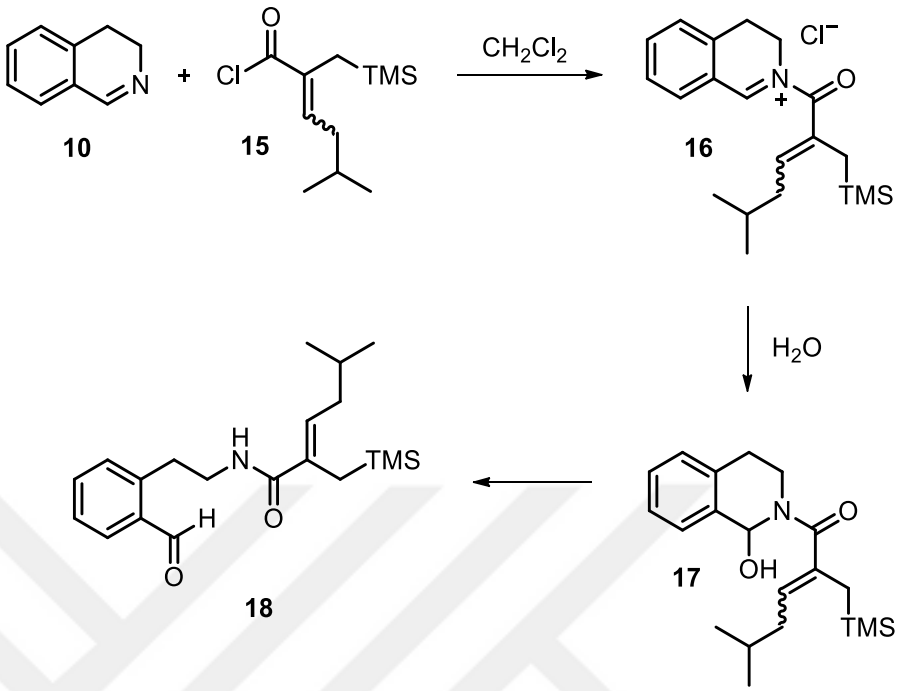

Scheme 10. Proposed pathway for the hydrolysis of *N*-acyliminium intermediate **16**.

Unfortunately, the isolation of the side product from the crude mixture of an aza-Nazarov reaction proved to be challenging, and it could not be isolated in pure form. Therefore, in order to identify the side product and prove the aldehyde formation, a control experiment was conducted. For this purpose, we attempted to investigate first the reaction between 3,4-dihydroisoquinoline **10** and commercially available methacryloyl chloride **19**. The imine substrate **10** to be used in this reaction was obtained in single step starting from the commercially available 1,2,3,4-tetrahydroisoquinoline **9** in 84% yield following a literature procedure as shown in the Scheme 11.

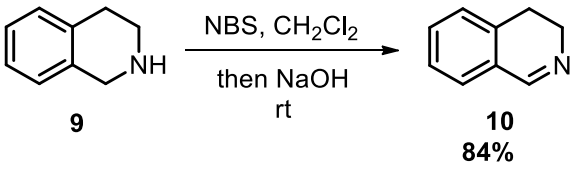

Scheme 11. Preparation of imine **10**.

The reaction of imine **10** with methacryloyl chloride **19**, which was selected as a simplified analogue of the acyl chloride substrate **15**, in an aqueous reaction medium afforded the hydrolysis product **20** after purification by flash column chromatography. The structural characterization of **20** was completed by ATR-FTIR, ^{1}H- and ^{13}C-NMR spectroscopies in addition of HRMS analysis.[15] The signals of **20** at 10.16 ppm in its ^{1}H-NMR spectrum and 193.9 ppm in its ^{13}C-NMR spectrum were assigned to the aldehyde group.

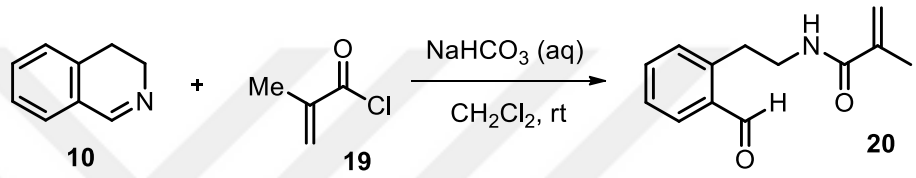

10 **19** **20**

Scheme 12. Reaction between imine **10** and methacryloyl chloride **19**.

As the next step, the hydrolysis reaction between imine **10** and acyl chloride **15** was investigated under the same reaction conditions. The acyl chloride derivative **15** required for this reaction was synthesized in four steps:[13] First, the deprotonation of the commercially available triethyl phosphonoacetate **11** with NaH followed by alkylation with $TMSCH_2I$ gave **12** with 57% yield (Scheme 13). Afterwards, the Horner-Wadsworth-Emmons (HWE) reaction using isoveraldehyde provided the α,β-unsaturated ester product **13** in 62% yield and with a diastereomeric ratio of 3:1 (*Z:E*). Hydrolysis of the ester under basic conditions followed by acidic work-up gave carboxylic acid product **14** in 52 % yield (dr = 3:1). Finally, conversion of the carboxylic acid group of **14** to acyl chloride was accomplished with the use of oxalyl chloride, and the final acyl chloride product **15** was isolated in 90% yield. We should note that the diastereomeric ratio is retained throughout this process, and the final product **15** was also obtained with a dr of 3:1. Finally, it should be emphasized that the acyl

chloride derivative **15** is prone to decomposition and therefore, was used immediately in the subsequent reaction after analysis by ^{1}H-NMR spectroscopy.

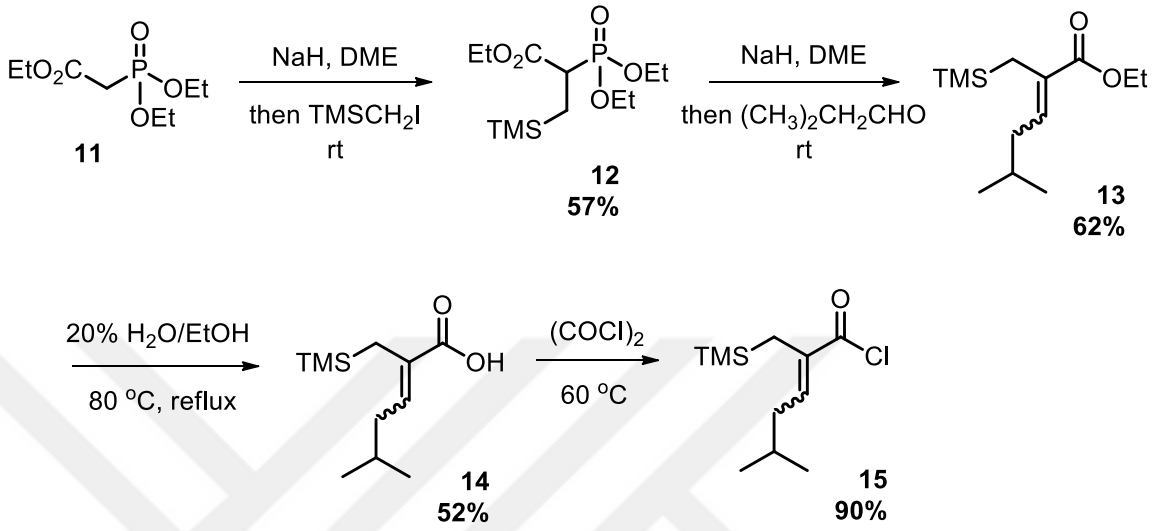

Scheme 13. Synthesis of α-β- unssturated acyl chloride **15**.

When the reaction between imine **10** and acyl chloride **15** under the same aqueous reaction conditions was investigated, a similar aldehyde-containing product **18** was obtained (Scheme 14). The signals of this product **18** were found to match exactly those signals of the suspected side product in the crude ^{1}H-NMR spectrum of the aza-Nazarov reaction. Based on these results, it can be concluded that hydrolysis of the *N*-acyliminium intermediate is a significant potential problem in these aza-Nazarov reactions and therefore, having an anhydrous reaction medium, and running the reactions under an inert atmosphere and using pre-dried glassware are crucial for obtaining high product yields in aza-Nazarov reactions.

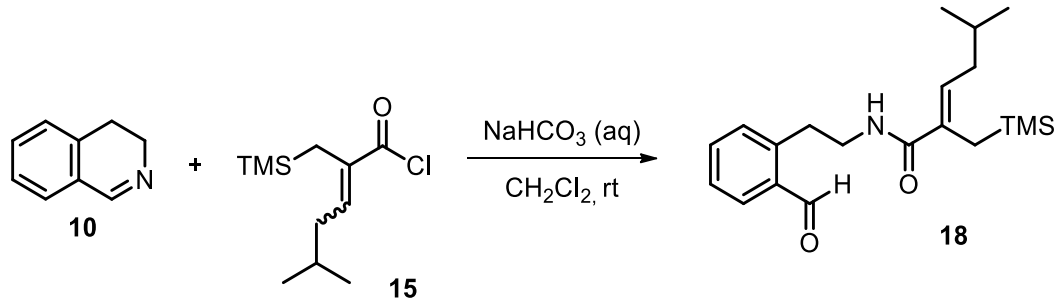

Scheme 14. Reaction between imine **10** and acyl chloride **15** in the presence of H_2O.

1.2.2. Aza-Nazarov Cyclization Reaction Promoted by Hydrogen Bond Donors

Aza-Nazarov cyclization between an imine substrate and an α,β-unsaturated acyl chloride takes place successfully under the optimized reaction conditions using a sub-stoichiometric amount of AgOTf as an anion exchange agent.[13] This part of the study aimed to investigate the aza-Nazarov cyclization reaction using different hydrogen bond donors as achiral anion binding catalysts. In the area of organocatalysis, thiourea and squaramide derivatives were demonstrated to bind anions strongly as hydrogen bond (HB) donors.[16] In this work, we opted to test the effectiveness of the HB donors listed in Figure 1 in the aza-Nazarov reaction. These HB donors include the achiral thiourea derivative **20**,[16] squaramide derivatives **21** and **22**,[17] and the triple HB donor thiophosphoramide derivative **23**.[18]

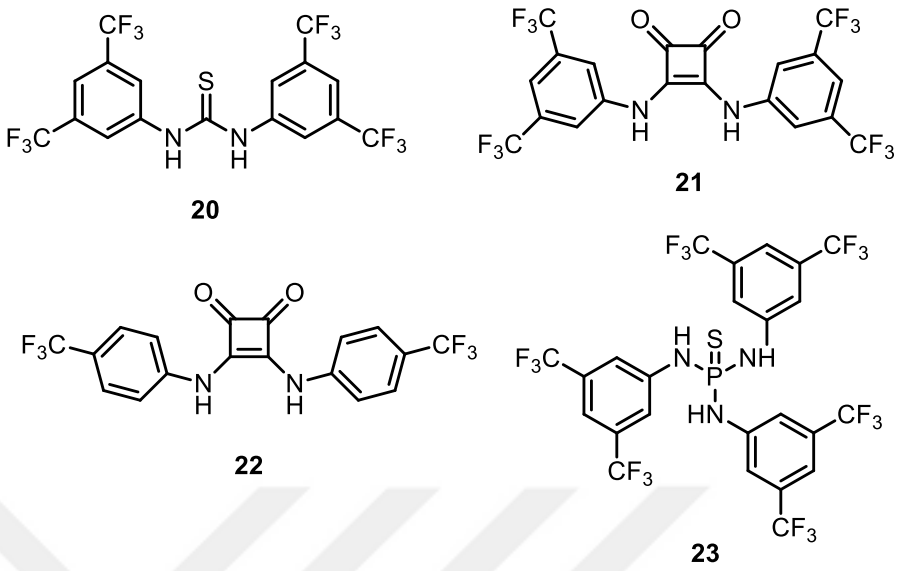

Figure 1. The hydrogen bond donors to be tested as anion binding catalysts.

In this part, the aza- Nazarov reaction between imine **10** and acyl chloride **15** was investigated under various conditions with the use of hydrogen bond donors **20**-**23** in substoichiometric or stoichiometric amounts. The results are summarized in Table 1. The characterization of the aza-Nazarov product **24** was carried out by ^{1}H-NMR, ^{13}C-NMR and FTIR-ATR spectroscopies, HRMS (high resolution mass spectrometry).

Table 1. The screening of aza-Nazarov reaction with hydrogen bond donors.

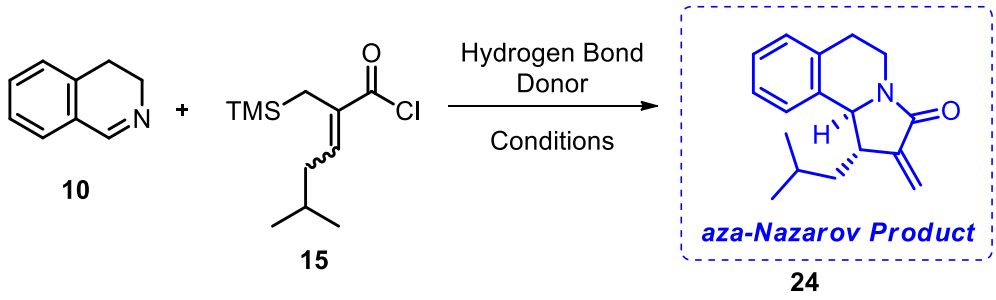

Entry[a]	Catalyst	Catalyst Loading (equiv)	Solvent	Temperature (°C)	Yield[b] (%)
1	**20**	0.20	CH_2Cl_2	23	ND[c]
2	**20**	0.20	MeCN	80	40
3	**20**	1.20	CH_2Cl_2	23	15
8	**21**	1.20	CH_2Cl_2	23	22
5	**21**	0.20	MeCN	80	48
6	**22**	1.20	CH_2Cl_2	23	17
7	**22**	0.20	MeCN	80	59
4	**23**	1.20	CH_2Cl_2	23	25

[a]1 equiv. imine **10** and 1.3 equiv. acyl chloride **15** used. [b]Isolated product yields.

[c] The formation of aza-Nazarov product was not detected.

Initially, the aza-Nazarov reaction in the presence of 20 mol% of the thiourea derivative **20** provided the product in 40% yield at 80 °C in acetonitrile, whereas product formation was not observed at 23 °C with the same catalyst loading in CH_2Cl_2 (Table 1, entries 1 and 2). When the hydrogen bond donor **20** was used in stoichiometric amount at 23 °C, reaction gave product in 15% yield (entry 3). It should be emphasized here that

instead of using urea-containing catalyst, thiourea-based catalyst was utilized since the stronger hydrogen bond-donating ability of thioureas is desired to make H-bonding stronger to chloride anion, which is crucial for the overall success of the reaction. In addition to this improvement, squaramide-derived catalysts **21** and **22** gave aza-Nazarov product **24** in 48 % and 59 % yields, respectively at 80 °C when they were used with 20 mol% loading (entries 5 and 7). For the reactions with these catalysts under stoichiometric condition, aza-Nazarov product **24** was isolated in 17% and 22% yields, respectively (entries 6 and 8). These results expectedly showed that squaramide-based catalysts **21** and **22** performed with higher yields than thiourea-derived catalyst **20**. Finally, thiophosphoramide-based catalyst **23**, which was developed by Shea and co-workers, was tested under stoichiometric condition at rt, and product was isolated in 25% yield (entry 4). Unlike thiourea and squaramide derivative catalysts, thiophosphoramide-based catalyst **23** contains three N-H groups. This property facilitated with stronger H-bonding to chloride ion compared to thiourea **20** and squaramide **21** and **22** catalysts. We hereby concluded that among the achiral anion binding catalysts used for aza-Nazarov reaction in this section, thiophosphoramide based catalyst **23** is found to be the most effective as having three HB donor groups. In addition to this, with squaramide derivatives **21** and **22**, aza-Nazarov product was obtained in good yields due to electronic factors that enabled catalyst to make more strongly hydrogen bonding with chloride ion. These results clearly demonstrate that the use of strong hydrogen bond donors as anion-binding catalysts holds great promise for this type of aza-Nazarov reactions, but further catalyst optimization is required to attain results comparanle to those obtained with AgOTf.

1.2.3. Studies on Understanding of the Reaction Mechanism

Although, a reaction mechanism for the aza-Nazarov cyclization between imine **10** and acyl chloride **15** was previously proposed,[13] studies to better grasp its mechanism are insufficient and control experiments to understand individual steps of the proposed mechanism have yet to be conducted. Therefore, in this part, we aimed to deal with different aspects of this particular reaction mechanism and reveal details of specific steps. In terms of reaction mechanism, imine **10** was proposed to react with acyl chloride **15** to form an *N*-acyliminium salt. Then, anion-binding agent would capture the chloride ion, and the resulting naked and activated *N*-acyliminium cation would undergo the aza-Nazarov cyclization. Since a single diastereoisomer **24** was obtained in all aza-Nazarov reactions between various 3,4-dihydroisoquinoline derivatives and α,β-unsaturated acyl chlorides so far, we hypothesized that among the *E* and *Z* isomers of acyl chloride **15**, only the *E* isomer, which is the major diastereomer, participates in the aza-Nazarov cyclization. In order to check this hypothesis, we decided to first separate *E* and *Z* isomers of ester **13** by flash column chromatography, and then transform these isomers to the corresponding pure acyl chlorides for use in aza-Nazarov reactions with imine **10** separately. With this intention, initially, an appropriate solvent system that provides a successful separation of the *E* and *Z* isomers of ester **13** was sought. It should be emphasized here that the separation process of these isomers was highly challenging since the two diastereomers have almost similar R_f values and were found to have very close spots to each other in TLC analysis. After substantial efforts, the mixture of trifluorotoluene and hexanes was determined to be a suitable solvent system for the separation of alkene isomers **13a** and **13b**. With the use of this solvent system as mobile phase, *E* isomer **13b** and *Z* isomer **13a** were successfully separated by flash column chromatography, and

each diastereomer was characterized by ^{1}H-NMR, ^{13}C-NMR and NOESY spectroscopic analysis.

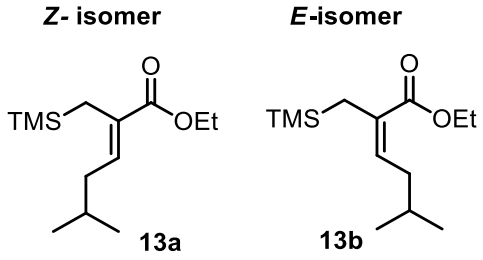

Figure 2. *E* and *Z* isomers of ester **13**.

Afterwards, hydrolysis reactions of the *E*- (minor) **13b** and *Z*- (major) **13a** isomers under basic conditions gave the corresponding carboxylic acid products **14b** and **14a**, which were also isolated after purification by flash column chromatography. Their purity analyses and characterization were done by ^{1}H-NMR, ^{13}C-NMR and NOESY stıudies. The results of these reactions demonstrated that the hydrolysis processes were highly diasterospecific and did not lead to isomerization. In other words, carboxylic acid products were isolated as single diastereomers. In the next step, chlorination reactions of the carboxylic acids were carried out with the use of oxalyl chloride to obtain acyl chlorides **15b** and **15a**. It is important to clarify here that the configuration of the major alkene of **15a** is (*E*) rather than (*Z*) and, the configuration of the minor alkene is (Z) rather than (*E*), since chlorine atom has a higher priority than silicon according to the Cahn-Ingold-Prelog priority rules.[19] Additionally, the (*E*) and (*Z*) acyl chloride derivatives were obtained as single diastereomers after purification by column chromatography.

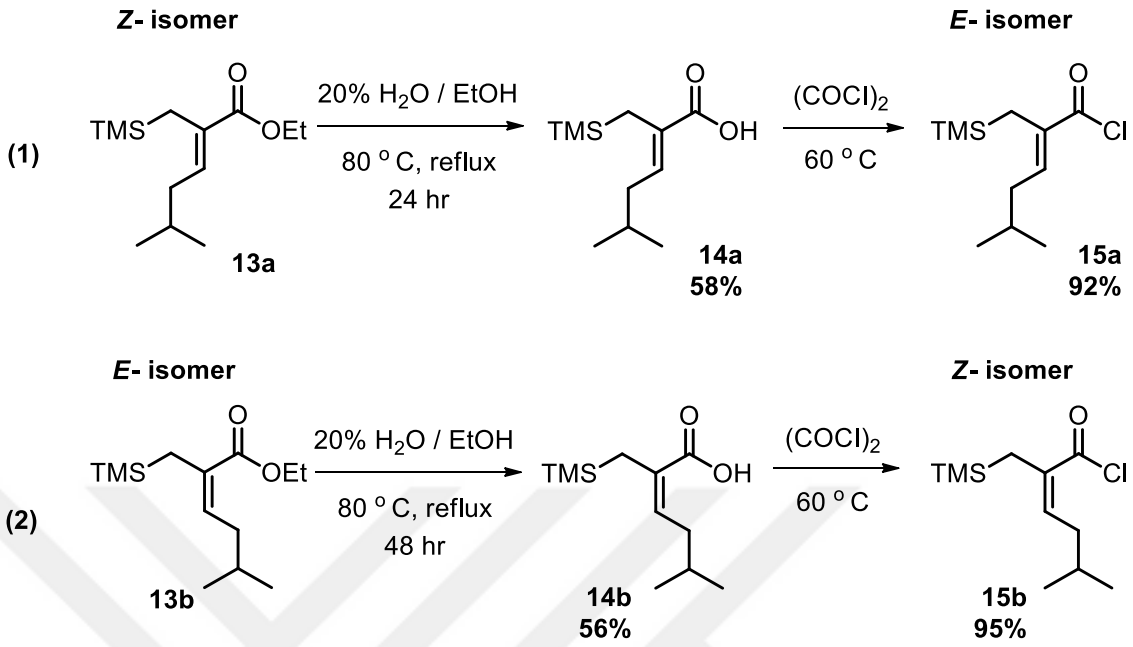

Scheme 15. *E* and *Z* isomers of the carboxylic acid and acyl chloride derivatives.

The aza-Nazarov reaction was performed separately between imine **10** and the *E*- (**15a**) and *Z*- (**15b**) isomers of the acyl halide under the optimal reaction condition.

Table 2. Aza-Nazarov reaction of the *E*- (**15a**) and *Z*- (**15b**) isomers with imine **10**.

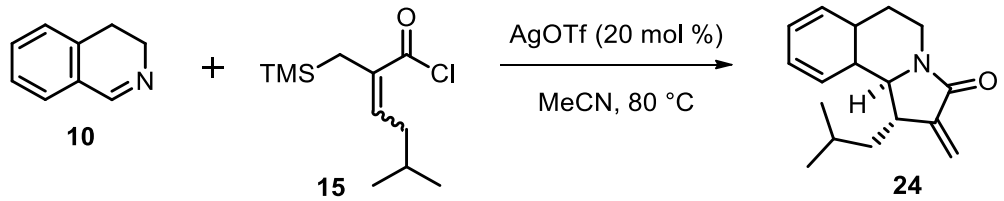

acyl chloride 15;

a. (*E*)-isomer
b. (*Z*)-isomer

Entry	Solvent	Yield[c] (%)
1[a]	MeCN	52
2[b]	MeCN	24

[a]1 equiv. imine **10** and 1 equiv. acyl chloride **15a**. [b]1 equiv. imine **10** and 1 equiv. acyl chloride **15b**.
[c] Isolated product yield.

The results of these reactions were unexpected according to our hypothesis, yet it provided crucial information about the mechanism of this particular reaction. We showed that not only *E*- (major) isomer of the acyl chloride **15** gave aza-Nazarov product **24** in 52% yield, but also the *Z*- (minor) isomer participates in aza-Nazarov reaction affording exactly the same diastereomer of the final product **24**, albeit in a lower yield (24% yield, Table 2). The lower product yield obtained when the (*Z*) isomer was used is not surprising, especially when the steric bulkiness of the isobutyl group is considered. In addition, when the proposed reaction mechanism is taken into consideration, even if *Z*-minor isomer is involved in the reaction, the product would be the other diastereomer of **24** due to the stereochemistry of minor isomer. Based on these results and inferences, we noticed that a separate and previously unconsidered step might be involved in the reaction mechanism, which would be responsible for the formation of the same diastereomer of the product from the *(E)*- and *(Z)*-acyl chloride isomers. Herein, we propose that an alkene isomerization prior to Nazarov cyclization might be taking place so that the same product diastereomer would be obtained. A plausible mechanism for this type of an alkene isomerization is described below in Scheme 16. After the minor acyl chloride isomer **15b** binds to imine **10**, they are expected to form an iminium salt. At this stage, we propose that an alkene isomerization may take place on *N*-acyliminium ion so that the minor isomer **15b** yields the same diastereoisomer of the aza-Nazarov product **24** as the major acyl chloride isomer. The 1,4-conjugate addition of chloride (Cl^-) to the α,β-unsaturated carbonyl moiety could give zwitterionic intermediate **25**, which in turn could give the isomerized *N*-acyliminium **16** upon elimination of Cl^-.

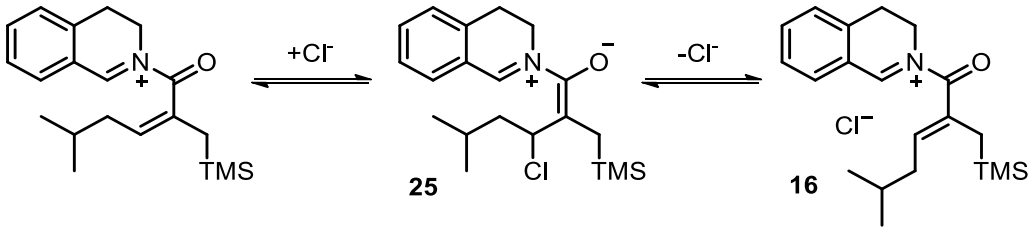

Scheme 16. A plausible mechanism for olefin isomerization under reaction conditions.

Another discussion to understand better the mechanism was about considering two different reaction pathways, which could provide aza-Nazarov product **24** (Scheme 17). In pathway I, the initial reaction between imine **10** and acyl chloride **15** would give the *N*-acyliminium salt **16**, which would then undergo an intramolecular cyclization to afford the final product **24**. In the alternative pathway II, α,β-unsaturated acyl chloride would first attack imine **10** in a manner similar to an aza-Hosomi-Sakurai allylation to give intermediate **26**, which would then undergo a lactam formation to give the final product.

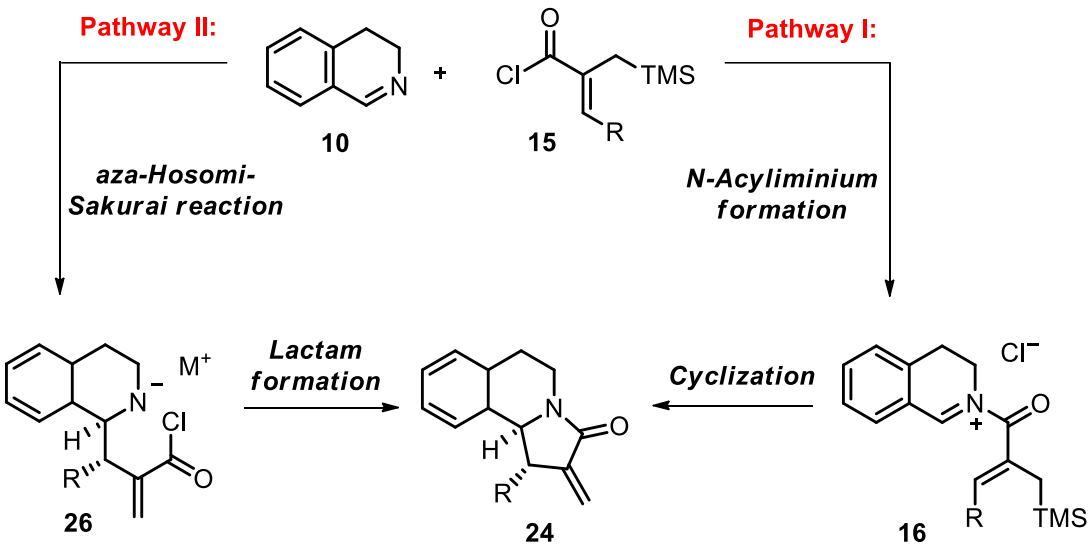

Scheme 17. Two possible pathways for the Aza-Nazarov reaction.

The formation of the aldehyde-containing hydrolysis product **18** in the presence of water as described in Section 1.2.1. supports pathway I for the aza-Nazarov reaction (Scheme 17). However, we still wanted to check the feasibility of pathway II in an indirect way through investigation of the reaction between imine **10** and an α,β-unsaturated ester instead of an acyl chloride. It should also be stated here that, *n*-propyl-substituted ester **27** was preferred instead of isobutyl-substituted ester **13** to minimize steric effects on the reaction. The synthesis of ester **27** required for this reaction was conducted in two steps: first, the deprotonation of the commercially available triethyl phosphonoacetate **11** with NaH followed by alkylation with $TMSCH_2I$ gave **12** in 57% yield (Scheme 18). Thereafter, the Horner-Wadsworth-Emmons (HWE) reaction using butyraldehyde provided the α,β-unsaturated ester product **27** in 31% yield and with a diastereomeric ratio of 2:1 (*Z:E*).

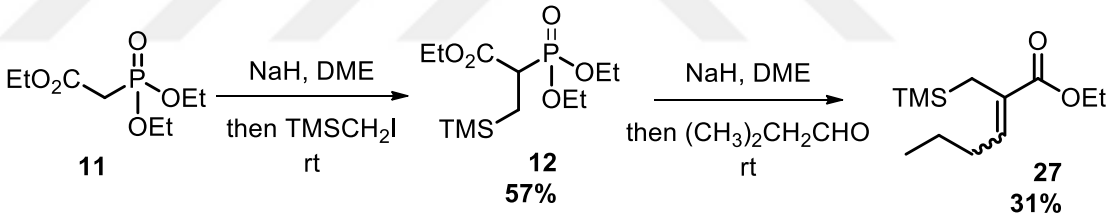

Scheme 18. Synthesis of α,β-unsaturated ester **27**.

In order to inspect this possibility, aza- Hosomi-Sakurai reaction between imine **10** and ester **27** was examined by utilizing different Lewis acids.

Table 3. Aza- Hosomi-Sakurai reaction between imine **10** and ester **27**.

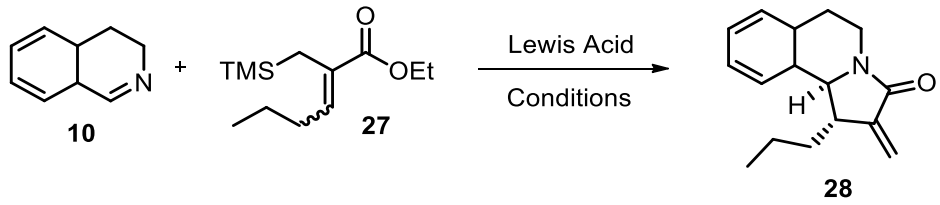

10 **27** **28**

Entry[a]	Lewis Acid	Catalyst (mol%)	Solvent	Temperature (°C)	Result[b]
1	$Zn(OTf)_2$	20	MeCN	70	NP
2	$ZnBr_2$	20	MeCN	70	NP
3	$CuCl_2$	20	MeCN	70	NP
4	Tf_2NH	20	MeCN	70	NP
5	$BF_3.Et_2O$	20	CH_2Cl_2	23	NP
6	AgOTf	20	MeCN	80	NP

[a]1 equiv. imine **10** and 1 equiv. ester **27** used. [b]Crude ^{1}H-NMR analysis.

1.2.4. Aza-Nazarov Cyclization Reaction with Thiophene-Based Imine

In the first part of this work, the synthesis of aza-Nazarov product **24** was achieved with the use of 3,4-dihydroisoquinoline **10** as a core imine structure and acyl chloride **15**. Considering the structures of biologically active molecules and pharmaceuticals, thiophene-based heterocyclic scaffolds constitute a significant portion of these heterocycles. With this in mind, we opted to test the feasibility of using a heterocyclic imine with a heteroatom other than nitrogen, particularly with a thiophene ring, in the aza-Nazarov reaction. Therefore, this part of the study focused on the aza-Nazarov reaction with 6,7-dihydrothieno[3,2-c]pyridine **32** and acyl chlorides **15** and **30**. The synthesis of thiophene-based imine **32** required for this reaction was synthesized in 2 steps (Scheme 19). Initially, formylation of the commercially

available thiophene-2-ethylamine using ethyl formate afforded **31** in 95% yield. The subsequent Bischler–Napieralski reaction with phosphoryl chloride at room temperature provided **32** in 21% yield. The low yield of the latter step was due to the difficulties encountered during the isolation process.

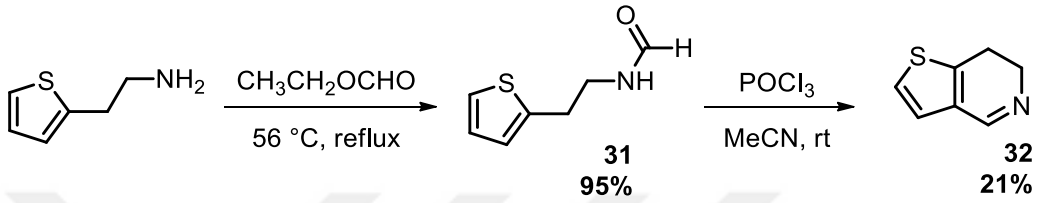

Scheme 19. Synthesis of thiophene-based imine **32**.

The aza-Nazarov reactions performed between thiophene-based imine **32** and acyl chlorides **15** and **30** by utilizing different Lewis acids are described below (Table 4).

Table 4. Aza-Nazarov reactions performed between thiophene-based imine **32** and acyl chlorides **15** and **30**.

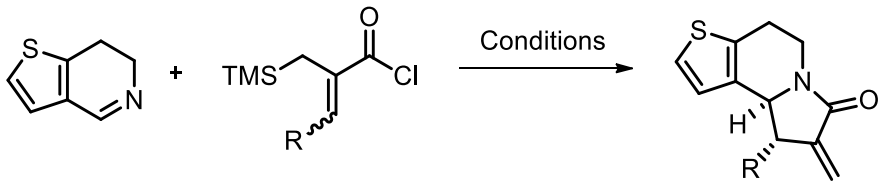

a. R : *n*-propyl
b. R : *i*-butyl

Entry	Catalyst	Lewis acid (equiv.)	Solvent	Temperature (°C)	Yield[c] (%)
1[a]	AgOTf	1.2	CH_2Cl_2	23	40
2[a]	$BF_3.OEt_2$	0.2	MeCN	80	ND
3[b]	AgOTf	0.2	MeCN	80	ND
4[b]	$BF_3.OEt_2$	0.2	MeCN	80	ND

[a]1 equiv. thiophene based imine **32** and 1.3 equiv. acyl chloride **15** used. [b]1 equiv. thiophene-based imine **32** and 1.3 equiv. acyl chloride **30** used. [c]Isolated yield.

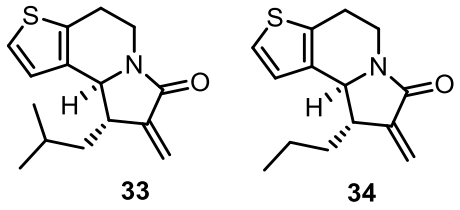

33 **34**

Figure 3. Thiophene-based aza-Nazarov products **33** and **34**.

The reaction between thiophene-based imine **32** and isobutyl-substituted acyl chloride **15** afforded the aza-Nazarov product **33** with 40% yield using stoichiometric amount of AgOTf at 23 °C. In addition, the same reaction also performed with catalytic amount of $BF_3.OEt$ at 80 °C and provided aza-Nazarov product **33**. It is important to mention that the yield percentage for the second reaction unfortunately could not be determined due to the solubility problem of the product **33** in MeCN. We realized the solubility problem after carrying out

the reaction with AgOTf and BF_3.OEt under catalytic condition in MeCN. Because we had limited amount of thiophene-based imine **32** at the beginning, we were only able to operate the same reaction with AgOTf under stoichiometric condition in CH_2Cl_2 and isolated yield % could be determined. Furthermore, the aza-Nazarov product **34** synthesized using thiophene based imine **32** and isopropyl substituted acyl chloride **30** under catalytic condition using AgOTF and $BF_3.OEt_2$ as a Lewis acids. In these reactions, we again encountered solubility problem of product **34** in MeCN and isolated yield percentage could not be determined as well. Although experimental problems interfered the purification process of the products, the aza-Nazarov reaction performed successfully using thiophene based imine **32** and corresponding acyl chlorides. The synthesized of thiophene based aza-Nazarov products **33** and **34** analyzed by ^{1}H-NMR, ^{13}C-NMR, FTIR-ATR spectroscopies and MS-TOF analysis.

1.2.5. Experiments Aiming to Observe Direct β-Si Effect

In the area of organosilicon chemistry, *β*-silicon effect is defined as a special type of hyperconjugation, which influences the stability of a carbocation due to the presence of silicon atom at the *β*-position of a positive charge. Within the scope of this project, in order to take advantage of this *β*-silicon effect, substrates containing trimethylsilyl group was utilized for the aza-Nazarov cyclization reactions. As illustrated in Scheme 20, TMS group is proposed to contribute to aza-Nazarov reaction in three ways: first, the alkene of the α,β-unsaturated carbonyl group becomes more electron-rich through strong hyperconjugation of C-Si bond. Secondly, after cyclization takes place, carbocation intermediate is stabilized due to the presence of silicon atom at the *β*-position of positively charged carbon atom. It should be underlined that stabilization effect on this carbocation facilitates with reducing the activation energy of the reaction and therefore increases the rate of the reaction. The effect

of the -TMS group at the *β*-position on the reaction rate and stabilization of the carbocation intermediate was supported through computational studies.[13] Finally, TMS group reacts with chloride ion through covalent bonding and forms TMSCl as a by-product of the reaction.

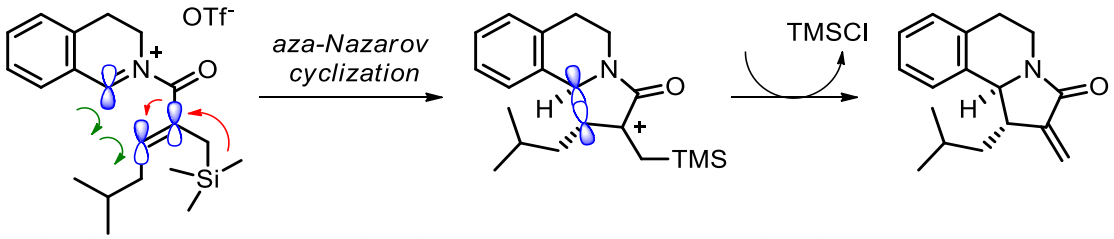

Scheme 20. *β*-silicon effect on stabilization of **24** carbocation.

Considering these significant contributions of *β*-silicon stabilization effect, in this part of the study, we aimed to exploit this effect in a different context for the development of a related aza-Nazarov reaction. For this purpose, we designed a new acyl chloride **41**, which includes only TMS group directly bound to the alkene group. The aza-Nazarov reaction between imine **10** and acyl chloride **41** was expected to form *N*-acyliminium ion **35**, which would subsequently undergo a 4π conrotatory electrocyclization to afford the targeted aza-Nazarov product **36**.

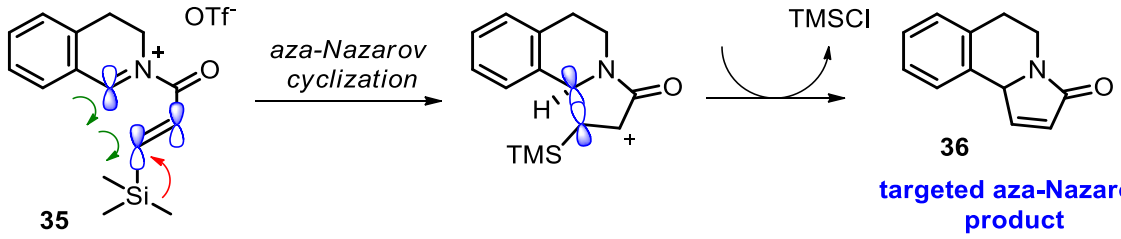

Scheme 21. *β*-silicon effect on stabilization of **36** carbocation.

In order to conduct this particular reaction, initially, new acyl chloride **41** was synthesized. The synthesis of **41** included four steps based on literature procedures: first, double deprotonation of commercially available propargyl alcohol **37** followed by addition of TMSCl gave **38** in 90% yield. Then, the reduction of **38** with $LiAlH_4$ provided full

conversion to the *trans* alkene **39**, which was subsequently used for oxidation reaction with Jones' reagent to afford **40** in 85% yield. Finally, carboxylic acid group of **40** was converted to acyl chloride by using oxalyl chloride to obtain **41** in 90% yield. It should be noted here that acyl chloride **41** is sensitive under open air, and therefore, was used immediately in the subsequent reaction after analysis by ^{1}H-NMR spectroscopy.

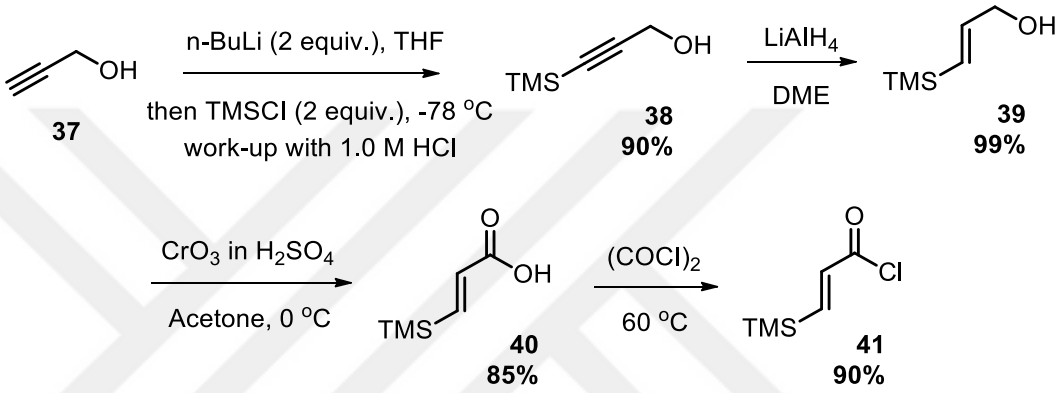

Scheme 22. Synthesis of acyl chloride **41**.

The aza-Nazarov reaction between imine **10** and acyl chloride **41** was investigated under various conditions to attempt the synthesis of product **36** as shown in Table 5.

Table 5. Aza-Nazarov reaction between imine **10** and acyl chloride **41**.

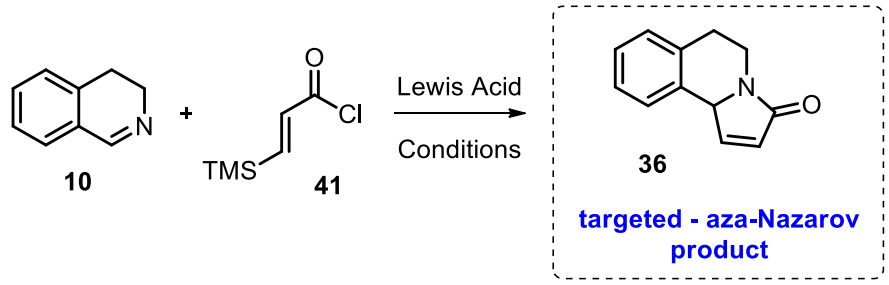

Entry[a]	Catalyst	Catalyst (equiv.)	Solvent	Temperature (°C)	Results[b]
1	AgOTf	1.2	MeCN	rt	NP
2	AgOTf	0.2	MeCN	80	NP
3	AgOTf	1.2	MeCN	80	NP
4	AgOTf	1.2	CH_2Cl_2	23	NP
5	Ferrocene	0.1	MeCN	80	NP
6	$BF_3{\cdot}OEt_2$	0.2	MeCN	80	NP

[a]1 equiv. imine **10** and 1.2 equiv. acyl chloride **41** used. [b]Crude ^{1}H-NMR analysis.

Despite all attempts to obtain aza-Nazarov product **36** under the reaction conditions listed on Table 5, we could not observe the formation of the desired product **36**. This unfortunate result can be explained by comparing the structural features of acyl chlorides **15** and **41**: nucleophilicity of the alkene of the α,β-unsaturated carbonyl group of **15** is anticipated to be much higher than that of **41** according to reactivity scales table developed by Mayr and co-workers.[20] This is because acyl chloride **15** possesses a -CH_2TMS group at adjacent position of the carbonyl, which provided an increased electron density for alkene group. On the other hand, acyl chloride **41** has only TMS

group directly bound at the *β*– position of the α,β-unsaturated carbonyl moiety. Additionally, acyl chloride **15** comprises an isobutyl substituent, which renders the alkene group more electron-rich. From these results, it was concluded that handling the *β*-silicon stabilization effect with a different approach to the aza-Nazarov reaction did not work to afford targeted product **36**, yet it provided a crucial information: the design of acyl chloride **15** for the aza-Nazarov reactions studied in this work plays an important role in terms of the positioning and the electronic effects of the silicon-containing substituents to yield the desired aza-Nazarov products.

1.3. CONCLUSION

This chapter of thesis outlined the developments of aza-Nazarov reaction mechanism between acyl chloride **15** and imine **10**, in which we mainly focused to understand the each steps of the reaction. This chapter included five parts; initially, the side product of the aza-Nazarov reaction was investigated and, it was isolated successfully with the help of control experiments. In the second part, HB donor anion binding catalyst were utilized to perform aza-Nazarov reaction and their effectiveness in term of hydrogen binding to chloride ion was tested. In the following part, the mechanism of this aza-Nazarov reaction were examined in detailed to bring light to behavior of the (*E)* and (*Z)* isomers of acyl chloride **15** during the reaction. Mechanistic works with this purpose provided significant findings to this thesis work; we proved that both isomers contributes to the aza-Nazarov product formation and minor isomer achieve this ability due to alkene isomerization during the reaction. In addition to this, aza-Nazarov product formation was considered following different pathways in the mechanism; the possibility of aza-Hosomi-Sakurai reaction was taken into account; it was concluded that the formation aza-Nazarov product only afforded by forming *N*-acyliminium salt. This particular aza-Nazarov reaction was operated with thiophe-based imine, which provides both nitrogen and sulfur containing heterocyclic scaffolds for the future synthesis of biologically active natural products. Finally, we paid attention to prominence of *β*-silicon effect, which benefits with stabilization of carbocation intermediate during the aza-Nazarov reactions. We attempt to perform aza-Nazarov reaction with a different approach to proceed cyclization step only supporting by TMS group with a new acyl chloride **41**. Although, the targeted aza-Nazarov product was not observed at all, these findings indicated that the design of the acyl chloride **15** has remarkable importance in the mechanism of the aza-Nazarov reaction.

2. DEVELOPMENT OF TEMPLATE-DIRECTED PHOTOCHEMICAL [2+2] CYCLOADDITION REACTIONS

2.1. INTRODUCTION

2.1.1. Photochemical [2+2] Cycloaddition Reaction

Many natural products and biologically active compounds possess cyclic scaffolds; therefore, their synthesis attracted remarkable attention in the field of synthetic organic chemistry. Although, well-established procedures for the syntheses of six-membered and five-membered rings are usually available on literature, comprehensive studies for cyclobutane chemistry have yet to be developed. The addition of two π systems containing four electrons under a light source is a reaction that has been investigated by organic chemists to produce cyclobutane rings, and is known as photochemical symmetry-allowed [2+2] cycloaddition reaction.

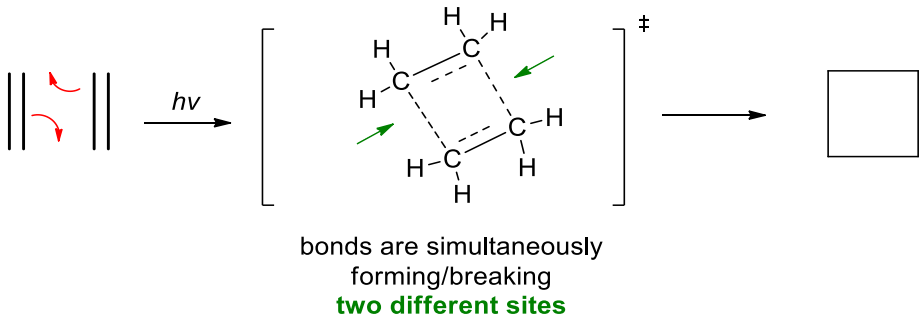

Scheme 23. Synthesis of cyclobutane using ethene molecules.

In terms of mechanism, the interaction between SOMO (π^*) of one alkene system and LUMO (π) of the second alkene takes place in a one-step concerted way, in which two σ bonds have to be established at the same time that subsequently two π bonds broken in the transition state. According to Woodward-Hoffman rules, this transformation is facilitated only under photochemical conditions to meet the orbital symmetry conditions; transition of

electron in π-bonding orbital to higher energy π^* - antibonding orbital is only possible when required energy for this process is provided generally by a UV-light source. In this favorable situation, there is constructive orbital overlap observed on both reacting site (Figure 4).

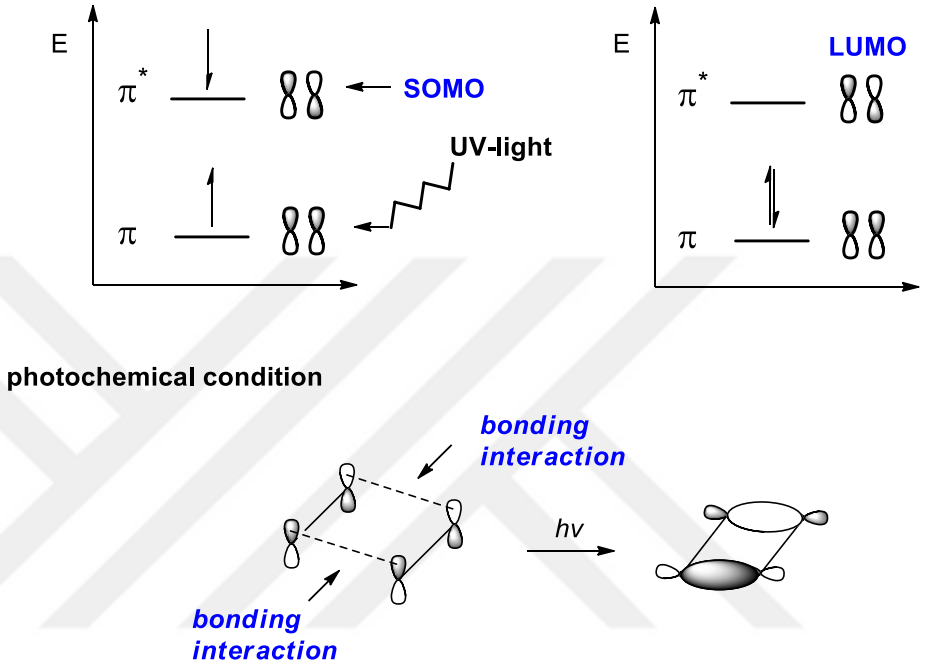

Figure 4. [2+2] cycloaddition reaction under photochemical condition.

Under thermal conditions, in which heat is used as the energy source, electron is not excited to the π^* - antibonding orbital, hereby, the symmetries of the HOMO (π) and LUMO (π) orbitals do not match. This results in only one σ bond forming as one of the two reactive sites experience constructive orbital overlap, and the other one ends with antibonding interaction. Under this circumstance, [2+2] cycloaddition does not work to produce cyclobutane (Figure 5).

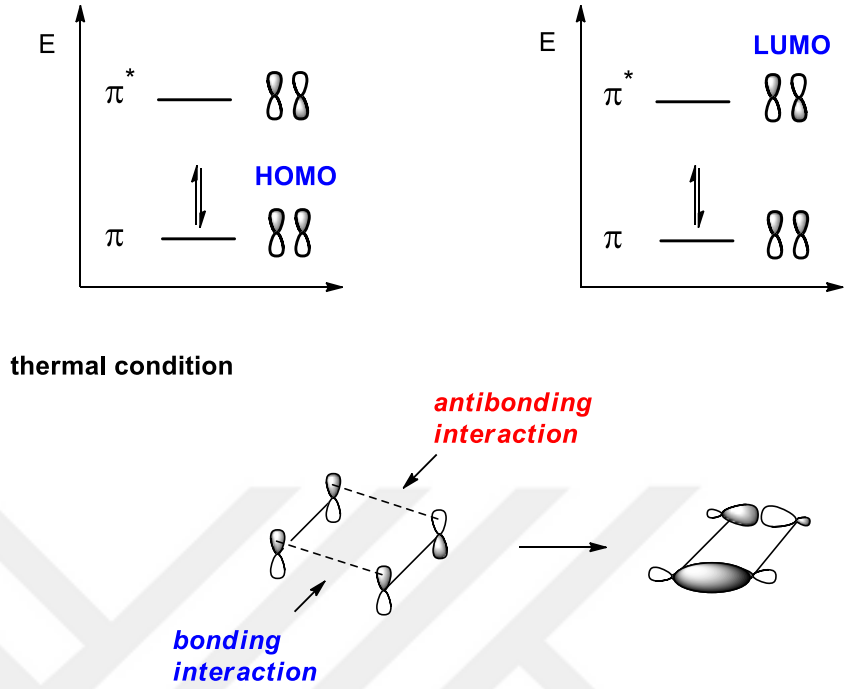

Figure 5. [2+2] cycloaddition reaction under thermal condition.

2.1.2. Advances on Photochemical [2+2] Cycloaddition Reaction

In 1908, Italian chemist and one of the pioneers of photochemistry, Giacomo Ciamician placed carvone **42** in solution under sunlight for months, and obtained carvonecamphor compound which formed via an intramolecular photochemical [2+2] cycloaddition.[21]

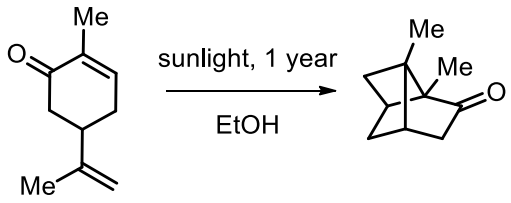

42

Scheme 24. Photochemical synthesis of carvonecamphor compound.

After this finding, in 1950s, Buchi and Goldman confirmed the structure of the camphor formed in this photochemical reaction. They conducted valuable research to

demonstrate synthetic value of the photochemical [2+2] reactions by examining the mechanism of irradiation reaction in detail.[22] Intermolecular photochemical [2+2] reactions in solution phase are found to be more difficult since UV-light generally causes *cis-trans* isomerization, and as a result, complex mixtures of products are obtained. In this way, the *chemo-*, *regio-* and *stereoselectivity* of this particular photochemical process proved to be challenging. On the other hand, Schmidt focused on the study of photochemical [2 + 2] reactions between two alkenes in solid state in 1971. Their work showed that the α- and β-polymorphic structures of *trans*-cinnamic acid could be transformed into α-truxillic acid and β-truxinic acid products, respectively, by photochemical [2 + 2] reaction in solid state.[23] Moreover, with a thorough analysis, they discovered that (1) the two alkenes must be positioned one on top of each other; (2) the two alkenes must be aligned parallel to each other, and (3) the distance between alkene centers must be between 3.5-4.2 Å in order to enter the photochemical reaction [2 + 2] in solid state. These are referred to as 'Schmidt criteria' in the literature, and are extremely valuable for design of new photochemical [2 + 2] reactions in solid state.

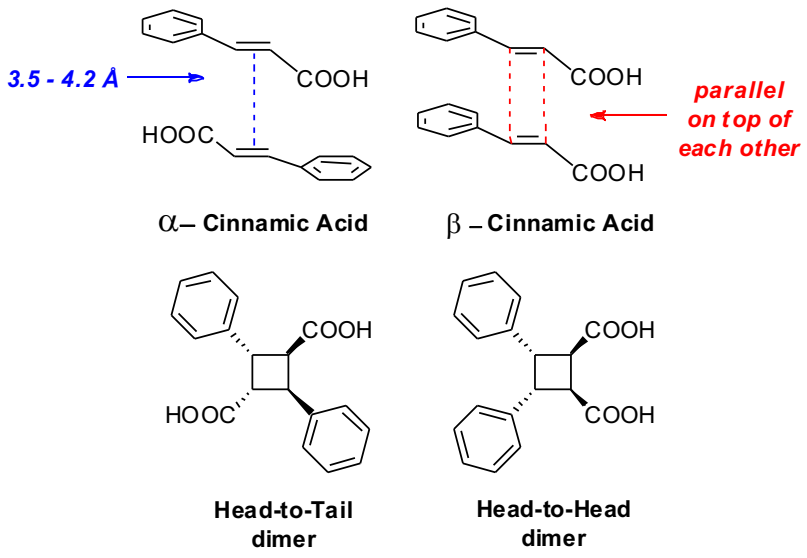

Figure 6. Dimerization of *trans*-cinnamic acid and the Schmidt criteria.

However, a very small number of molecules crystallize in this manner, and this situation makes photochemical [2 + 2] reaction in solid state quite challenging. In order to overcome these difficulties, template molecules are used to direct photochemical [2+2] cycloadditions in the solid state in which, the *chemo*-, *regio*- and *stereoselectivity* for such reactions could be achieved. In their pioneering work, the MacGillivray research group has been studying since 2000 template-directed photochemical [2 + 2] homodimerization reactions of alkenes containing pyridine and carboxylic acid units using a variety of interactions such as hydrogen bonding and metal coordination.[24] For instance, the photochemical homodimerization of 1,2-di(4-pyridyl)ethylene complexed with resorcinol as template in the solid state afforded very efficiently the symmetrical [2 + 2] homodimerization product (Scheme 25a).[24] In another study by MacGillivray and co-workers reported in 2008, a bis-pyridine-containing molecule was identified as a highly effective hydrogen bonding template for the photochemical homodimerization of fumaric acid (Scheme 25b).[25] Additionally, Resnati and Metrangolo groups published a groundbreaking study related to utilization of halogen bonds for the first time in such template molecules in 2004 for the homodimerization of 1,2-di(4-pyridyl)ethylene (Scheme 25c).[26]

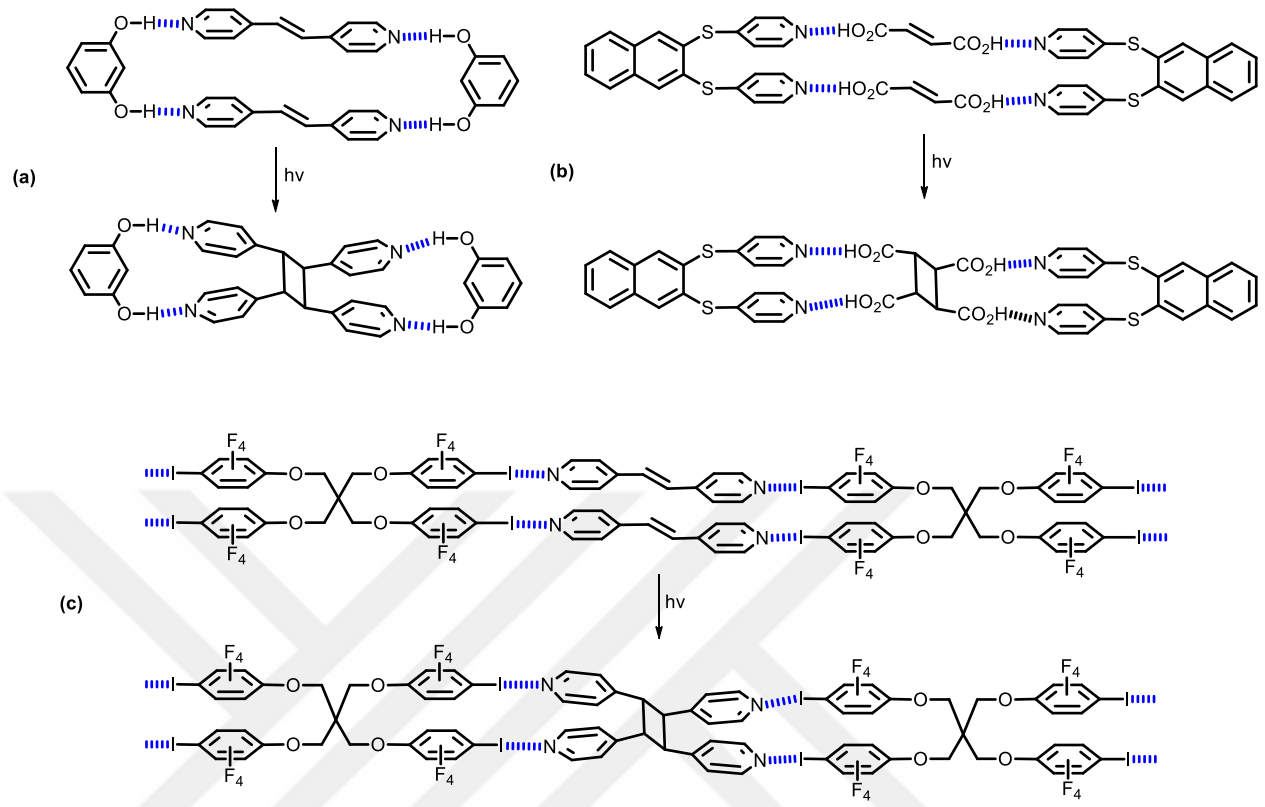

Scheme 25. Advances on photochemical [2+2] reaction.

Another study belongs to Wolf group used a template molecule containing two pyridines in the photochemical homodimerization of fumaric acid (Scheme 26).[27] Although the reaction works efficiently with 99>%, synthesizing template molecule in 2 steps and achieving only homodimerization of related acids stands for disadvantageous situation for this study.

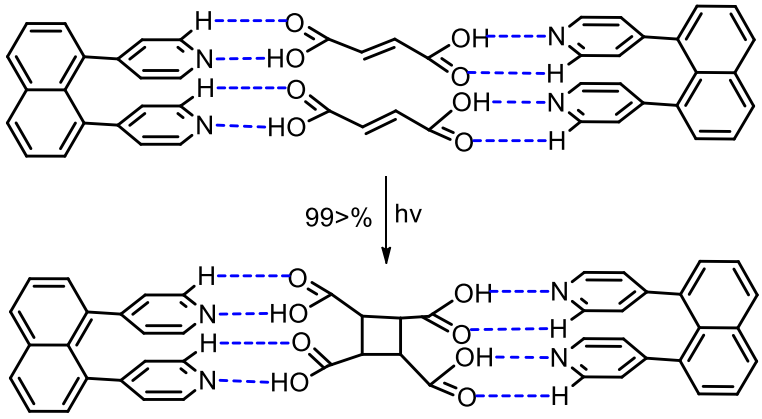

Scheme 26. Template- directed photodimerization of fumeric acid.

When all these studies are taken into consideration, recently, photochemical [2 + 2] cycloaddition reactions have been investigated with different approaches using template molecules. However, it is seen that all these reactions in the literature are homodimerization reactions, meaning that the same two alkene molecules participate in these photochemical dimerization reactions. In this way, only symmetrical cyclobutane rings could be afforded, which results in restricted number of products and limited diversity among the products due to their symmetry. In the studies mentioned above, template molecules allow only one type of interaction, preventing the selective interaction of two different alkenes with the template molecule. These circumstances pose a problem in synthetic organic chemistry field, since natural products with a cyclobutane ring that demonstrate biological activity possess unsymmetrical cyclobutane scaffolds (Figure 7).[28-31] Therefore, new methods are required to be developed to make possible the synthesis of such natural products containing biologically active cyclobutane as well as other unnatural compounds that have the potential to be used as pharmaceuticals.

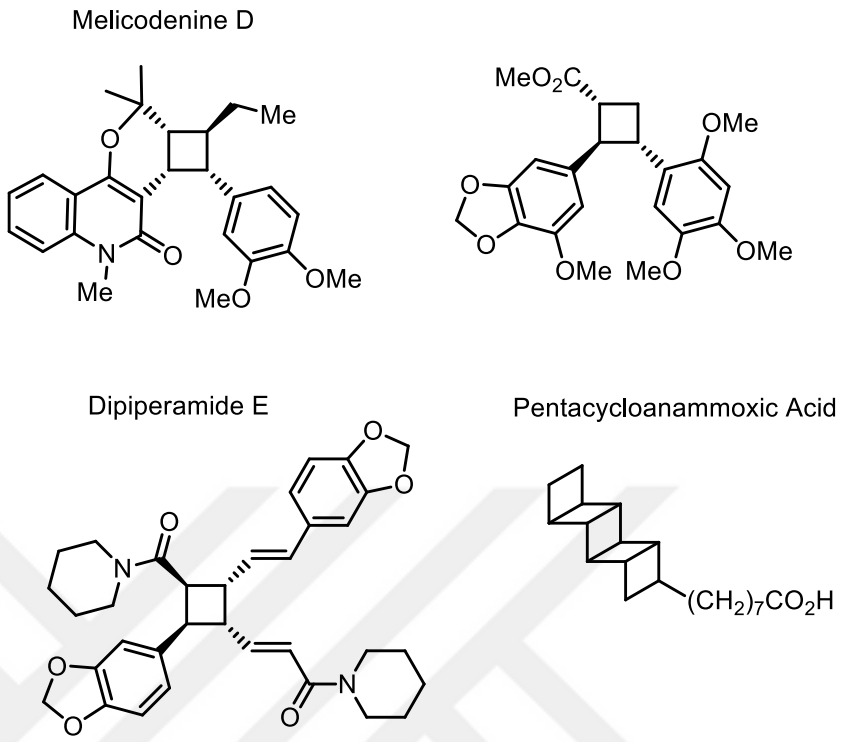

Figure 7. Examples of natural products containing cyclobutane ring.

2.1.3. Aim of This Project

Considering the contents of the studies about development of photochemical [2+2] reaction along with their drawbacks, we proposed a novel reaction pathway for the selective synthesis of cyclobutanes using a template molecule. This template-directed reaction pathway was intended to provide unsymmetrical cyclobutene products as the ultimate goal of this thesis work. For this purpose, 1,8-dihydronaphthalene (DHN) will be utilized as a template molecule. The design of this newly developed reaction pathway includes three consecutive steps: firstly, *trans*-cinnamic acid derivatives will be used to form 1,8-diester compounds **(A)** by using DCC as a coupling reagent and DMAP as a catalyst. In the second step, 1,8-diester compounds will be irradiated with 400 W medium-pressure Hg lamp to afford cyclobutane compounds **(B)** in solid state. Finally, hydrolysis of cyclobutane derivatives under basic conditions will provide the final truxinic acid products **(C),** and the

template of the reaction will be recovered as well. The template molecule, 1,8-DHN, will help to align two alkene molecules in an appropriate geometry so that the conditions proposed in Schmidt's work [27] to observe cyclobutane ring formation will be fulfilled. In this design, we aimed to obtain symmetrical truxinic acid derivatives.

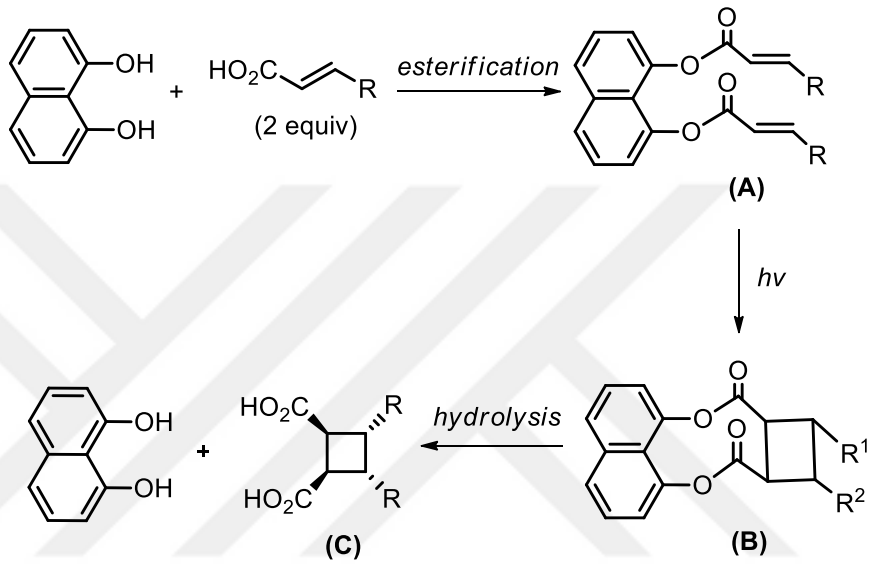

Scheme 27. Proposed synthetic pathway for the synthesis of symmetrical truxinic acids**.**

Our strategy towards the selective heterodimerization reactions of cinnamic acids is described below in Scheme 28. In this design, 1,8-DHN template will initially be transformed to mono-ester **48** by using one equivalent of acyl chloride **47**. The synthesis of unsymmetrical 1,8-diester compound **49** will be achieved using *trans*- 4-trifluoromethyl-cinnamic acid with DCC and DMAP as well. Subsequently, irradiation of asymmetric 1,8- diester compound **49** will provide cyclobutane **53**, which will undergo hydrolysis reaction under basic conditions to achieve asymmetric truxinic acid **56**.

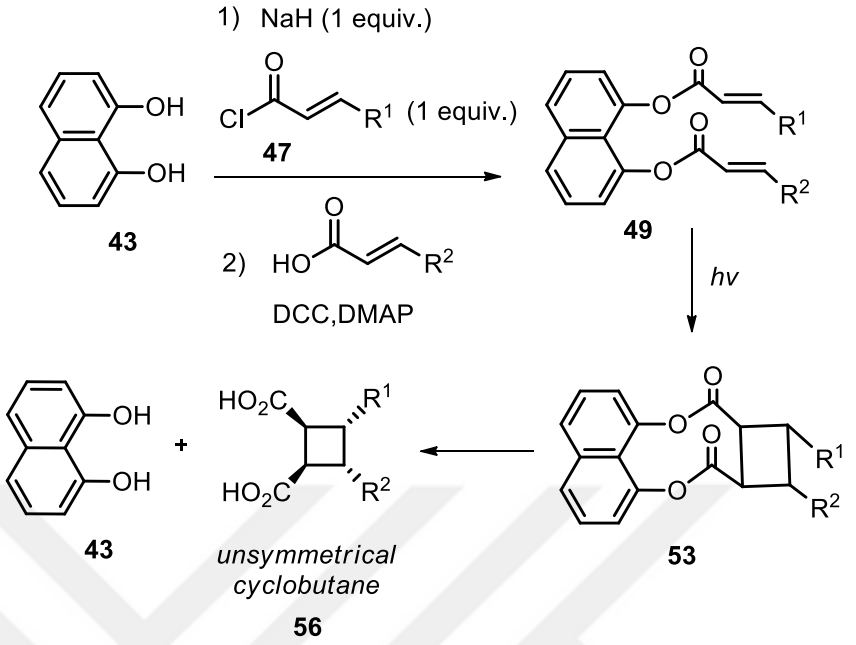

Scheme 28. Proposed synthetic pathway for the synthesis of asymmetric truxinic acids.

2.2. RESULTS AND DISCUSSION

2.2.1. Synthesis of Symmetrical 1,8-Diester Compounds

The synthesis of symmetrical 1,8-diester compounds was achieved through Steglich esterification reaction by utilizing 2 equivalents of corresponding trans-cinnamic acid derivatives and 1,8-dihydronaphthalene (1,8-DHN) in the presence of dicyclohexylcarbodiimide (DCC) as a coupling reagent and *N*,*N*-dimethylaminopyridine (DMAP) as catalyst. Purification of 1,8 -diester compounds was carried out by flash column chromatography and each compound was characterized by ^{1}H-NMR and ^{13}C-NMR spectroscopy, ATR-IR spectroscopy and HRMS.

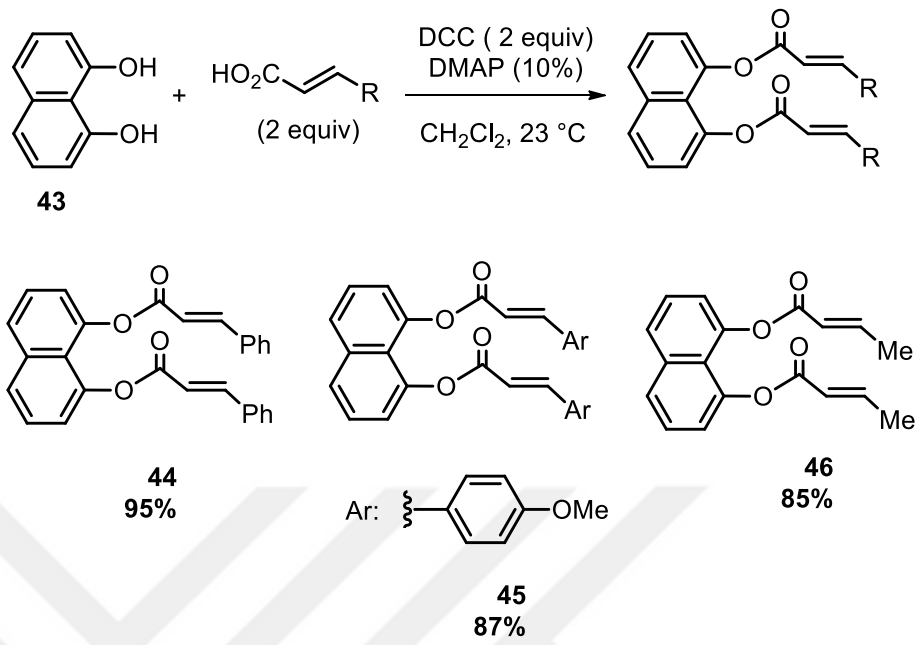

Scheme 29. Synthesis of 1,8- diester compounds using **43** and trans- cinnamic acid derivatives.

Esterification reaction of between 1,8-DHN **43** and unsubstituted *trans*-cinnamic acid afforded the 1,8-diester **44** in 95% yield (Scheme 29). The same reaction between **43** and *trans*-4-methoxycinnamic acid provided 1,8-diester **45** in 87% yield. Finally, when crotonic acid was used as the carboxylic acid component in the esterification reaction, 1,8-diester **43** was obtained in 85% yield. It should be stated that Steglich esterification reaction is quite efficient for the synthesis of these 1,8- diester compounds with high yields under mild reaction conditions.

In order to gain insight on the geometrical orientations of the two alkenes present in diester **44** with respect to one another, we opted to analyze its solid state structure by single-crystal X-ray crystallography. Single crystals of diester **44** were obtained by the vapor-diffusion crystallization technique using a CH_2Cl_2 and pentane as the components of the solvent system, and the structure was solved by Dr. Yunus Zorlu at Gebze Technical

University. Excitingly, in the X-ray structure of diester **44**, the alkenes are oriented perfectly parallel to each other, and the distance between the two alkene centers is 3.63 Å, which is in perfect agreement with the Schmidt criteria (Figure 8).[23] This crystallographic analysis demonstrated clearly that 1,8-DHN is an excellent template molecule for such photochemical reactions from a geometrical perspective.

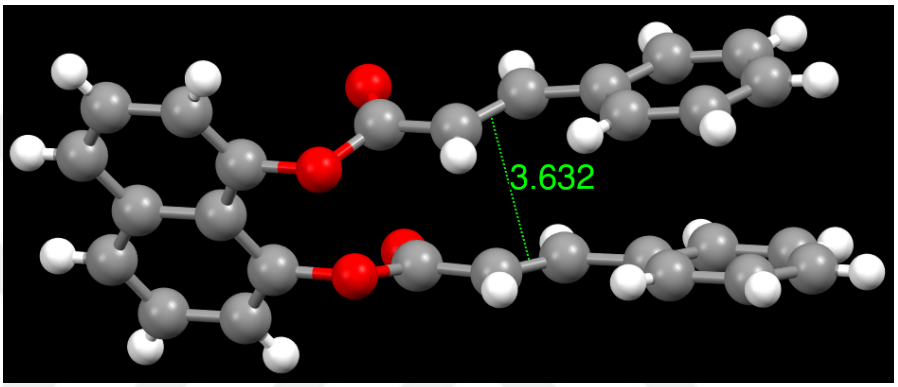

Figure 8. X-ray structure of diester **44**.

2.2.2. Synthesis of Unsymmetrical 1,8-Diester Compound

In order to synthesize an unsymmetrical 1,8-diester compound, a different reaction procedure was followed rather than Steglich esterification reaction. This is because mono-esterification with this procedure was not efficient even when one equivalent of the carboxylic acid was used, and the formation of a mixture of mono- and di-esterification prodcuts was observed. Therefore, a different approach was undertaken. First, the carboxylic acid group of *trans*-cinnamic acid was converted to acyl chloride **47** via chlorination reaction by using oxalyl chloride (Scheme 30a). In the second step, the esterification reaction between 1,8- DHN **43** and one equivalent of acyl chloride **47** provided monoester **48** in 82% yield (Scheme 30b). This product was analyzed by both ^{1}H-NMR and ^{13}C-NMR spectroscopy.

Additionally, phenol peak 3388 at cm^{-1} and a carbonyl peak at 1704 cm^{-1} in FTIR-ATR spectrum of **48** provided an additional support for the presence of monoester **48**.

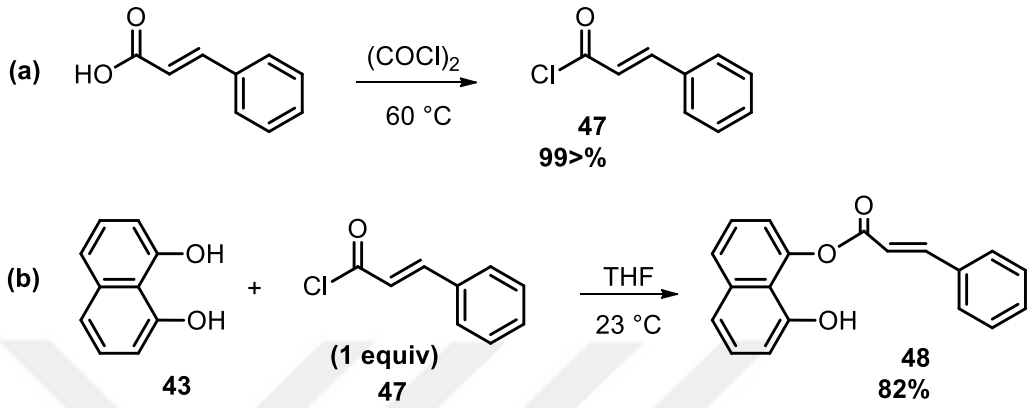

Scheme 30. Synthesis of monoester 48 using acyl chloride **47**.

Later, monoester **48** provided an important scaffold for the synthesis of unsymmetrical 1,8-diester **49** via a subsequent Steglich esterification. For this purpose, monoester **48** was reacted with *trans*- 4-(trifluoromethyl)cinnamic acid in the presence of DCC and catalytic amount of DMAP at 23 °C to afford unsymmetrical 1,8-diester **49** in 71% yield.

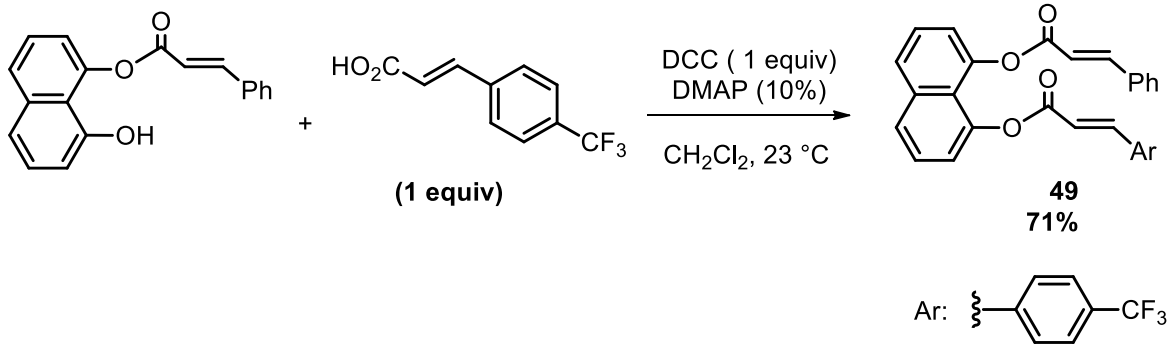

Scheme 31. Synthesis of unsymmetrical 1,8-diester **49**.

2.2.3. Investigation of the Photochemical [2+2] Homo- and Heterodimerization Reactions

The synthesis of cyclobutane products was examined starting from the 1,8-diester compounds through photochemical [2+2] cycloaddition reactions. As a general procedure, 1,8-diester compound was ground and placed homogeneously between microscopic slides, and placed vertically in front of UV-light source. For these reactions, we utilized 400 W broadband medium-pressure Hg lamp as UV-light source, which is enclosed with a safety cabinet to prevent any UV-light leakage to the surroundings.

In order to test the efficiency of our UV-light source, initially, *trans*-cinnamic acid was irradiated for four hours continuously as a control experiment. After 4 hours, the resulting reaction powder was directly analyzed with ^{1}H-NMR to check the formation of α-truxillic acid **54**. ^{1}H-NMR spectroscopic analysis indicated full conversion to α-truxillic acid, which indicated that our UV set-up operated successfully.

The first trial of photochemical [2+2] cycloaddition reaction started with 1,8-diester **44** in order to optimize the irradiation time for the full conversion of 1,8-diester **44** to cyclobutane **50**.

Table 6. Optimization studies for the synthesis of cyclobutane **50**.

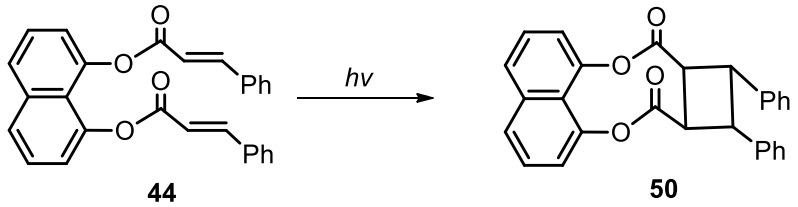

44 **50**

Entry	Irradiation Time (h)	Conversion to Product (%)[a]	Yield (%)
1	2	17	ND
4	8	44	ND
5	8	>99	95
3	4	>99	92
2	2	90	ND

[a] Determined by ^{1}H-NMR analysis of the crude reaction mixture.

Initially, 1,8-diester **44** was treated for 2 h continuously, and the cyclobutane product **50** was determined to form with only 17% conversion (Table 6, entry 1). When the same reaction was performed with 8 h of continuous irradiation, 44% conversion to product was observed as determined by ^{1}H-NMR analysis (entry 4). From these results, we assumed that diester reactant molecules at the surface could be irradiated successfully, however, the intermediate layers of solid reaction powder stayed unreacted (Figure 9, (1)). Therefore, we decided to mix reaction powder with a clean spatula every 2 hours of irradiation so that unreacted 1,8-diester molecules could move upper layers to ensure homogenous reaction powder between the slides (Figure 9, (2)).

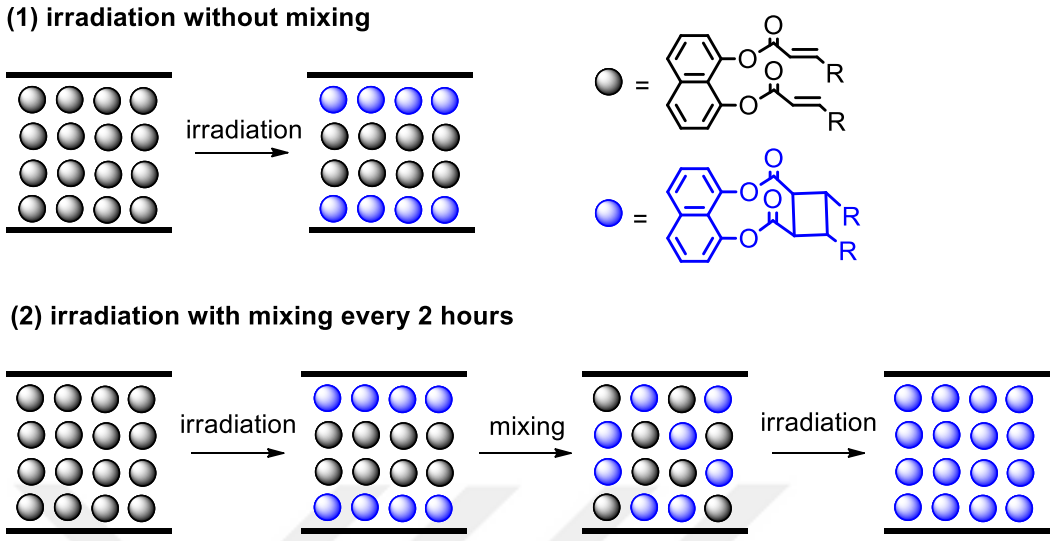

Figure 9. Illustration of mixing process and impact on reaction medium.

After this decision, 1,8-diester **44** was treated with UV-light source for 8 h, and every 2 h, reaction powder was mixed with a spatula. This technique proved to be very beneficial, and full conversion to cyclobutane **50** was achieved in this experiment (Table 6, entry 5). This method worked efficiently for 4 h of irradiation as well (entry 3). Finally, we repeated the irradiation reaction for 2 h with mixing only once at the end of the first hour in order to decrease reaction time. However, this treatment ended with 90% conversion to cyclobutane **50** (entry 2). In order to visualize this process, stacked ^{1}H-NMR spectra of the crude mixtures of each trial is shown in Figure 10. It should be emphasized here that mixing the reaction powder every 2 hours of irradiation process is essential to observe high or full conversion to the desired product. Moreover, ^{1}H-NMR spectroscopic analysis indicated no side product or by-product formation during the reaction photochemical reactions.

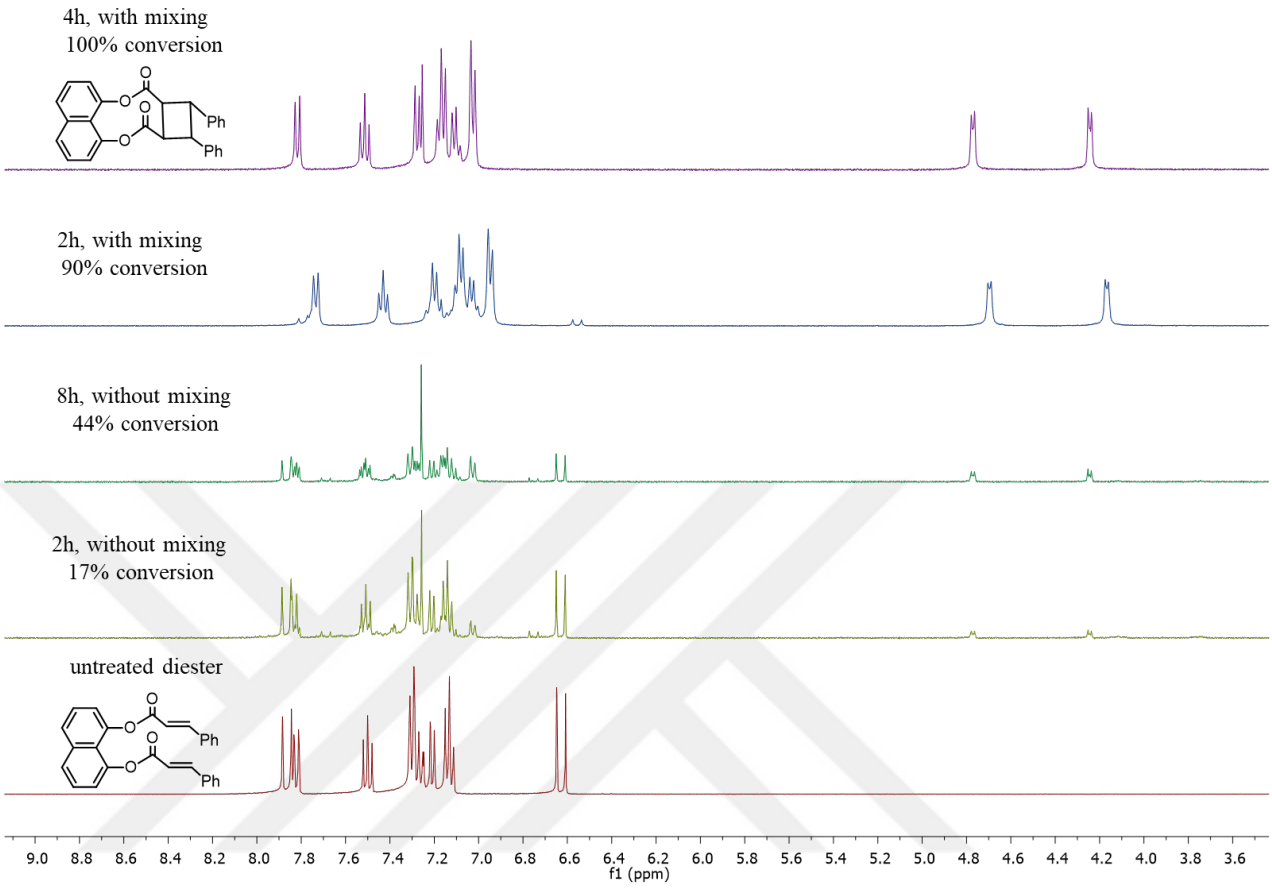

Figure 10. Stacked 1H-NMR spectra of cyclobutane **50** with different irradiation times.

Unequivocal structural characterization of the photochemical [2 + 2] cycloaddition product **50** was achieved by single-crystal X-ray diffraction analysis. The X-ray structure of the product did not only confirm the cyclobutane formation, but also provided the stereochemical assignment for the relative configurations of the stereocenters of the cyclobutane ring (Figure 11).

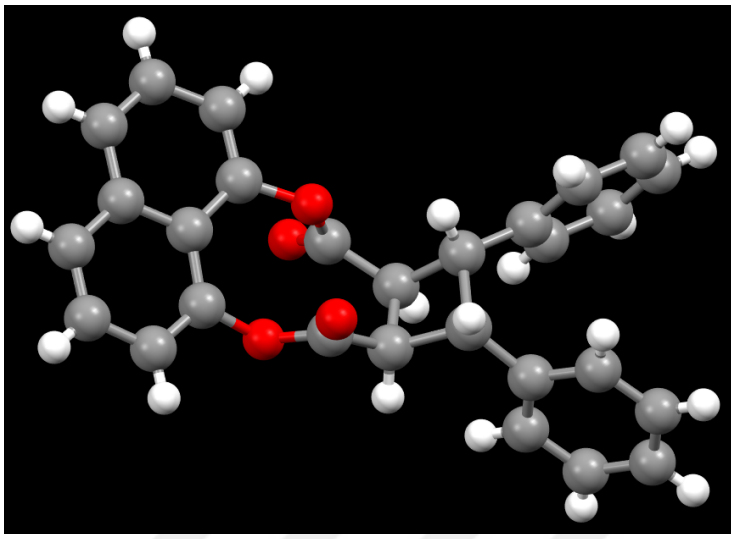

Figure 11. X-ray structure of cyclobutane **50**.

Afterwards, the photochemical [2+2] cycloaddition reactions were performed for other 1,8-diester compounds following the same procedure with mixing the reaction powder every 2 hours as listed in Table 7.

Table 7. Irradiation reaction conditions and results of 1,8- diester compounds.

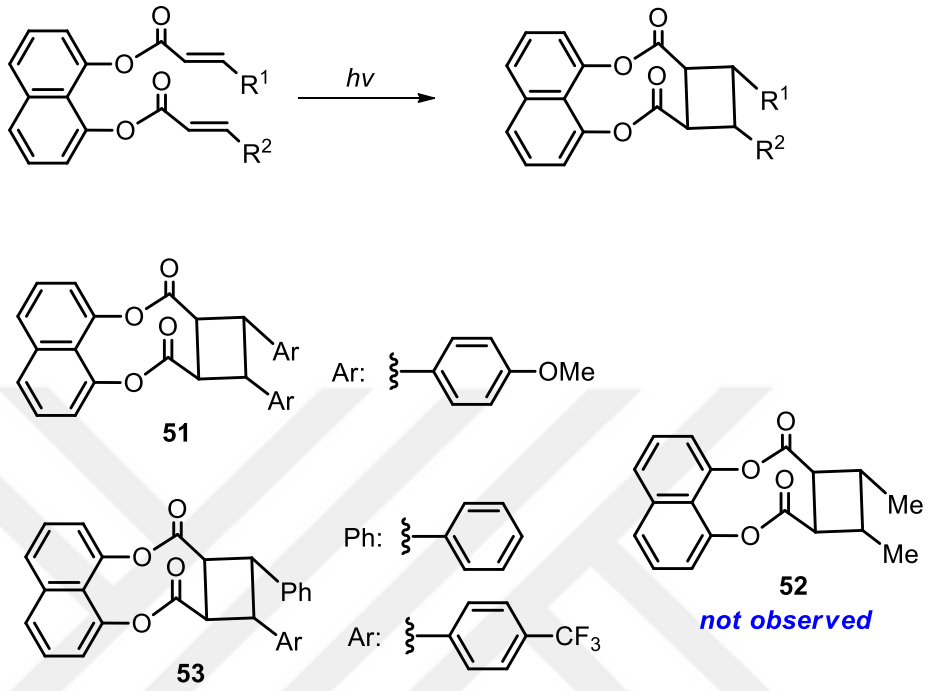

Entry[a]	1,8-Diester Reactant	Irradiation Time (h)	Conversion to Product (%)[b]	Yield (%)[c]
1	**51**	4	33	ND
2	**51**	8	67	ND
3	**51**	12	>99	78
4	**53**	6	95	88
5	**53**	8	>99	ND
6	**52**	6	0	ND

[a]25 mg of DHN diester compounds used. [b]Crude H-NMR analysis. [c]Isolated yields. ND: not determined.

The synthesis of symmetrical cyclobutane **51** having 4-methoxyphenyl substituents was tested in three different experiments. In the first trial, we observed only 33% conversion

to product at the end of 4 h of irradiation (Table 7, entry 1). When the same reaction was performed in a second experiment with an irradiation time of 8 h, the conversion doubled and increased to 67% (Table 7, entry 2). After this observation, the reaction powder was treated with UV-light for an additional four hours and full conversion to cyclobutane **51** was achieved at the end of 12 h of irradiation (entry 3). Afterwards, the synthesis of the unsymmetrical cyclobutane **53** was attempted twice starting from the unsymmetrical 1,8-diester **49**. When diester **49** was irradiated for 6 hours, 95% conversion to product was observed (entry 4). ^{1}H-NMR analysis of the crude reaction mixture showed that only 5% of starting diester was left as an unreacted starting compound, therefore the product was isolated by flash column chromatography in 88% yield. In order to achieve full conversion to unsymmetrical cyclobutane **56**, we extended the irradiation time to 8 h. Although this trial resulted in almost full conversion of product, around 5% of side product signals were determined in crude ^{1}H-NMR analysis. In addition to these, the cycloaddition reaction for 1,8-diester **46**, which was derived from crotonic acid, could not be observed at all after 4 hours of irradiation. ^{1}H-NMR spectroscopic analysis indicated that the reactant diester **46** remained intact at the end of the reaction with no indication of the formation of the [2+2] cycloaddition product (entry 6).

In addition to these studies, two control experiments were performed under thermal conditions in order to prove that [2+2] cycloaddition reactions only work under photochemical activation with a UV-light source. To this end, the first control experiment was carried out in solution, in which 1,8-diester **44** was heated in toluene at 90 °C for 6 h (Scheme 32a). After directly evaporating toluene, ^{1}H-NMR analysis of the crude mixture expectedly indicated that 1,8-diester **44** remained completely unreacted. Furthermore, solid state reaction of 1,8-diester **44** in the absence of any solvent allowed to take place at 90 °C

as a second control experiment. This time, 1,8-diester **44** was placed between microscope slides and placed onto 90 °C ceramic heater (Scheme 32b). After 6 h, the reaction powder was analyzed with ^{1}H-NMR spectroscopy, and no cyclobutane product formation was observed. These control experiments demonstrated proof of principle for the [2+2] cycloaddition reactions in this study works only under photochemical conditions.

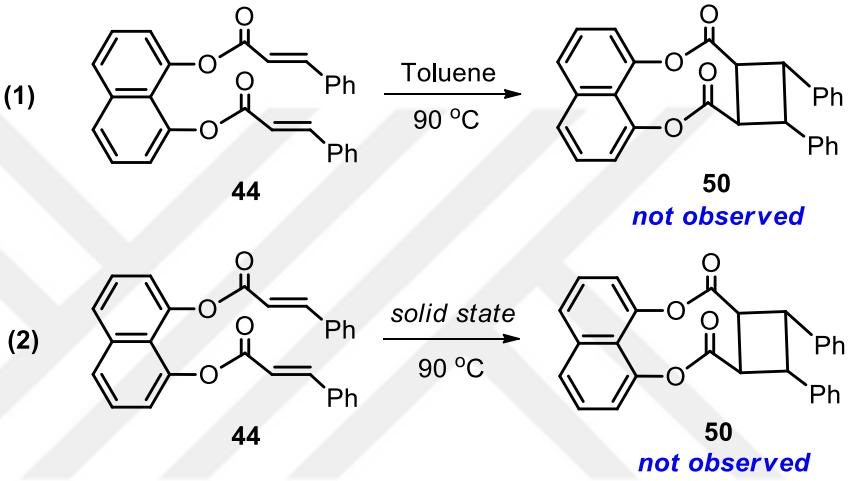

Scheme 32. Control experiments of 1,8-diester **44** under thermal conditions.

2.2.4. Hydrolysis of Photochemical [2+2] Reaction Products

In the last part of this study, the synthesis of truxinic acid compounds was investigated through the hydrolysis of the ester groups in [2+2] reaction products. The hydrolysis of ester groups in these cyclobutane compounds is simple yet a convenient way to obtain truxinic acid products as carboxylic acid derivatives. In addition, even though 1,8-DHN **43** is commercially available and inexpensive, its recovery at the end of the reaction is still highly valuable. It should be indicated here that reusability of such chemicals has also a great contribution to green chemistry field in terms of reducing the amount of waste chemicals.

Hydrolysis reaction of cyclobutene products was conducted under basic conditions using KOH as a base, and acidic work-up followed by purification by flash column chromatograph afforded truxinic acid compounds, which were analyzed by ^{1}H-NMR and ^{13}C-NMR spectroscopy.

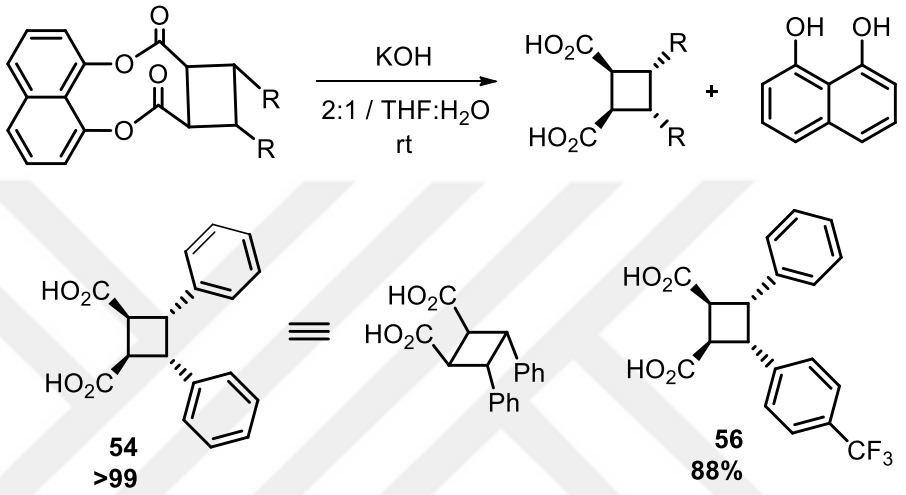

Scheme 33: Hydrolysis reaction conditions and results of cyclobutane compounds.

Firstly, the hydrolysis reaction of cyclobutane **50** was investigated, and the progress of the reaction was monitored by TLC analysis until complete consumption of cyclobutane **50** was observed. Additionally, ^{1}H-NMR analysis of the crude reaction mixture showed the presence of only truxinic acid **54** and free 1,8-DHN template without any side product. After this observation, truxinic acid **54** and 1,8- DHN **43** were isolated by flash column chromatography in >99% yield for both compounds. The same procedure was applied to cyclobutane **53** as well, and the truxinic acid product **56** were purified in 88% yield. Although synthesis of symmetrical truxinic acid derivatives is known in the literature, isolation of truxinic acid **56**, to the best of our knowledge, is the first example of a template-directed, photochemical heterodimerization reaction targeting the synthesis of an unsymmetrical truxinic acid derivative.

2.3. CONCLUSION

This part of the thesis demonstrated a groundbreaking work on development of development of template- directed photochemical [2+2] reaction. For this particular reaction, considering the contents of the studies up to this date, we proposed a novel reaction pathway for the selective synthesis of cyclobutanes using a template molecule. Moreover, template-directed reaction pathway provided unsymmetrical cyclobutene products as the ultimate goal of this thesis work. With this intention, 1,8-dihydronaphthalene (DHN) was utilized as a template molecule. Template molecule was modified successfully with *trans*-cinnamic acid derivatives by esterification reaction under mild conditions. The wise chocice of template molecule ensured that *trans*-cinnamic acid derivatives aligned in an appropriate geometry to undergo photochemical [2+2] reaction to afford cyclobutane compounds with high yields, which finally provided symmetrical and unsymmetrical truxinic acid derivatives for the first time.

The developed reaction has also remarkable contribution to green chemistry field due to its elegant design in terms of the use of chemicals and atom-economic purposes. It should be emphasized that template molecule was a cheap molecule and fully recovered at the end of the synthesis of truxinic acid derivatives. In addition to this, irradiation reactions were carried out in solid state without using any solvent and even thought reactions were operated with small scales of reactants, high yields % were achieved successfully without any formation of side-products. This thesis work demonstrated an illuminating discussion about the development of a novel and photochemical [2+2] cycloaddiaition reaction using a reusable template.

3. EXPERIMENTAL PART

3.1. Materials and Methods

In order to obtain all compounds, reactions were monitored by thin-layer chromatography (TLC) using aluminum-backed plates pre-coated with silica gel (Merck, Silica Gel 60 F_{254}), and the spots were visualized with 254 nm UV light. For TLC visualization of non-UV active compounds, $KMnO_4$ and PMA (phosphomolybdic acid) staining solutions were used. Flash column chromatography purifications were performed by using Silicycle 40-63 μm (230-400 mesh) flash silica gel. All reactions performed using oven- or flame-dried glassware under an inert atmosphere of nitrogen. All chemicals for the experiments supplied from Acros Organics, Merck, TCI, Sigma-Aldrich, Alfa Aesar, and Carlo Erba, and they used without further purification. CH_2Cl_2, MeCN, pentane, DME, DMF, MeOH, EtOH were obtained from Sigma Aldrich. Other solvents used in synthesis and column chromatography were technical grade; they were purified by distillation and, dried with using drying agents. NMR spectra were obtained from a Bruker spectrometer at 400 MHz for ^{1}H-NMR spectra, 100 MHz for ^{13}C-NMR spectra and, 376 MHz for ^{19}F NMR calibrated from internal standard (TMS, 0 ppm) or residual solvent signals (chloroform at 7.26 ppm, DMSO at 2.50 ppm) for ^{1}H spectra and, (chloroform at 77.16 ppm, DMSO at 39.52 ppm) for ^{13}C spectra and, (trifluoroacetic acid at -76.55 ppm) for ^{19}F NMR. ^{1}H-NMR data are reported as follows: chemical shift (parts per million, ppm), integration, multiplicit (s = singlet, d = doublet, t = triplet, q= quarted, dd = doublet of doublets, ddd = doublet of doublet of doublets, m = multiplet, br = broad, app = apparent), coupling constant (Hz). Infrared (FTIR) spectra were recorded on a Bruker Alpha-Platinum-ATR spectrometer with only selected peaks reported. Mass spectral analyses were performed on Agilent Technologies 6224 TOF LC/MS at UNAM-National Nanotechnology Research Center and Institute of Materials Science and Nanotechnology, Bilkent University,

and East Anatolia High Technology Application and Research Center, Atatürk University. Broadband medium pressure Hg lamp is known to produce UV-light predominantly at 365 nm along with irradiation at certain wavelengths between 254-440 nm.

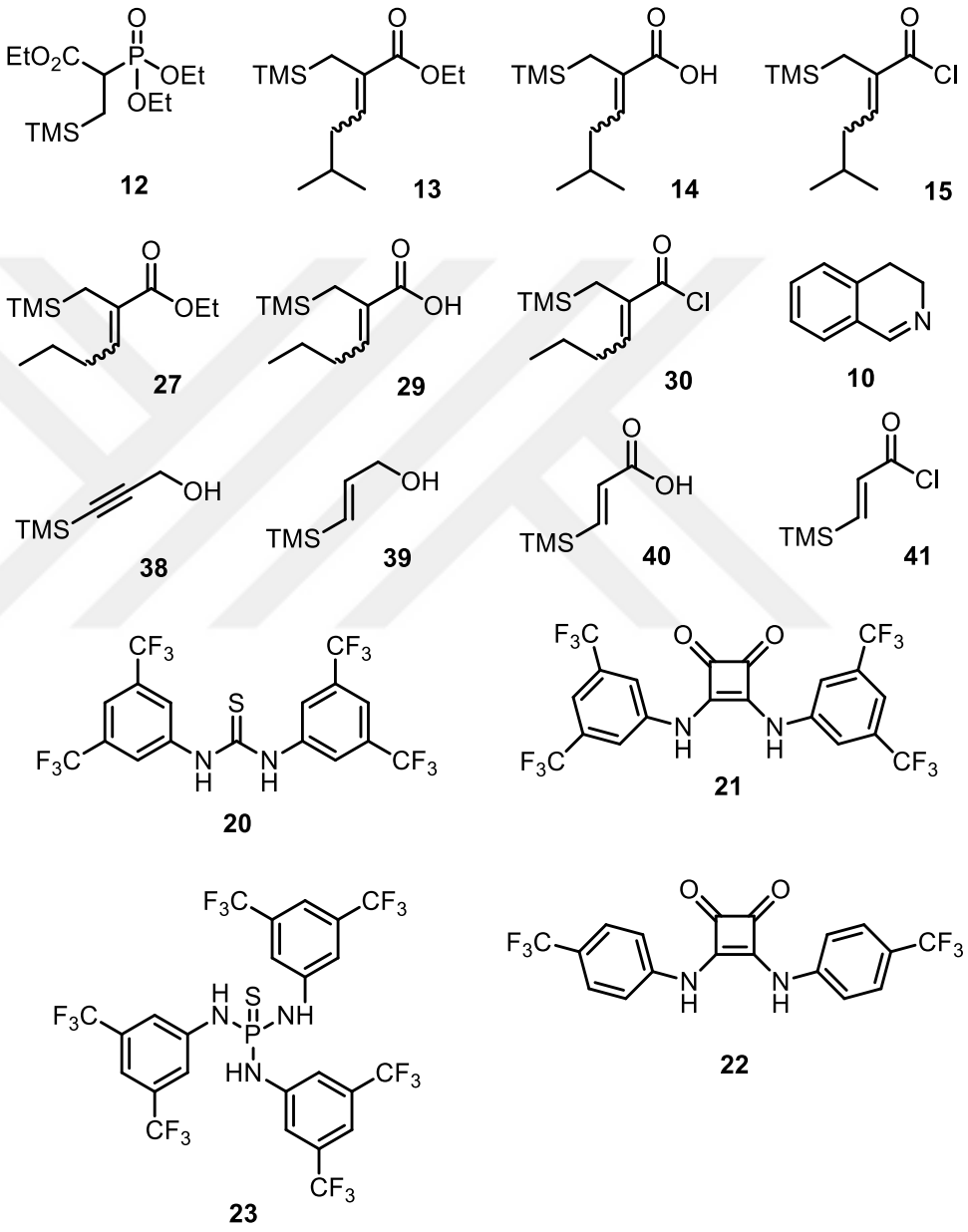

The previously known compounds **12, 13, 14,15 ,27, 29, 30, 10, 41**[13], **38**[32], **39**[33], **40**[34], **20**[16], **23**[18], **21, 22**[17] were prepared based on the literature procedures.

3.2. Reaction Procedures of Chapter 1

3.2.1. Compound 13a

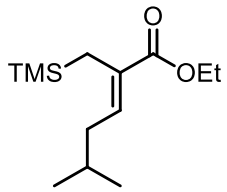

Purification of **13a** by flash column chromatography (10:1, hexanes: CF_3-Toluene) provided **13a** as a pure (*Z)* -isomer of **13**.

$\boldsymbol{R_f}$ = 0.68 (10:1, hexanes: $PhCF_3$)

TLC Visualization: UV active; stains with $KMnO_4$ solution.

^{1}H NMR (400 MHz; $CDCl_3$) δ: 6.62 (1H, t, *J* = 7.3 Hz), 4.15 (2H, q, *J* = 7.2 Hz), 1.96 (2H, t, *J* = 7.1 Hz), 1.78 (2H, s), 1.70 (1H, sept, *J* = 6.7 Hz), 1.27 (3H, t, *J* = 7.1 Hz), 0.91 (6H, d, *J* = 6.7 Hz), -0.02 (9H, s).

^{13}C NMR (100 MHz; $CDCl_3$) δ: 168.4, 137.5, 130.7, 60.4, 38.3, 28.5, 22.7, 17.4, 14.4, -0.9.

FTIR ν_{max} (ATR, film)/cm^{-1} 2956, 2902, 2872, 1710, 1636, 1465, 1368, 1330,1283.

3.2.2. Compound 13b

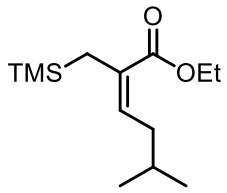

Purification of **13b** by flash column chromatography (10:1, hexanes: CF_3-Toluene) provided the **13b** as pure (*E)*-isomer of **13**.

R_f = 0.59 (10:1, hexanes: $PhCF_3$)

TLC Visualization: UV active; stains with $KMnO_4$ solution.

^{1}H NMR (400 MHz; $CDCl_3$) δ: 5.67 (1H, t, *J* = 7.6 Hz), 4.16 (2H, q, *J* = 7.2 Hz), 2.29 (2H, t, *J* = 7.2 Hz), 1.74 (2H, s), 1.66 (1H, sept, *J* = 6.7 Hz), 1.29 (3H, t, *J* = 7.1 Hz), 0.90 (6H, d, *J* = 6.7 Hz), -0.02 (9H, s).

^{13}C NMR (100 MHz; $CDCl_3$) δ: 168.7, 137.9, 130.1, 60.1, 38.7, 24.4, 22.6, 19.9, 14.4, 1.48.

FTIR ν_{max} (ATR, film)/cm^{-1} 2958, 2901, 2869, 1711, 1636, 1478, 1368, 1279.

3.2.3. Compound 14a

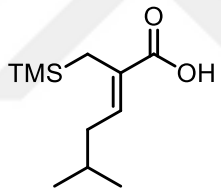

To a solution of **14a** (60 mg, 0.25 mmol) in 2:1 (v/v) EtOH/H_2O (2 mL), KOH (42.3 mg, 0.75 mmol) was added as solid at rt under N_2. The reaction mixture was placed in oil bath with a condenser to reflux at 85 °C for 24 h. Reaction was quenched with 1.0 M HCl (3 mL) and saturated NH_4Cl solution. The aqueous phase was extracted three times with CH_2Cl_2 (3×30 mL). The combined organic layers were dried over Na_2SO_4, filtered and concentrated under reduced pressure. The residue was purified by flash column chromatography (1:5, EtOAc: hexanes). Compound **14a** was obtained as pale orange solid (30 mg, 56% yield).

Note: 1.0 M HCl was directly added to the crude reaction mixture until pH came to 1-2. pH of the reaction medium was checked by pH paper by taking a small sample from the mixture.

R_f = 0.63 (1:5, EtOAc: hexanes)

TLC Visualization: UV active; stains with $KMnO_4$ solution.

^{1}H NMR (400 MHz; $CDCl_3$) δ: 6.81 (1H, t, *J* = 7.3 Hz), 2.02 (2H, t, *J* = 7.0 Hz), 1.80 (2H, s), 1.78-1.70 (1H, m), 0.94 (6H, d, *J* = 6.7 Hz), 0.02 (9H, s).

^{13}C NMR (100 MHz; $CDCl_3$) δ: 173.2, 140.5, 130.2, 38.5, 28.5, 22.7, 17.2, -0.8

FTIR ν_{max} (ATR, film)/cm^{-1} 2956, 2899, 2872, 1681, 1630, 1420, 1290, 1249.

3.2.4. Compound 14b

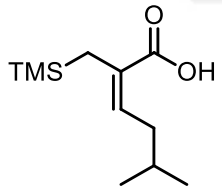

To a solution of **14b** (40 mg, 0.16 mmol) in 2:1 (v/v) EtOH/H_2O (2 mL), KOH (28.2 mg, 0.50 mmol) was added as solid at rt under N_2. The reaction mixture was placed in oil bath with a condenser to reflux at 85 °C for 48 h. Reaction was quenched with 1.0 M HCl (3 mL) and saturated NH_4Cl solution. The aqueous phase was extracted three times with CH_2Cl_2 (3×30 mL). The combined organic layers were dried over Na_2SO_4, filtered and concentrated under reduced pressure. The residue was purified by flash column chromatography (1:5, EtOAc: hexanes). Compound **14b** was obtained as pale orange oil (20 mg, 58% yield).

Note: 1.0 M HCl was directly added to the crude reaction mixture until pH came to 1-2. pH of the reaction medium is checked by pH paper by taking a small sample from the mixture.

R_f = 0.55 (1:5, EtOAc: hexanes)

TLC Visualization: UV active; stains with $KMnO_4$ solution.

^{1}H NMR (400 MHz; $CDCl_3$) δ: 5.86 (1H, t, *J* = 7.5 Hz), 2.40 (2H, t, *J* = 7.2 Hz), 1.77 (2H, s), 1.69 (1H, sept, *J* = 6.7 Hz), 0.93 (6H, d, *J* = 6.7 Hz), 0.01 (9H, s).

^{13}C NMR (100 MHz; $CDCl_3$) δ: 174.1, 141.8, 129.0, 38.9, 29.2, 24.1, 22.6, 1.49.

FTIR ν_{max} (ATR, film)/cm^{-1} 2956, 2898, 2872, 1686, 1625, 1425, 1248.

3.2.5. Compound 15a

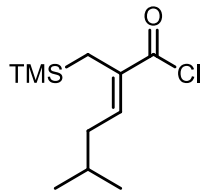

Oxalyl chloride (2 mL, 23.3 mmol) was directly added to **15a** (23.1 mg, 0.11 mmol) at rt under N_2. The reaction mixture was placed in oil bath at 60 °C, and stirred for 2 h. Then, excess amount of oxalyl chloride was carefully evaporated under reduced pressure by placing rotary evaporator inside well-ventilated fume hood. Compound **15a** was concentrated *in vacuo* as pale orange oil.

Note: 15a was prone to decomposition easily and highly volatile compound, therefore it was immediately used without further purification for the subsequent reaction.

^{1}H NMR (400 MHz; $CDCl_3$) δ: 7.12 (1H, t, *J* = 7.2 Hz), 2.10 (2H, t, *J* = 7.1 Hz), 1.84 (2H, s), 1.84-1.79 (1H, m), 0.97 (6H, d, *J* = 6.6 Hz), 0.07 (9H, s).

3.2.6. Compound 15b

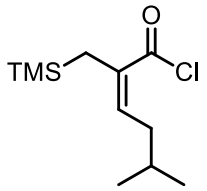

Oxalyl chloride (2 mL, 23.3 mmol) was directly added to **15b** (10.1 mg, 0.05 mmol) at rt under N_2. The reaction mixture was placed in oil bath at 60 °C, and stirred for 2 h. Then, excess amount of oxalyl chloride was carefully evaporated under reduced pressure by placing rotary evaporator inside well-ventilated fume hood. Compound **15b** was concentrated *in vacuo* as pale orange oil.

Note: 15b was prone to decomposition easily and highly volatile compound, therefore it was immediately used without further purification for the subsequent reaction.

^{1}H NMR (400 MHz; $CDCl_3$) δ: 5.74 (1H, t, *J* = 7.5 Hz), 2.21 (2H, t, *J* = 7.2 Hz), 1.93 (2H, s), 1.73-1.67 (1H, m), 0.92 (6H, d, *J* = 6.7 Hz), 0.00 (9H, s).

3.2.7. Compound 31

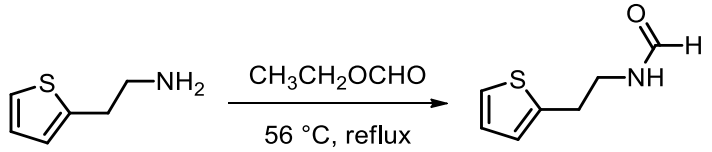

Ethyl formate (5 mL) was added directly to thiophene-2-ehylamine (200 mg, 1.57 mmol) at rt under N_2. The reaction mixture was placed in oil bath with a condenser to reflux at 56 °C. The product formation was followed by TLC analysis. After stirring the

reaction mixture for 24 h, ethyl formate was directly evaporated under reduced pressure. The residue was purified by flash column chromatography (EtOAc). Compound **31** was obtained as pale yellow oil (236 mg, 97% yield).

R_f = 0.43 (EtOAc)

TLC Visualization: UV active; stains with $KMnO_4$ solution.

^{1}H NMR (400 MHz; $CDCl_3$) δ: 8.11 (1H, s), 7.15 (1H, d, *J* = 5.1 Hz), 6.93 (1H, dd, *J* = 5.1, 3.6 Hz), 6.84 (1H, d, *J* = 2.4 Hz), 6.02 (1H, brs), 3.56 (2H, q, *J* = 6.5 Hz), 3.04 (2H, t, *J* = 6.7 Hz).

^{13}C NMR (100 MHz; $CDCl_3$) δ: 161.4, 141.0, 127.2, 125.6, 124.1, 39.5, 29.9.

FTIR ν_{max} (ATR, film)/cm^{-1} 3282, 3065, 2930, 2863, 1660, 1532, 1437, 1384, 1245.

HRMS (+ESI) Calcd for $C_7H_{10}NOS$ $[M+H]^+$ 156.0478, found: 156.0470.

3.2.8. Compound 32

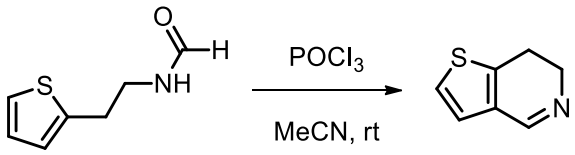

To a solution of **31** (434 mg, 2.78 mmol) in MeCN (2 mL), $POCl_3$ (417µL, 4.47 mmol) was added slowly at rt under N_2. The product formation was followed by TLC analysis. After stirring the reaction mixture for 24 h, reaction medium became green color, and MeCN was directly evaporated under reduced pressure. The residue was dissolved in water (3 mL) by heating a little bit to dissolve green residue completely, and saturated Na_2CO_3 solution was added slowly. H_2 gas leakage was observed during addition of saturated Na_2CO_3 solution, and the reaction medium became brown color.

The aqueous phase was extracted three times with CH_2Cl_2 (3×30 mL). The combined organic layers were dried over Na_2SO_4, filtered and concentrated under reduced pressure. The residue was purified by flash column chromatography (9:1, EtOAc: MeOH). Compound **32** is obtained as brownish solid (77 mg, 21% yield).

R_f = 0.23 (9:1, EtOAc: MeOH)

TLC Visualization: UV active; stains with $KMnO_4$ solution.

^{1}H NMR (400 MHz; $CDCl_3$) δ: 8.29 (1H, t, *J* = 2.1 Hz), 7.09 (1H, d, *J* = 5.1 Hz), 7.02 (1H, d, *J* = 5.1 Hz), 3.85-3.81 (2H, m), 2.89-2.85 (2H, m)

^{13}C NMR (100 MHz; $CDCl_3$) δ: 155.1, 142.6, 131.2, 124.7, 123.0, 47.9, 22.2.

FTIR ν_{max} (ATR, film)/cm^{-1} 3200, 3086, 2875, 2856, 1675, 1530, 1390, 1384, 1248.

HRMS (+ESI) Calcd for C_7H_8NS $[M+H]^+$ 138.0372, found: 138.0372.

3.2.9. Compound 20

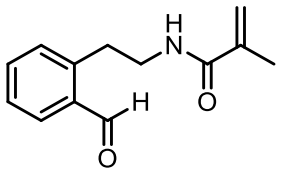

To a solution of **10** (200 mg, 1.53 mmol) in DCM (2 mL) and sat. $NaHCO_3$ solution (2 mL), methacrolyl chloride (186 µL, 1.91 mmol) in CH_2Cl_2 (2 mL) was added at rt under N_2. After stirring the reaction mixture for 1 h, reaction was quenched with 10% ammonia solution (10 mL) solution and brine (10 mL). The aqueous phase was extracted three times with EtOAc (3×30 mL). The combined organic layers were dried over Na_2SO_4, filtered and concentrated under reduced pressure. The residue was purified by flash column chromatography twice; first column, (1:1, EtOAc: hexanes,

Rf: 0.44) gave colorless oil, second column of this colorless oil, (2:1, toluene: acetone, ***Rf***: 0.56) provided compound **20** as white solid.

R_f = 0.56 (2:1, toluene: acetone)

TLC Visualization: UV active; stains with $KMnO_4$ solution.

^{1}H NMR (400 MHz; $CDCl_3$) δ: 10.16 (1H, s), 7.80 (1H, dd, *J* = 7.6, 1.4 Hz), 7.54 (1H, dt, *J* = 7.5, 1.5 Hz), 7.44 (1H, dt, *J* = 7.5, 1.2 Hz), 7.33 (1H, d, *J* = 7.5 Hz), 6.22 (1H, br s), 5.63-5.61 (1H, m), 5.29-5.27 (1H, m), 3.58 (2H, q, *J* = 6.9 Hz), 3.28 (2H, t, *J* = 6.9 Hz), 1.91 (3H, dd, *J* = 1.5, 0.9 Hz).

^{13}C NMR (100 MHz; $CDCl_3$) δ: 193.9, 168.6, 141.5, 140.1, 134.4, 134.3, 134.1, 132.1, 127.4, 119.6, 41.4, 32.4, 18.7.

FTIR ν_{max} (ATR, film)/cm^{-1} 3331, 2924, 2854, 1693, 1655, 1615, 1526, 1452, 1432.

HRMS (+ESI) Calcd for $C_{13}H_{16}NO_2$ $[M+H]^+$ 218.1176, found: 218.1191.

3.2.10. Compound 18

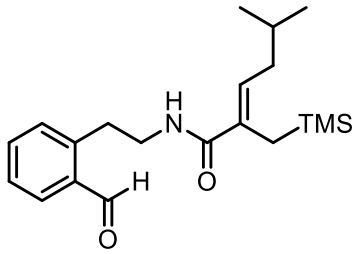

To a solution of **18** (59 mg, 0.45 mmol) in DCM (2 mL) and sat. $NaHCO_3$ solution (2 mL), acyl chloride **15** (130 mg, 0.56 mmol) in CH_2Cl_2 (2 mL) was added at rt under N_2. After stirring the reaction mixture for 1 h, the reaction was quenched with 10% ammonia solution (10 mL) solution and brine (10 mL). The aqueous phase was extracted three times with EtOAc (3×30 mL). The combined organic layers were dried

over Na_2SO_4, filtered and concentrated under reduced pressure. The residue was purified by flash column chromatography twice; first column, (1:2, EtOAc: hexanes, ***Rf***: 0.38) gave colorless oil, second column of this colorless oil, (9:1, toluene: acetone, ***Rf***: 0.40) provided compound **18** as white solid.

R_f = 0.40 (9:1, toluene: acetone)

TLC Visualization: UV active; stains with $KMnO_4$ solution.

^{1}H NMR (400 MHz; $CDCl_3$) δ: 10.18 (1H, s), 7.80 (1H, dd, *J* = 7.6, 1.5 Hz), 7.54 (1H, dt, *J* = 7.5, 1.5 Hz), 7.44 (1H, dt, *J* = 7.5, 1.3 Hz), 7.35 (1H, d, *J* = 7.5 Hz), 6.09 (1H, br s), 5.89 (1H, t, *J* = 7.0 Hz), 3.54 (2H, q, *J* = 7.1 Hz), 3.28 (2H, t, *J* = 7.1 Hz), 1.79 (1H, s), 1.73-1.63 (3H, m), 0.91 (6H, d, *J* = 6.7 Hz), -0.04 (9H, s).

Note: Multiplet signal between 1.73-1.63 ppm represents 1H, which originally supposed to give septet signal.

^{13}C NMR (100 MHz; $CDCl_3$) δ: 193.8, 170.6, 141.7, 140.1, 135.8, 134.5, 134.3, 134.1, 132.1, 129.6, 127.3, 41.4, 37.9, 32.6, 28.6, 22.7, 18.2, -0.9.

FTIR ν_{max} (ATR, film)/cm^{-1} 3339, 2954, 2897, 2870, 1695, 1650, 1615, 1525, 1428.

HRMS (+ESI) Calcd for $C_{20}H_{32}NO_2Si$ $[M+H]^+$ 346.2197, found: 346.2201.

3.3. General Procedure for Aza-Nazarov Products in Chapter 1

To a flame-dried Schlenk-flask (25 mL) imine reactant (1 mmol) **10** in freshly distilled anhydrous MeCN (0.5 mL), and the solution of acyl chloride **15** (for products **24** and **33**) or **30** (for product **33**) (1.33 mmol; *Z*:*E* = 3:1) in 0.5 mL anhydrous MeCN was added under nitrogen. The reaction mixture was allowed to mix for 5 minutes. After

addition of AgOTf (0.2 mmol) the reaction mixture was placed into preheated 80 °C oil bath and, stirred for 24 h. It was then quenched with saturated $NaHCO_3$ (3 mL) solution. The aqueous phase was extracted three times with EtOAc (3×20 mL). The combined organic layers were dried over Na_2SO_4, filtered and concentrated under reduced pressure. The residue was purified by flash column chromatography (1:1, EtOAc: hexanes).

3.3.1. Compound 24

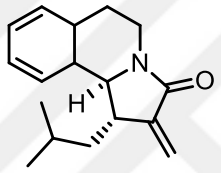

Following the general procedure, the synthesis of compound **24** was carried out using imine **10** (77 mg, 0.59 mmol) and acyl chloride **15** (178mg, 0.76 mmol) with AgOTf (30 mg, 0.12 mmol) in 1.0 mL anhydrous MeCN. Purification by column chromatography (1:1, EtOAc: hexanes) gave aza-Nazarov product as an orange oil (87 mg, 58% yield).

R_f = 0.61 (1:1, EtOAc: hexanes)

TLC Visualization: UV active; stains with $KMnO_4$ solution.

^{1}H NMR (400 MHz; $CDCl_3$) δ: 7.25-7.18 (3H, m), 7.12 (1H, d, *J* = 7.6 Hz), 6.03 (1H, d, *J* = 2.5 Hz), 5.31 (1H, d, *J* = 2.2 Hz), 4.42 (1H, d, *J* = 2.6 Hz), 4.34 (1H, ddd, *J* = 12.8, 6.3, 2.9 Hz), 3.23 (1H, ddd, *J* = 12.8, 10.7, 4.9 Hz), 3.08-3.00 (2H, m), 2.78-2.72 (1H, m), 1.95 (1H, sept, *J* = 6.7 Hz), 1.75 (1H, dt, *J* = 14.0, 7.0 Hz), 1.66 (1H, dt, *J* = 14.0, 7.2 Hz), 1.09 (3H, d, *J* = 6.5 Hz), 1.05 (3H, d, *J* = 6.6 Hz).

^{13}C NMR (100 MHz; $CDCl_3$) δ: 166.9, 144.7, 137.7, 134.5, 129.4, 127.3, 126.9, 124.6, 116.1, 61.3, 46.5, 42.2, 38.3, 28.3, 25.7, 23.1, 22.9

FTIR ν_{max} (ATR, film)/cm^{-1} 2955, 2927, 2871, 1685, 1656, 1457, 1420, 1302.

3.3.2. Compound 34

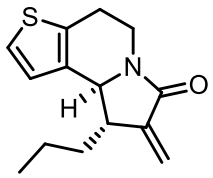

Following the general procedure, the synthesis of compound **34** was carried out using imine **32** (19 mg, 0.14 mmol) and acyl chloride **30** (39,4 mg, 0.18 mmol) with AgOTf (7.2 mg, 0.027 mmol) in 1.0 mL anhydrous MeCN. Purification by column chromatography (1:1, EtOAc: hexanes) gave aza-Nazarov product **34** as a colorless oil.

R_f = 0.49 (1:1, EtOAc: hexanes)

TLC Visualization: UV active; stains with $KMnO_4$ solution.

^{1}H NMR (400 MHz; $CDCl_3$) δ: 7.17 (1H, d, *J* = 5.2 Hz), 6.86 (1H, d, *J* = 5.3 Hz), 6.07 (1H, d, *J* = 2.9 Hz), 5.32 (1H, d, *J* = 2.5 Hz), 4.62-4.57 (1H, m), 4.42-4.40 (1H, m), 3.11 (1H, ddd, *J* = 12.7, 11.6, 4.8 Hz), 3.04-2.95 (1H, m), 2.85-2.80 (2H, m), 1.83-1.76 (2H, m), 1.62-1.53(2H, m), 1.04 (3H, t, *J* = 7.3 Hz).

^{13}C NMR (100 MHz; $CDCl_3$) δ: 167.0, 144.2, 139.7, 134.2, 136.6, 124.0, 123.8, 116.1, 59.7, 43.9, 42.1, 38.0, 37.2, 24.6, 20.1, 14.5.

FTIR ν_{max} (ATR, film)/cm^{-1} 2956, 2930, 2868, 1695, 1642, 1452, 1427, 1326.

HRMS (+ESI) Calcd for $C_{14}H_{18}NOS$ $[M+H]^+$ 248.1104, found: 248.1109.

3.3.3. Compound 33

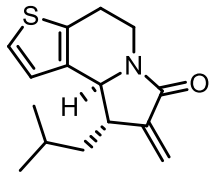

Following the general procedure, the synthesis of compound **33** was carried out using imine **32** (20 mg, 0.15 mmol) and acyl chloride **15** (44 mg, 0.19 mmol) with AgOTf (7.5 mg, 0.029 mmol) in 1 mL anhydrous MeCN. Purification by column chromatography (1:1, EtOAc: hexanes) provided aza-Nazarov product **33** as colorless oil . (15 mg, 40% yield)

R_f = 0.56 (1:1, EtOAc: hexanes)

TLC Visualization: UV active; stains with $KMnO_4$ solution.

^{1}H NMR (400 MHz; $CDCl_3$) δ: 7.17 (1H, d, *J* = 5.2 Hz), 6.84 (1H, d, *J* = 5.2 Hz), 6.05 (1H, d, *J* = 2.7 Hz), 5.32 (1H, d, *J* = 2.3 Hz), 4.61-4.56 (1H, m), 4.37-4.35 (1H, m), 3.11 (1H, ddd, *J* = 12.6, 11.6, 4.8 Hz), 3.04-2.95 (1H, m), 2.88-2.79 (2H, m), 1.92 (1H, sept, *J* = 6.6 Hz), 1.72-1.28 (3H, m), 1.08 (3H, d, *J* = 6.5 Hz), 1.03 (3H, d, *J* = 6.6 Hz).

^{13}C NMR (100 MHz; $CDCl_3$) δ: 167.1, 144.9, 135.9, 134.2, 124.1, 123.7, 116.3, 60.8, 45.6, 42.1, 38.1, 26.1, 24.6, 23.1, 22.9.

FTIR ν_{max} (ATR, film)/cm^{-1} 2954, 2924, 2868, 1694, 1657, 1452, 1420, 1326.

HRMS (+ESI) Calcd for $C_{15}H_{20}NOS$ $[M+H]^+$ 262.1261, found: 262.1259.

3.4. Reaction Procedures of Chapter 2

3.4.1. Compound 44

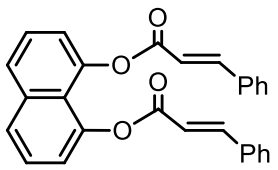

1,8-DHN **43** (100 mg, 0.62 mmol) was dissolved in 15 mL of anhydrous CH_2Cl_2 in a 100 mL, round-bottomed flask at 23 °C under nitrogen. Cinnamic acid (185 mg, 1.25 mmol), DCC (258 mg, 1.25 mmol) and DMAP (15.3 mg, 0.125 mmol) were added sequentially. The resulting cloudy, heterogeneous mixture was stirred at 23 °C for 24 h. TLC analysis indicated full consumption of 1,8-DHN **43**. The reaction mixture was quenched with a 10% (w/v) aqueous solution of citric acid (30 mL) and H_2O (10 mL). The two phases were partitioned. The organic phase was washed once with brine. It was then dried over anhydrous Na_2SO_4, filtered and concentrated under vacuum. Purification by column chromatography (SiO_2; CH_2Cl_2:hexanes = 1:1) afforded pure **44** (248 mg, 95%) as a pale yellow solid.

M.P. 222-223 °C ($CHCl_3$).

$\boldsymbol{R_f}$ = 0.56 (CH_2Cl_2:hexanes = 1:1)

TLC Visualization: UV active; stains with $KMnO_4$ solution.

^{1}H NMR (400 MHz; $CDCl_3$) δ: 7.86 (2H, d, *J* = 16.0 Hz), 7.82 (2H, d, *J* = 8.3 Hz), 7.50 (2H, t, *J* = 7.9 Hz), 7.31-7.25 (6H, m), 7.21 (2H, d, *J* = 7.3 Hz), 7.13 (4H, t, *J* = 7.6 Hz), 6.63 (2H, d, *J* = 16.0 Hz).

^{13}C NMR (100 MHz; $CDCl_3$) δ: 166.0, 147.1, 145.3, 136.9, 133.9, 130.7, 128.9, 128.3, 127.0, 126.2, 121.5, 120.7, 117.4.

FTIR ν_{max} (ATR, film)/cm^{-1} 3061, 2924, 2853, 1718, 1633, 1601, 1576, 1497, 1450.

HRMS (APCI+) Calcd for $C_{28}H_{20}NaO_4$ $[M+Na]^+$: 443.1254, found: 443.1255.

3.4.2. Compound 50

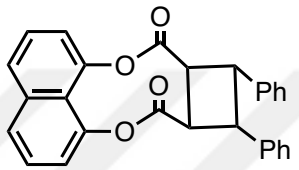

Diester **44** (25.6 mg, 0.061 mmol) was placed between two microscope slides as a solid powder. The sample was irradiated in a safety box using a 400 W broadband medium-pressure Hg lamp for 4 h. The solid powder was mixed with a spatula to ensure homogeneity after two hours. At the end of 4 h in total, the sample was transferred to a vial by washing with $CDCl_3$. ^{1}H-NMR spectroscopic analysis indicated full conversion of diester **44** to the cyclobutane product **50**. The presence of diester **44** or any other side product was not observed in this spectrum. Cyclobutane **50** was obtained as a light brown solid upon removal of the solvent (23.3 mg, 92%).

In another experiment, diester **44** (26.3 mg, 0.063) was irradiated using the same experimental set-up for 8 h. The solid powder was mixed with a spatula to ensure homogeneity every two hours. At the end of 8 h in total, the sample was transferred to a vial by washing with $CDCl_3$. ^{1}H-NMR spectroscopic analysis indicated full conversion of diester **44** to the cyclobutane product **50**. The presence of diester **44** or any other side product was not observed in this spectrum. Cyclobutane **50** was obtained as a light brown solid upon removal of the solvent (24.9 mg, 95%).

Experimental Set-up:

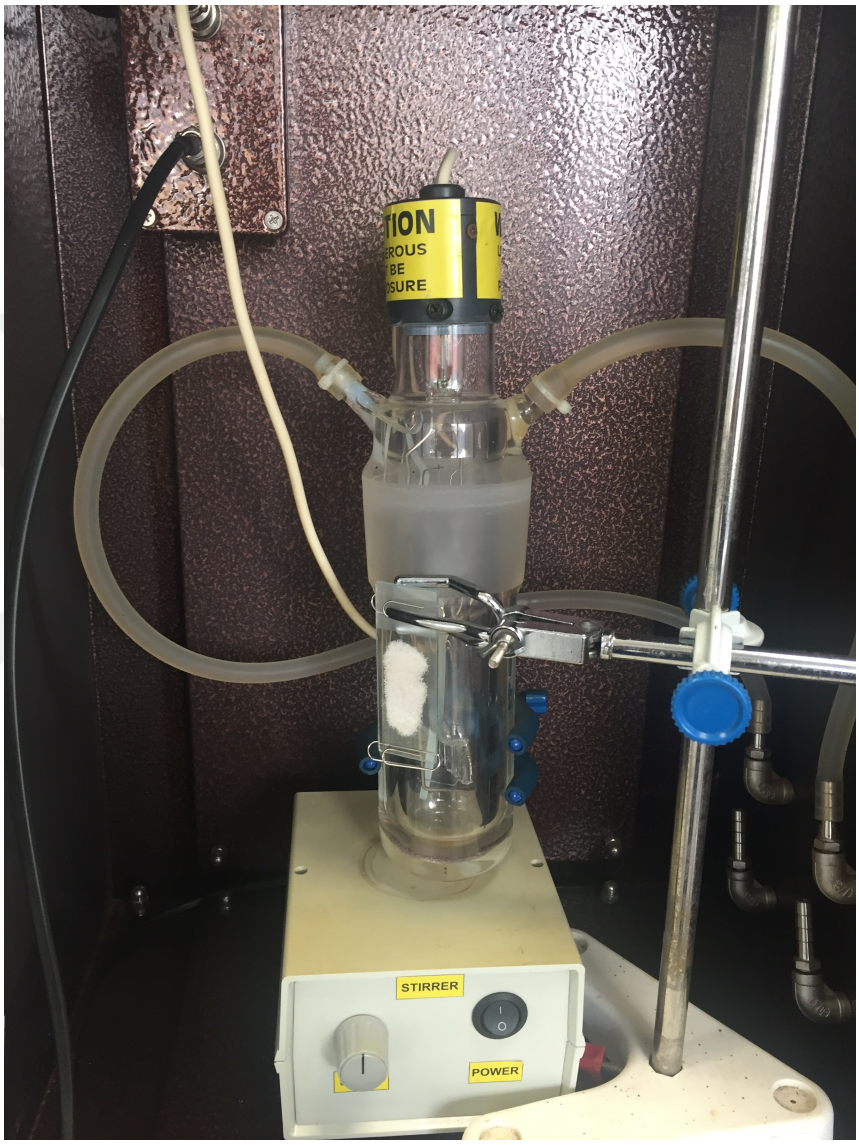

Figure 12. The appearance of the reaction set-up before the UV lamp is switched on.

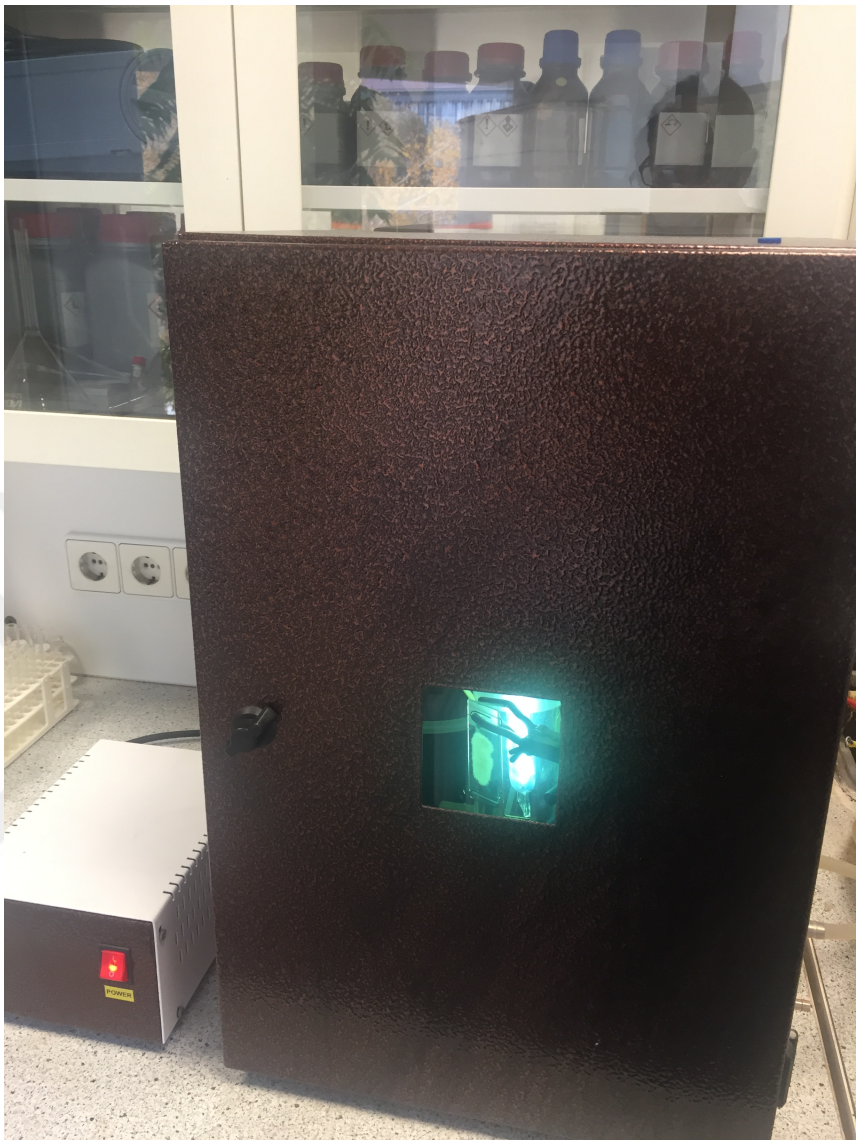

Figure 13. The appearance of the reaction set-up with the safety cabinet closed and the UV lamp switched on.

M.P. 228-229 °C ($CHCl_3$).

$\boldsymbol{R_f}$ = 0.62 (CH_2Cl_2:hexanes = 1:1)

TLC Visualization: UV active; stains slowly with $KMnO_4$ solution.

^{1}H NMR (400 MHz; $CDCl_3$) δ: 7.82 (2H, d, *J* = 8.3 Hz), 7.51 (2H, t, *J* = 7.9 Hz), 7.28 (2H, d, *J* = 7.5 Hz), 7.17 (4H, t, *J* = 7.3 Hz), 7.10 (2H, t, *J* = 7.2 Hz), 7.03 (4H, d, *J* = 7.2 Hz), 4.77 (2H, app d, *J* = 6.0 Hz), 4.24 (2H, app d, *J* = 6.0 Hz).

^{13}C NMR (100 MHz; $CDCl_3$) δ: 170.1, 145.5, 138.2, 137.1, 128.3, 127.9, 127.1, 126.8, 126.5, 121.1, 119.6, 44.9, 44.3.

FTIR ν_{max} (ATR, film)/cm^{-1} 2924, 2853, 1762, 1607, 1497, 1452, 1366.

HRMS (APCI+) Calcd for $C_{21}21_3O_4$ $[M+H]^+$: 421.1435, found: 421.1436.

3.4.3. Compound 54

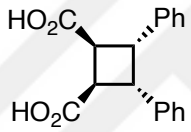

In a 20-mL scintillation vial, cyclobutane **50** (25 mg, 0.059 mmol) was dissolved in 2.0 mL of THF. Afterwards, distilled water (1.0 mL) and KOH (65 mg, 1.13. mmol) were added. The resulting mixture was stirred at 23 °C for 2 h. It was then quenched with 1.0 M HCl solution until pH was adjusted to 1-2. The aqueous phase was extracted three times with EtOAc. The combined organic phase was then dried over anhydrous Na_2SO_4, filtered and concentrated under vacuum. Purification by column chromatography (SiO_2; 0.5% (v/v) AcOH in EtOAc: hexanes = 1:1) afforded pure **54** (18 mg, 100%) as a yellow solid, and pure 1,8-DHN **43** (10 mg, 100%) as a black solid.

$\boldsymbol{R_f}$ = 0.20 (0.5% (v/v) AcOH in EtOAc: hexanes = 1:1)

TLC Visualization: UV inactive; stains slowly with $KMnO_4$ solution.

^{1}H NMR (400 MHz; $CDCl_3$) δ: 12.44 (2H, br s), 7.09-6.97 (10H, m), 4.21 (2H, d, *J* = 6.0 Hz), 3.80 (2H, d, *J* = 6.0 Hz).

^{13}C NMR (100 MHz; DMSO-*d*^{6}) δ: 174.0, 139.3, 127.9, 127.8, 126.0, 44.5, 42.7.

FTIR ν_{max} (ATR, film)/cm^{-1} 3070, 2834, 1762, 1685, 1597, 1452, 1366.

3.4.4. Compound 45

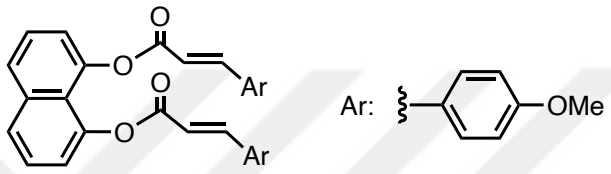

1,8-DHN **43** (100 mg, 0.62 mmol) was dissolved in 15 mL of anhydrous CH_2Cl_2 in a 100 mL, round-bottomed flask at 23 °C under nitrogen. 4-Methoxycinnamic acid (223 mg, 1.25 mmol), DCC (258 mg, 1.25 mmol) and DMAP (15.3 mg, 0.125 mmol) were added sequentially. The resulting cloudy, heterogeneous mixture was stirred at 23 °C for 24 h. The reaction mixture was quenched with a 10% (w/v) aqueous solution of citric acid (30 mL) and H_2O (10 mL). The two phases were partitioned. The organic phase was washed once with brine. It was then dried over anhydrous Na_2SO_4, filtered and concentrated under vacuum. Purification by column chromatography (SiO_2; only CH_2Cl_2) afforded pure **45** (250 mg, 87%) as a pale yellow solid.

M.P. 231-232 °C ($CHCl_3$).

R_f = 0.50 (only CH_2Cl_2)

TLC Visualization: UV active; stains with $KMnO_4$ solution.

^{1}H NMR (400 MHz; $CDCl_3$) δ: 7.81 (2H, d, *J* = 7.7 Hz), 7.79 (2H, d, *J* = 15.9 Hz), 7.49 (2H, t, *J* = 7.9 Hz), 7.23 (4H, d, *J* = 8.7 Hz), 7.19 (2H, d, *J* = 7.5 Hz), 6.64 (4H, d, *J* = 8.7 Hz), 6.48 (2H, d, *J* = 16.0 Hz), 3.79 (6H, s).

^{13}C NMR (100 MHz; $CDCl_3$) δ: 166.4, 161.6, 146.6, 145.5, 136.9, 130.0, 126.9, 126.8, 126.2, 121.7, 120.8, 114.9, 114.3, 55.3.

FTIR ν_{max} (ATR, film)/cm^{-1} 2923, 2842, 1718, 1633, 1601, 1572, 1513.

HRMS (APCI+) Calcd for $C_{30}H_{24}NaO_6$ $[M+Na]^+$: 503.1466, found: 503.1466.

3.4.5. Compound 51

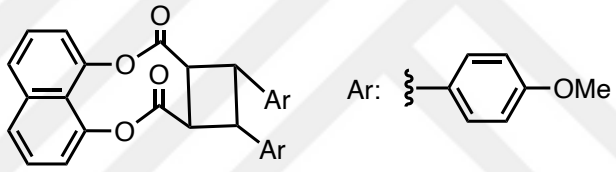

Diester **45** (16.1 mg, 0.034 mmol) was placed between two microscope slides as a solid powder. The sample was irradiated in a safety box using a 400 W broadband medium-pressure Hg lamp for 12 h. The solid powder was mixed with a spatula to ensure homogeneity every two hours. The reaction was stopped at the end of 12 h in total. Purification by column chromatography (SiO_2; only CH_2Cl_2) afforded pure **51** (12.5 mg, 78%) as a yellow solid.

$\boldsymbol{R_f}$ = 0.66 (only CH_2Cl_2)

TLC Visualization: UV active; stains slowly with $KMnO_4$ solution.

^{1}H NMR (400 MHz; $CDCl_3$) δ: 7.80 (2H, d, *J* = 8.2 Hz), 7.50 (2H, t, *J* = 7.9 Hz), 7.27 (2H, d, *J* = 7.7 Hz), 6.93 (4H, d, *J* = 8.6 Hz), 6.71 (4H, d, *J* = 8.6 Hz), 4.66 (2H, app d, *J* = 6.0 Hz), 4.16 (2H, app d, *J* = 5.9 Hz), 3.71 (6H, s).

^{13}C NMR (100 MHz; $CDCl_3$) δ: 170.2, 158.4, 145.5, 137.1, 130.4, 129.0, 127.0, 126.5, 121.1, 119.7, 113.8, 55.3, 45.2, 43.7.

HRMS (APCI+) $C_{30}H_{24}NaO_6$ $[M+Na]^+$: 503.1466, found: 503.1476.

3.4.7. Compound 46

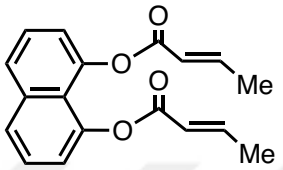

1,8-DHN **43** (100 mg, 0.62 mmol) was dissolved in 15 mL of anhydrous CH_2Cl_2 in a 100 mL, round-bottomed flask at 23 °C under nitrogen. Crotonic acid (108 mg, 1.25 mmol), DCC (258 mg, 1.25 mmol) and DMAP (15.3 mg, 0.125 mmol) were added sequentially. The resulting cloudy, heterogeneous mixture was stirred at 23 °C for 24 h. The reaction mixture was quenched with a 10% (w/v) aqueous solution of citric acid (30 mL) and H_2O (10 mL). The two phases were partitioned. The organic phase was washed once with brine. It was then dried over anhydrous Na_2SO_4, filtered and concentrated under vacuum. Purification by column chromatography (SiO_2; CH_2Cl_2:hexanes = 1:1) afforded pure **46** (158 mg, 85%) as a white solid with >96% purity. A portion of this product was further purified via recrystallization from heptane to give an analytically pure sample of **46**.

M.P. 153-154 °C (heptane).

$\boldsymbol{R_f}$ = 0.42 (CH_2Cl_2:hexanes = 1:1)

TLC Visualization: UV active; stains with $KMnO_4$ solution.

^{1}H NMR (400 MHz; $CDCl_3$) δ: 7.77 (2H, d, *J* = 8.2 Hz), 7.45 (2H, t, *J* = 7.9 Hz), 7.22-7.15 (2H, m), 7.12 (2H, d, *J* = 7.7 Hz), 6.04 (2H, app dd, *J* = 15.6, 1.6 Hz), 1.96 (6H, dd, *J* = 6.9, 1.5 Hz).

^{13}C NMR (100 MHz; $CDCl_3$) δ: 165.3, 147.0, 145.3, 136.9, 126.9, 126.1, 122.6, 121.6, 120.6, 18.3.

FTIR ν_{max} (ATR, film)/cm^{-1} 3057, 2922, 2850, 1742, 1659, 1603, 1442, 1377, 1312.

HRMS (APCI+) Calcd for $C_{18}H_{16}NaO_4$ $[M+Na]^+$: 319.0941, found: 319.0940.

Irradiation of Diester 46:

Diester **46** (23 mg, 0.078 mmol) was placed between two microscope slides as a solid powder. The sample was irradiated in a safety box using a 400 W broadband medium-pressure Hg lamp for 4 h. The solid powder was mixed with a spatula to ensure homogeneity after two hours. At the end of 4 h in total, the sample was transferred to a vial by washing with $CDCl_3$. ^{1}H-NMR spectroscopic analysis indicated no formation of the desired cyclobutene product, and the reactant **46** was observed to remain intact.

3.4.8. Compound 48

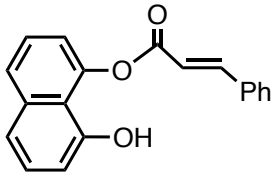

In a 100-mL round-bottomed flask, *trans*-cinnamic acid (520 mg, 3.51 mmol) was dissolved in 2 mL of oxalyl chloride at 23 °C under an inert atmosphere of nitrogen. The clear solution was heated at 60 °C for 2 h. Afterwards, it was cooled back to ambient

temperature, and the volatiles were removed by the use of a rotary evaporator to give acyl chloride **47** (575 mg, 99%) as yellow solid.

In another 100-mL round-bottomed flask, 1,8-DHN **43** (500 mg, 3.12 mmol) was dissolved in 10 mL of anhydrous THF under an inert atmosphere of nitrogen. The clear solution was cooled to 0 °C in an ice bath, and NaH (137 mg, 3.43 mmol, 60% dispersion in mineral oil) was added carefully in portions. The reaction mixture was stirred at this temperature for 20 min. Acyl chloride **47** (520 mg, 3.12 mmol), which was prepared as described above, was dissolved in 5 mL of anhydrous THF, and this solution was added slowly via syringe to the reaction mixture at 0 °C. Afterwards, the reaction mixture was stirred at 23 °C for 75 min. TLC analysis indicated full consumption of 1,8-DHN **43**. The reaction mixture was quenched with 50 mL of saturated aqueous NH_4Cl solution. The aqueous phase was extracted three times with CH_2Cl_2. The combined organic phase was dried over anhydrous Na_2SO_4, filtered and concentrated under vacuum. Purification by column chromatography (SiO_2; EtOAc:hexanes = 1:5) afforded pure **48** (740 mg, 82%) as an orange solid.

M.P. 119-120 °C (CH_2Cl_2).

$\boldsymbol{R_f}$ = 0.27 (EtOAc:hexanes = 1:5)

TLC Visualization: UV active; stains with $KMnO_4$ solution.

^{1}H NMR (400 MHz; $CDCl_3$) δ: 7.91 (1H, d, *J* = 16.0 Hz), 7.67 (1H, t, *J* = 8.3 Hz), 7.56-7.54 (2H, m), 7.41-7.37 (5H, m), 7.30-7.28 (2H, m), 7.20 (1H, d, *J* = 7.3 Hz), 6.82 (1H, d, *J* = 7.6 Hz), 6.68 (1H, d, *J* = 15.9 Hz).

^{13}C NMR (100 MHz; $CDCl_3$) δ: 164.7, 152.1, 148.2, 146.2, 137.0, 133.9, 131.3, 129.2, 128.6, 127.2, 126.6, 125.6, 120.4, 118.6, 117.2, 116.5, 111.5.

FTIR ν_{max} (ATR, film)/cm^{-1} 3388 (br s), 3058, 2924, 2853, 1704, 1633, 1601, 1579, 1449.

HRMS (APCI+) Calcd for $C_{19}H_{14}NaO_3$ $[M+Na]^+$: 313.0836, found: 313.0839.

3.4.9. Compound 49

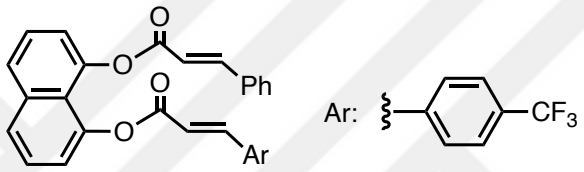

Monoester **48** (100 mg, 0.35 mmol) was dissolved in 10 mL of anhydrous CH_2Cl_2 in a 100 mL, round-bottomed flask at 23 °C under nitrogen. 4-Trifluoromethylcinnamic acid (75 mg, 0.35 mmol), DCC (72 mg, 0.35 mmol) and DMAP (4.2 mg, 0.035 mmol) were added sequentially. The resulting orange, heterogeneous mixture was stirred at 23 °C for 24 h. The reaction mixture was quenched with a 10% (w/v) aqueous solution of citric acid (30 mL). The aqueous phase was extracted with CH_2Cl_2 (3×30 mL). The combined organic phase was then dried over anhydrous Na_2SO_4, filtered and concentrated under vacuum. Purification by column chromatography (SiO_2; hexanes: $CHCl_3$ = 1:5) afforded pure **49** (120 mg, 71%) as a white solid.

M.P. 172-173 °C (CH_2Cl_2).

R_f = 0.36 (hexanes:$CHCl_3$ = 1:5)

TLC Visualization: UV active; stains with $KMnO_4$ solution.

^{1}H NMR (400 MHz; $CDCl_3$) δ: 7.85-7.79 (4H, m), 7.51-7.46 (2H, m), 7.56-7.54 (2H, m), 7.30-7.27 (4H, m), 7.25-7.19 (5H, m), 7.07 (2H, t, J = 7.7 Hz), 6.67 (1H, d, J = 16.1 Hz), 6.59 (1H, d, J = 16.1 Hz).

^{13}C NMR (100 MHz; $CDCl_3$) δ: 165.9, 165.4, 147.0, 145.3, 145.1, 144.9, 137.1 (q, $^{4}J_{C\text{-}F}$ = 1.4 Hz), 137.0, 133.7, 131.9 (q, $^{2}J_{C\text{-}F}$ = 33.9 Hz), 131.0, 128.9, 128.3, 128.2, 127.2, 127.1, 126.3, 126.2, 125.8 (q, $^{3}J_{C\text{-}F}$ = 3.7 Hz), 123.8 (q, $^{1}J_{C\text{-}F}$ = 272 Hz), 121.4, 120.9, 120.7, 120.1, 117.4.

^{19}F NMR (376 MHz; $CDCl_3$) δ: -61.8 (s).

FTIR ν_{max} (ATR, film)/cm^{-1} 3064, 2925, 1731, 1716, 1642, 1332.

HRMS (APCI+) Calcd for $C_{29}H_{20}F_3NaO_4$ $[M+Na]^+$: 511.1128, found: 511.1128.

3.4.10. Compound 53

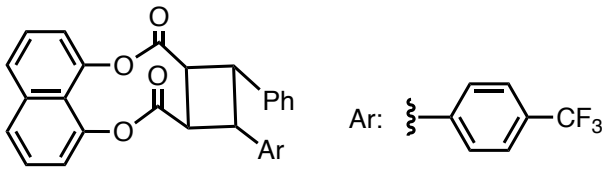

Diester **49** (25.5 mg, 0.052 mmol) was placed between two microscope slides as a solid powder. The sample was irradiated in a safety box using a 400 W broadband medium-pressure Hg lamp for 8 h. The solid powder was mixed with a spatula to ensure homogeneity every two hours. At the end of 8 h in total, the sample was transferred to a vial by washing with $CDCl_3$. ^{1}H-NMR spectroscopic analysis indicated full conversion of diester **49** to the cyclobutane product **53**. Cyclobutane **53** was obtained as a brown solid upon removal of the solvent (22.5 mg, 88%).

R_f = 0.43 (hexanes:CH_2Cl_2 = 1:1)

TLC Visualization: UV active; stains with $KMnO_4$ solution.

^{1}H NMR (400 MHz; $CDCl_3$) δ: 7.84-7.82 (2H, m), 7.55-7.50 (2H, m), 7.42 (2H, d, *J* = 8.2 Hz), 7.30-7.28 (2H, m), 7.21-7.17 (2H, m), 7.12 (3H, d, *J* = 7.6 Hz), 7.02 (2H,d, *J* = 6.9 Hz), 4.85-4.78 (2H, m), 4.25 (2H, d, *J* = 5.4 Hz).

^{13}C NMR (100 MHz; $CDCl_3$) δ: 169.8, 169.7, 142.3, 142.4 (q, $^4J_{C\text{-}F}$ = 1.5 Hz), 137.6, 137.1, 129.92 128.9, 128.6, 128.2, 127.9 (q, $^2J_{C\text{-}F}$ = 35.2 Hz), 127.2, 127.1, 126.6, 126.5, 125.3, (q, $^3J_{C\text{-}F}$ = 3.9 Hz), 121.1, 121.0, 119.5, 44.9, 44.7, 44.2, 44.1.

FTIR ν_{max} (ATR, film)/cm^{-1} 3064, 2925, 1731, 1716, 1642, 1332.

HRMS (APCI+) Calcd for $C_{29}H_{20}F_3O_4$ $[M+H]^+$: 489.1309, found: 489.1297.

3.4.11. Compound 56

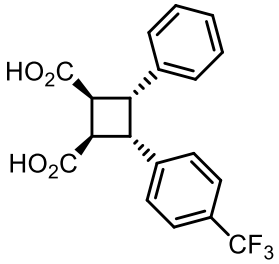

In a 20-mL scintillation vial, cyclobutane **53** (19 mg, 0.038 mmol) was dissolved in 2.0 mL of THF. Afterwards, distilled water (1.0 mL) and KOH (42 mg, 0.74 mmol) were added. The resulting mixture was stirred at 23 °C for 2 h. It was then quenched with 1.0 M HCl solution until pH was adjusted to 1-2. The aqueous phase was extracted three times with EtOAc. The combined organic phase was then dried over anhydrous Na_2SO_4, filtered and concentrated under vacuum. Purification by column chromatography (SiO_2;

0.5% (v/v) AcOH in EtOAc: hexanes = 1:1) afforded pure **56** (12.5 mg, 88%) as a colorless oil, and pure 1,8-DHN **43** (10 mg, 100%) as a black solid.

$\boldsymbol{R_f}$ = 0.28 (0.5% (v/v) AcOH in EtOAc: hexanes = 1:1)

TLC Visualization: UV inactive; stains slowly with $KMnO_4$ solution.

^{1}H NMR (400 MHz; $CDCl_3$) δ: 7.27 (2H, d, *J* = 8.1 Hz), 7.17-7.09 (3H, m), 7.03 (2H, d, *J* = 8.1 Hz), 6.94 (2H, d, *J* = 8.1 Hz), 4.60-4.40 (2H, m), 4.0-3.9 (2H, m).

4. BIBLIOGRAPHY

[1] Kurti, L.; Czakó, B. Strategic applications of named reactions in organic synthesis, Elsevier, **2005.**

[2] Vinogradov, M. G.; Turova, O. V.; Zlotin, S. G. *Organic & Biomolecular Chemistry* **2017**, *15*, 8245-8269.

[3] Vaidya, T.; Eisenberg, R.; Frontier, A. J. *ChemCatChem* **2011**, *3*, 1531-1548.

[4] Woodward, R. B.; Hoffmann, R. *Journal of the American Chemical Society* **1965**, *87*, 395-397.

[5] Williams, D. R.; Robinson, L. A.; Nevill, C. R.; Reddy, J. P. *Angewandte Chemie International Edition* **2007**, *46*, 915-918.

[6] Karthikeyan, I.; Arunprasath, D.; Sekar, G. *Chemical Communications* **2015**, *51*, 1701-1704.

[7] Ji, W.; Liu, Y. A.; Liao, X. *Angewandte Chemie International Edition* **2016**, *55*, 13286-13289.

[8] Klumpp, D. A.; Zhang, Y.; O'Connor, M. J.; Esteves, P. M.; de Almeida, L. S. *Organic Letters* **2007**, *9*, 3085-3088.

[9] Sai, K. K. S.; O'Connor, M. J.; Klumpp, D. A. *Tetrahedron Letters* **2011**, *52*, 2195-2198.

[10] Narayan, R.; Daniliuc, C. G.; Würthwein, E. U. *European Journal of Organic Chemistry* **2012**, *2012*, 6021-6032.

[11] Ghavtadze, N.; Fröhlich, R.; Würthwein, E. U. *European Journal of Organic Chemistry* **2008**, *2008*, 3656-3667.

[12] Shimada, N.; Ashburn, B. O.; Basak, A. K.; Bow, W. F.; Vicic, D. A.; Tius, M. A. *Chemical Communications* **2010**, *46*, 3774-3775.

[13] Donmez, S. E.; Soydaş, E.; Aydın, G. k. e.; Şahin, O.; Bozkaya, U. u.; Türkmen, Y. E. *Organic Letters* **2019**, *21*, 554-558.

[14] Rasapalli, S.; Sammeta, V. R.; Murphy, Z. F.; Huang, Y.; Boerth, J. A.; Golen, J. A.; Savinov, S. N. *Organic Letters* **2019**, *21*, 9824-9828.

[15] Ihara, M.; Kirihara, T.; Kawaguchi, A.; Tsuruta, M.; Fukumoto, K.; Kametani, T. *Journal of the Chemical Society, Perkin Transactions 1* **1987**, 1719-1726.

[16] Rodriguez, A. A.; Yoo, H.; Ziller, J. W.; Shea, K. J. *Tetrahedron Letters* **2009**, *50*, 6830-6833.

[17] Rostami, A.; Colin, A.; Li, X. Y.; Chudzinski, M. G.; Lough, A. J.; Taylor, M. S. *The Journal of Organic Chemistry* **2010**, *75*, 3983-3992.

[18] Cranwell, P. B.; Hiscock, J. R.; Haynes, C. J.; Light, M. E.; Wells, N. J.; Gale, P. A. *Chemical Communications* **2013**, *49*, 874-876.

[19] Cahn, R. S.; Dermer, O. C. Introduction to chemical nomenclature, Butterworth-Heinemann, **2013.**

[20] Mayr, H.; Patz, M. *Angewandte Chemie International Edition in English* **1994**, *33*, 938-957.

[21] Ciamician, G.; Silber, P. *Ber. dtsch. chern. Ces* **1908**, *41*, 1928.

[22] Büchi, G.; Goldman, I. *Journal of the American Chemical Society* **1957**, *79*, 4741-4748.

[23] Schmidt, G., *Pure Appl. Chem* **1971**, *27*, 647-678.

[24] MacGillivray, L. R.; Reid, J. L.; Ripmeester, J. A. *Journal of the American Chemical Society* **2000**, *122*, 7817-7818.

[25] Macgillivray, L. R.; Papaefstathiou, G. S.; Friščić, T.; Hamilton, T. D.; Bučar, D.-K.; Chu, Q.; Varshney, D. B.; Georgiev, I. G. *Accounts of Chemical research* **2008**, *41*, 280-291.

[26] Caronna, T.; Liantonio, R.; Logothetis, T. A.; Metrangolo, P.; Pilati, T.; Resnati, G. *Journal of the American Chemical Society* **2004**, *126*, 4500-4501.

[27] Mei, X.; Liu, S.; Wolf, C. *Organic Letters* **2007**, *9*, 2729-2732.

[28] Dembitsky, V. M. *Journal of natural medicines* **2008**, *62*, 1-33.

[29] Dembitsky, V. M. *Phytomedicine* **2014**, *21*, 1559-1581.

[30] Damsté, J. S. S.; Strous, M.; Rijpstra, W. I. C.; Hopmans, E. C.; Geenevasen, J. A.; van Duin, A. C.; Van Niftrik, L. A.; Jetten, M. S. *Nature* **2002**, *419*, 708-712.

[31] Li, Y. Z.; Tong, A. P.; Huang, J. *Chemistry & Biodiversity* **2012**, *9*, 769-776.

[32] Yang, Q.; Draghici, C.; Njardarson, J. T.; Li, F.; Smith, B. R.; Das, P. *Organic & biomolecular chemistry* **2014**, *12*, 330-344.

[33] Anzo, T.; Suzuki, A.; Sawamura, K.; Motozaki, T.; Hatta, M.; Takao, K.-i.; Tadano, K.-i. *Tetrahedron Letters* **2007**, *48*, 8442-8448.

[34] Fleming, I.; Gil, S.; Sarkar, A. K.; Schmidlin, T. *Journal of the Chemical Society, Perkin Transactions 1* **1992**, 3351-3361.

5. APPENDIX

5.1. XRD Analysis

5.1.1. XRD Analysis of Compound 44.

10 mg of diester **44** was dissolved in 1.0 mL of CH_2Cl_2 in a small vial, which was placed in a 20-mL scintillation via containing 3 mL of pentane. The outer vial was sealed with a screw cap, and left at ambient temperature for crystallization. Colorless crystals were obtained after three days.

A suitable crystal was selected and [] on a Bruker APEX-II CCD diffractometer. The crystal was kept at 298 K during data collection. Using Olex2[1], the structure was solved with the XT[2], structure solution program using Intrinsic Phasing and refined with the XL[3], refinement package using Least Squares minimisation.

Table 12. Crystal data and structure refinement for Diester **44.**

Identification code	20gtu101_BBY_1_186_0m
Empirical formula	$C_{28}H_{20}O_4$
Formula weight	420.44
Temperature/K	298
Crystal system	monoclinic
Space group	$P2_1/n$
a/Å	10.258(14)
b/Å	12.725(18)
c/Å	16.47(3)
α/°	90

β/°	92.26(3)
γ/°	90
Volume/Å^3	2148(5)
Z	4
ρ_{calc}g/cm^3	1.300
μ/mm^{-1}	0.086
F(000)	880.0
Crystal size/mm^3	0.35 × 0.25 × 0.2
Radiation	MoKα (λ = 0.71073)
2Θ range for data collection/°	5.896 to 50.048
Index ranges	-6 ≤ h ≤ 12, -15 ≤ k ≤ 10, -19 ≤ l ≤ 19
Reflections collected	8010
Independent reflections	3738 [R_{int} = 0.0847, R_{sigma} = 0.1180]
Data/restraints/parameters	3738/0/290
Goodness-of-fit on F^2	0.991
Final R indexes [I>=2σ (I)]	R_1 = 0.0848, wR_2 = 0.2164
Final R indexes [all data]	R_1 = 0.1122, wR_2 = 0.2421
Largest diff. peak/hole / e Å^{-3}	0.47/-0.41

Table 13. Bond Lengths for Diester **44**.

Atom	Atom	Length/Å	Atom	Atom	Length/Å
O1	C1	1.400(4)	C12	C13	1.335(4)
O1	C11	1.385(4)	C13	C14	1.460(4)
O2	C11	1.195(4)	C14	C15	1.395(4)
O3	C9	1.410(4)	C14	C19	1.385(4)
O3	C20	1.368(3)	C15	C16	1.372(5)
O4	C20	1.197(3)	C16	C17	1.367(5)
C1	C2	1.357(5)	C17	C18	1.382(5)
C1	C10	1.422(5)	C18	C19	1.373(5)
C2	C3	1.401(5)	C20	C21	1.452(4)
C3	C4	1.361(6)	C21	C22	1.336(4)
C4	C5	1.408(5)	C22	C23	1.451(4)
C5	C6	1.423(5)	C23	C24	1.395(4)
C5	C10	1.436(4)	C23	C28	1.392(4)
C6	C7	1.356(5)	C24	C25	1.377(5)
C7	C8	1.393(5)	C25	C26	1.358(5)
C8	C9	1.367(5)	C26	C27	1.380(5)
C9	C10	1.422(4)	C27	C28	1.371(5)
C11	C12	1.451(4)			

5.1.2. XRD Analysis of Compound 50.

10 mg of cyclobutane **50** was dissolved in 1.0 mL of CH_2Cl_2 in a small vial, which was placed in a 20-mL scintillation via containing 3 mL of pentane. The outer vial was sealed with a screw cap, and left at ambient temperature for crystallization. Colorless crystals were obtained after five days.

A suitable crystal was selected and [] on a Bruker APEX-II CCD diffractometer. The crystal was kept at 298 K during data collection. Using Olex2[1], the structure was solved with the SHELXT[2], structure solution program using Intrinsic Phasing and refined with the SHELXL[3], refinement package using Least Squares minimisation.

Table 14. Crystal data and structure refinement for cyclobutane **50.**

Identification code	20gtuu116_BBY_1_188_0m
Empirical formula	$C_{28}H_{20}O_4$
Formula weight	420.44
Temperature/K	298
Crystal system	monoclinic
Space group	$P2_1/c$
a/Å	13.5533(19)
b/Å	10.6923(15)
c/Å	16.080(2)
α/°	90
β/°	101.612(2)
γ/°	90
Volume/Å^3	2282.6(6)
Z	4
ρ_{calc}g/cm^3	1.223
μ/mm^{-1}	0.081
F(000)	880.0

Crystal size/mm^3	0.231 × 0.214 × 0.12
Radiation	MoKα (λ = 0.71073)
2Θ range for data collection/°	6.138 to 50.054
Index ranges	-16 ≤ h ≤ 16, -8 ≤ k ≤ 12, -19 ≤ l ≤ 19
Reflections collected	11066
Independent reflections	4011 [R_{int} = 0.0408, R_{sigma} = 0.0503]
Data/restraints/parameters	4011/0/289
Goodness-of-fit on F^2	1.029
Final R indexes [I>=2σ (I)]	R_1 = 0.0565, wR_2 = 0.1360
Final R indexes [all data]	R_1 = 0.1007, wR_2 = 0.1573
Largest diff. peak/hole / e Å^{-3}	0.16/-0.17

Table 15. Bond Lengths for cyclobutane 50.

Atom	Atom	Length/Å	Atom	Atom	Length/Å
O2	C11	1.186(3)	C12	C27	1.563(4)
O3	C9	1.405(3)	C13	C14	1.502(4)
O3	C28	1.360(3)	C13	C26	1.576(3)
O4	C28	1.198(3)	C14	C15	1.377(4)
O5	C1	1.404(3)	C14	C19	1.382(4)
O5	C11	1.363(3)	C15	C16	1.377(4)
C1	C2	1.361(4)	C16	C17	1.369(5)
C1	C10	1.405(4)	C17	C18	1.368(4)

C2	C3	1.395(5)	C18	C19	1.376(4)
C3	C4	1.346(6)	C20	C21	1.377(4)
C4	C5	1.412(6)	C20	C25	1.379(4)
C5	C6	1.418(5)	C20	C26	1.500(3)
C5	C10	1.422(4)	C21	C22	1.381(4)
C6	C7	1.346(6)	C22	C23	1.368(4)
C7	C8	1.412(5)	C23	C24	1.359(4)
C8	C9	1.350(4)	C24	C25	1.387(4)
C9	C10	1.421(4)	C26	C27	1.543(3)
C11	C12	1.501(4)	C27	C28	1.498(4)
C12	C13	1.545(3)			

[1]Dolomanov, O.V.; Bourhis, L. J.; Gildea, R. J.; Howard, J. A. K.; Puschmann, H. *J. Appl. Cryst.* **2009**, *42*, 339-341.

[2] Sheldrick, G.M. *Acta Cryst.* **2015**, *A71*, 3-8.

[3] Sheldrick, G.M. *Acta Cryst.* **2008**, *A64*, 112-122.

5.2. NMR Spectra

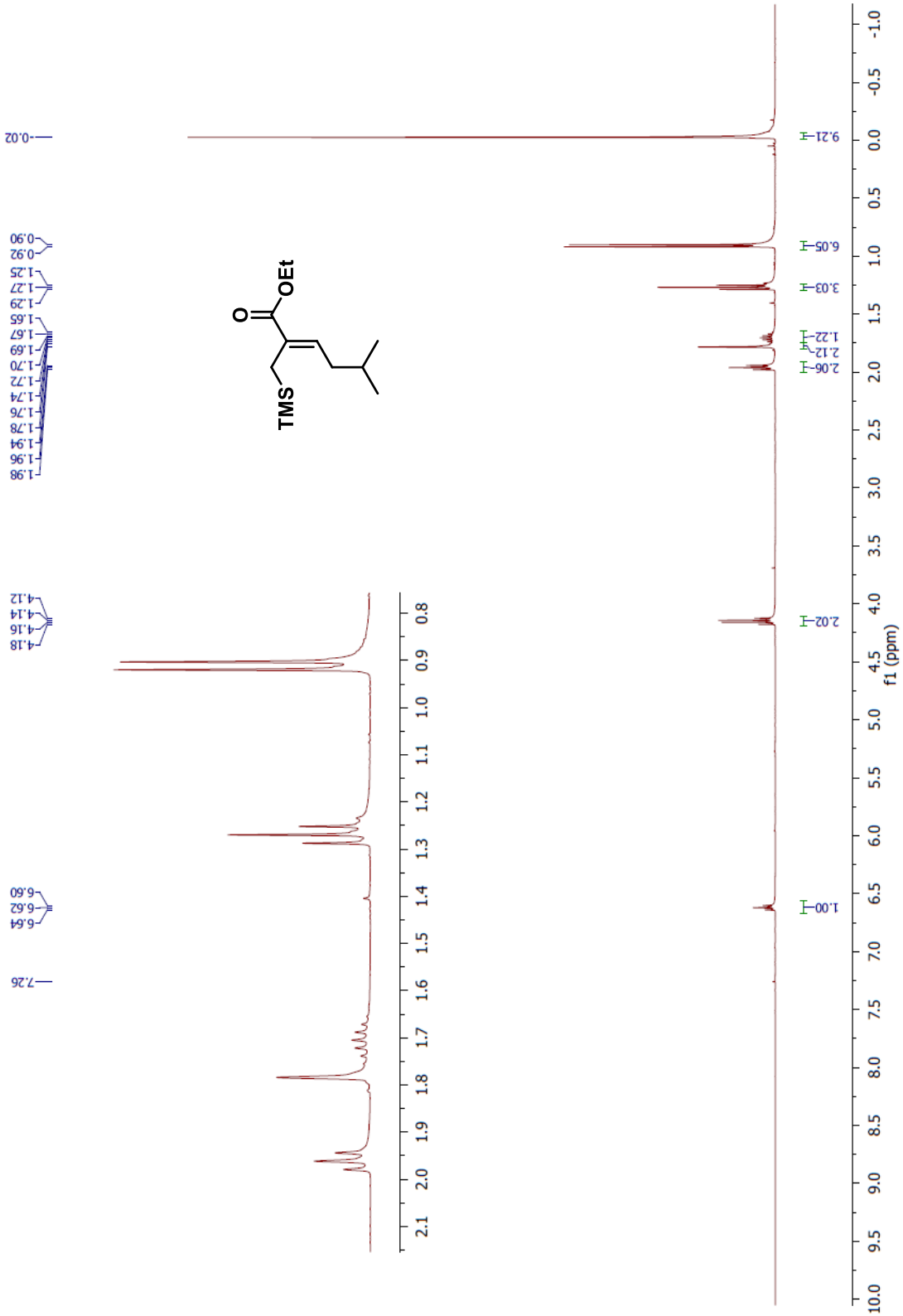

Figure 14. ^{1}H-NMR spectrum of **13a** in $CDCl_3$.

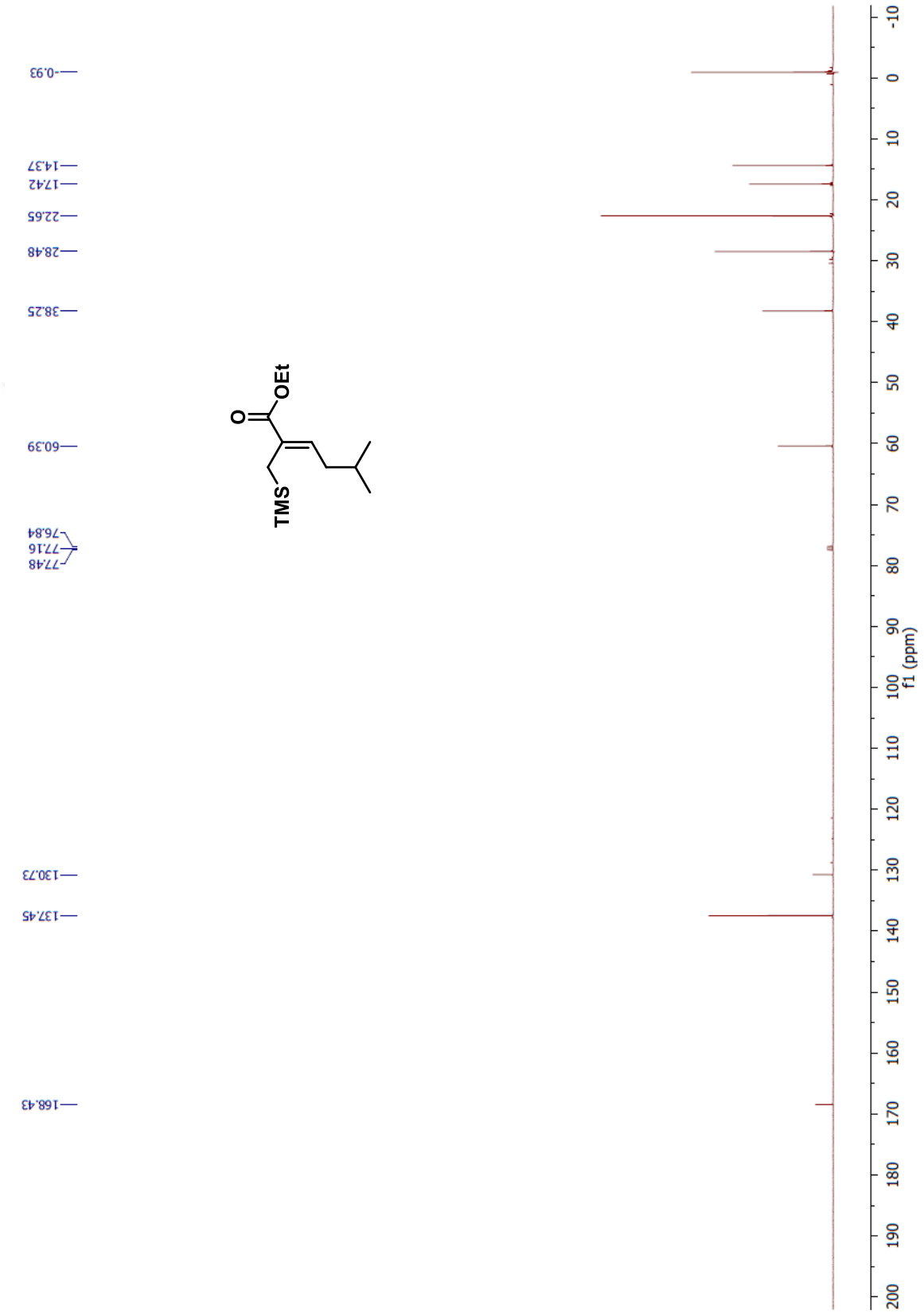

Figure 15. ^{13}C-NMR spectrum of **13a** in $CDCl_3$.

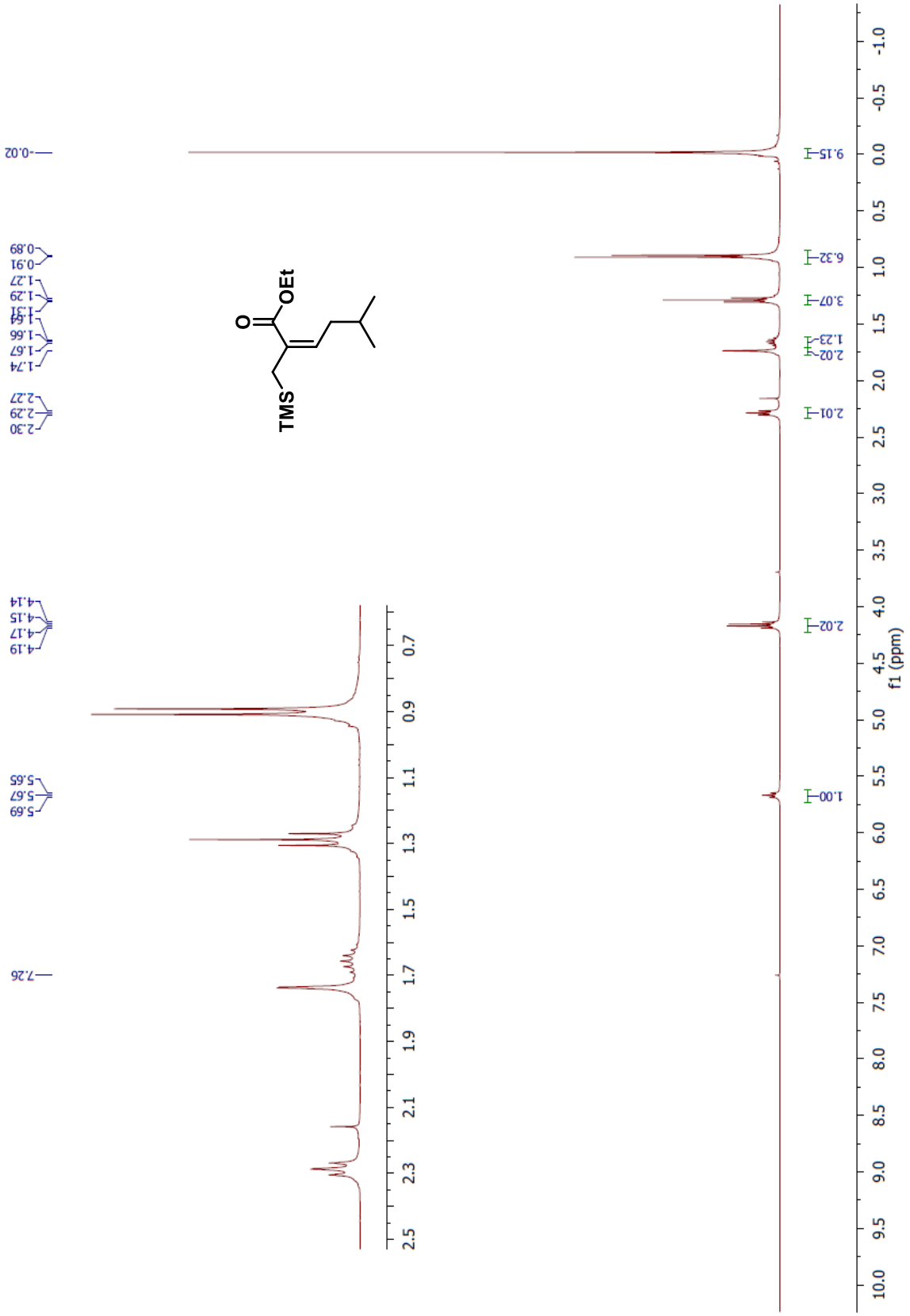

Figure 16. ^{1}H-NMR spectrum of **13b** in $CDCl_3$.

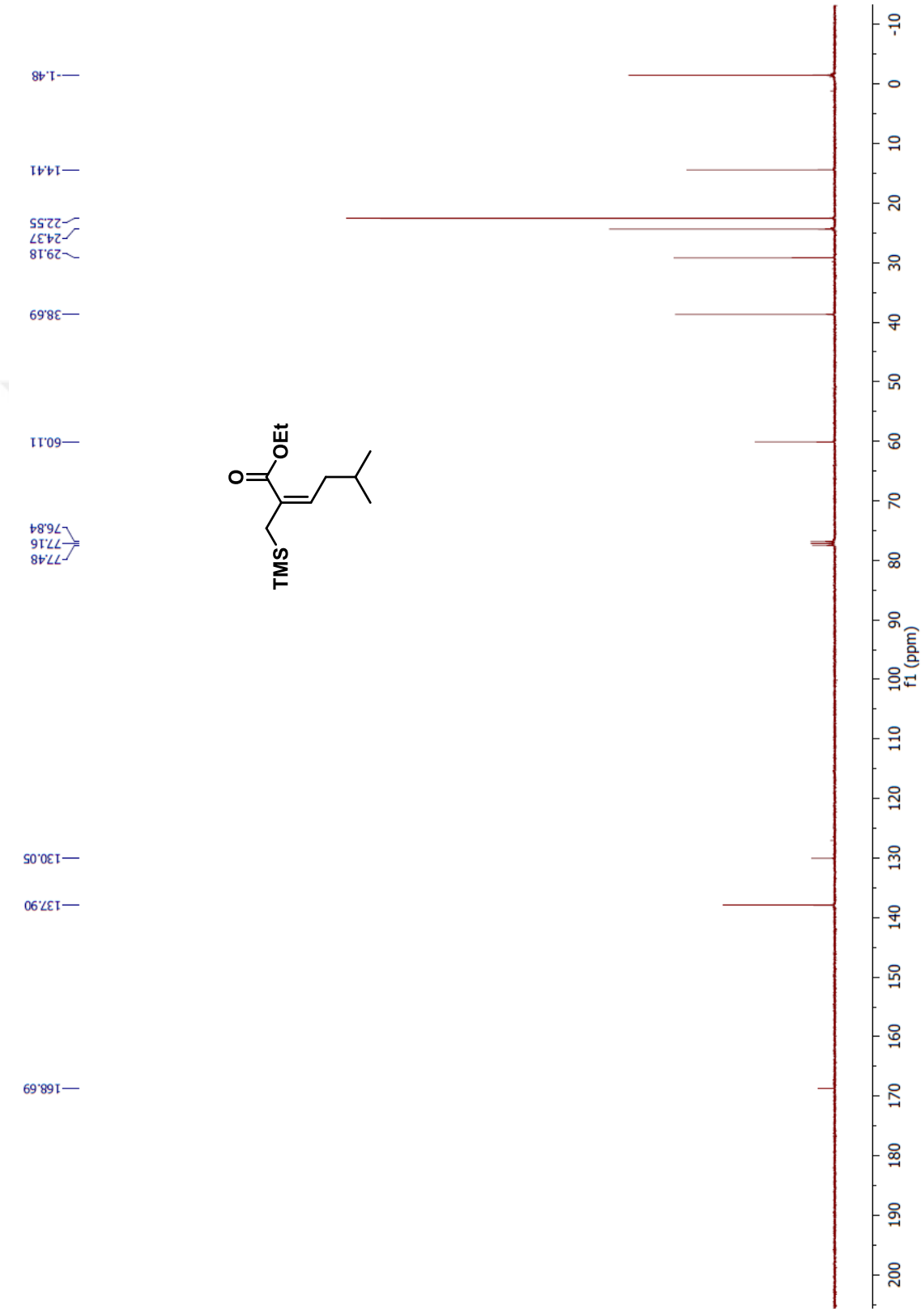

Figure 17. ^{13}C-NMR spectrum of **13b** in $CDCl_3$.

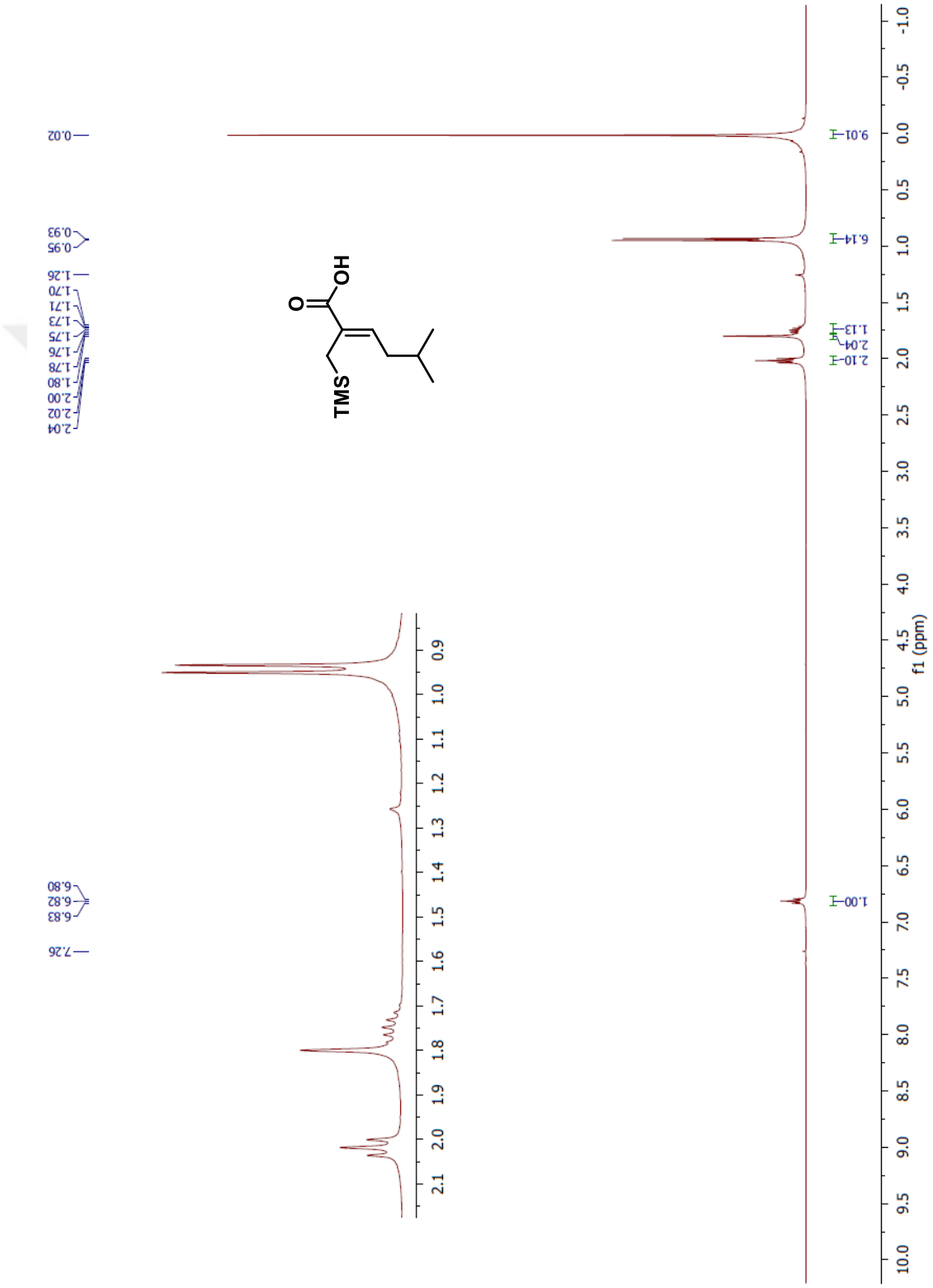

Figure 18. ^{1}H-NMR spectrum of **14a** in $CDCl_3$.

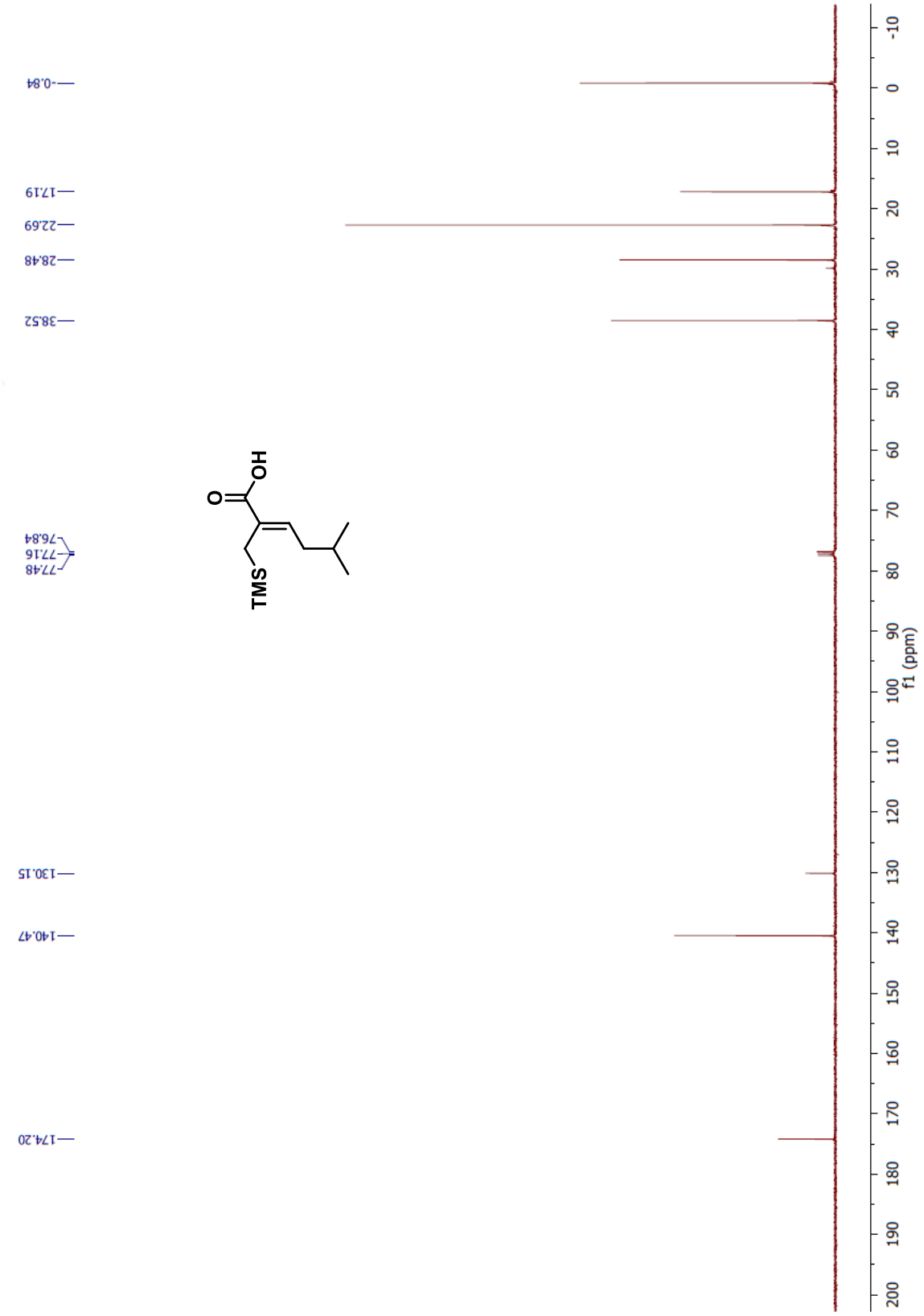

Figure 19. ^{13}C-NMR spectrum of **14a** in $CDCl_3$.

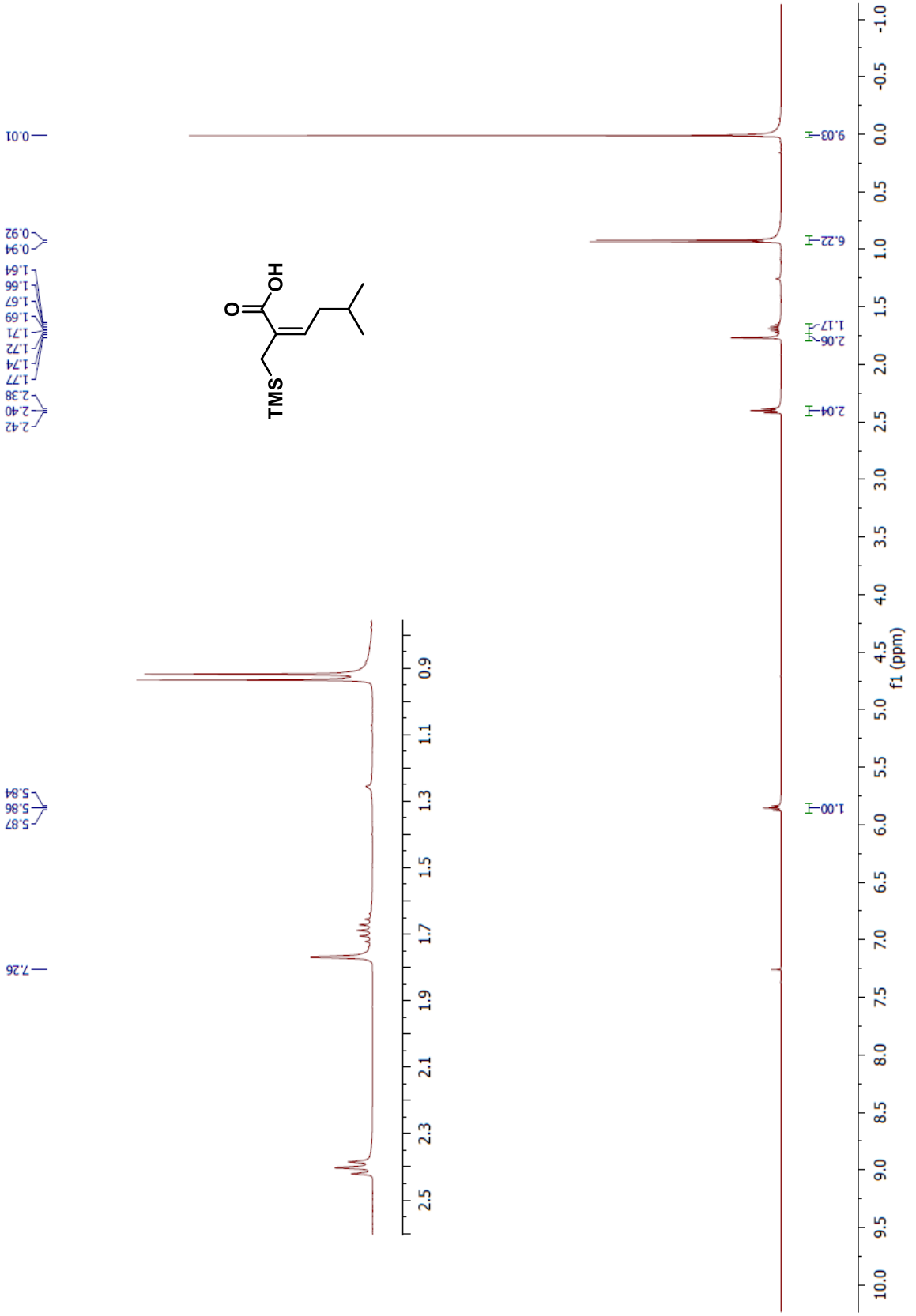

Figure 20. ^{1}H-NMR spectrum of **14b** in $CDCl_3$.

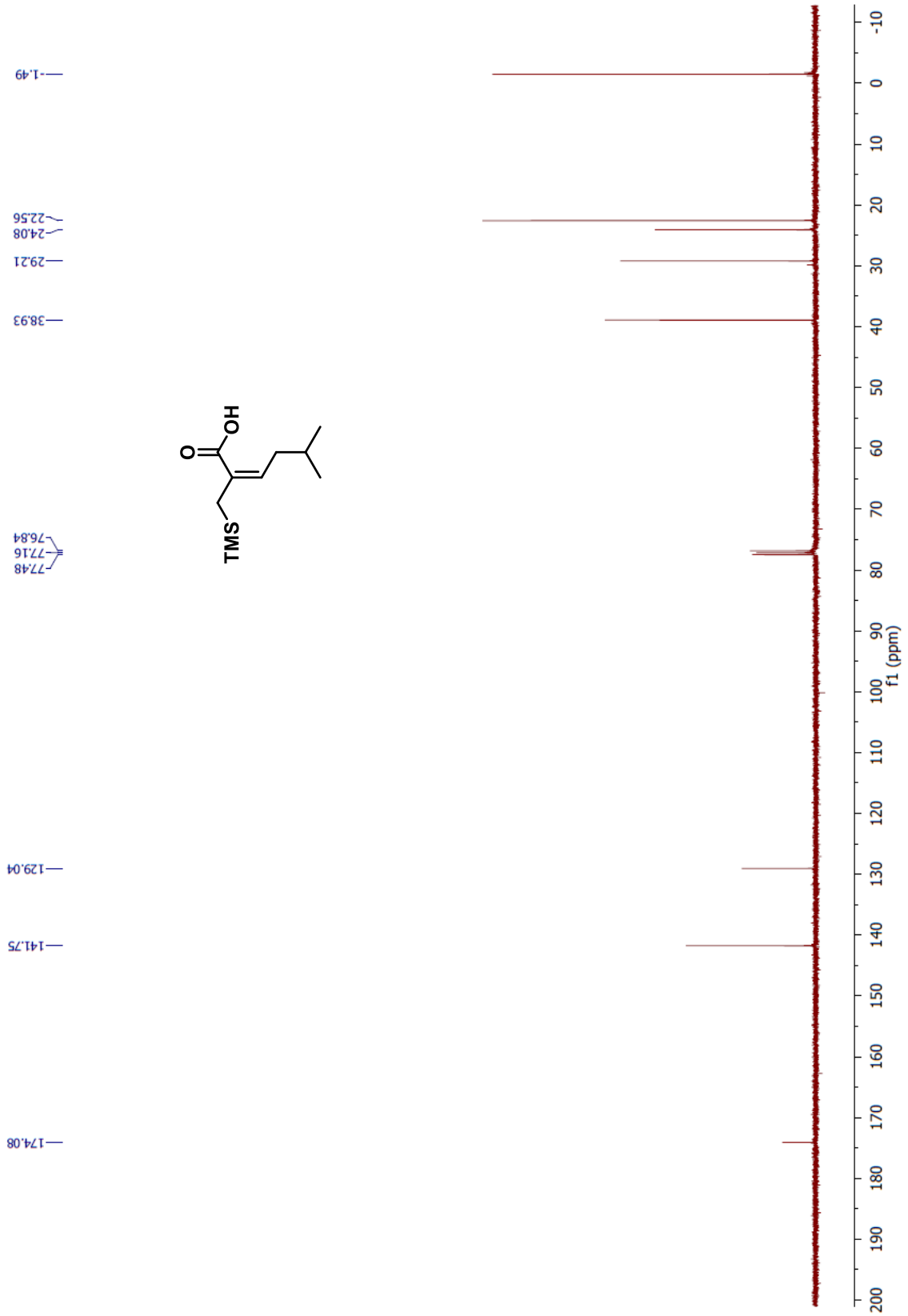

Figure 21. ^{13}C-NMR spectrum of **14b** in $CDCl_3$.

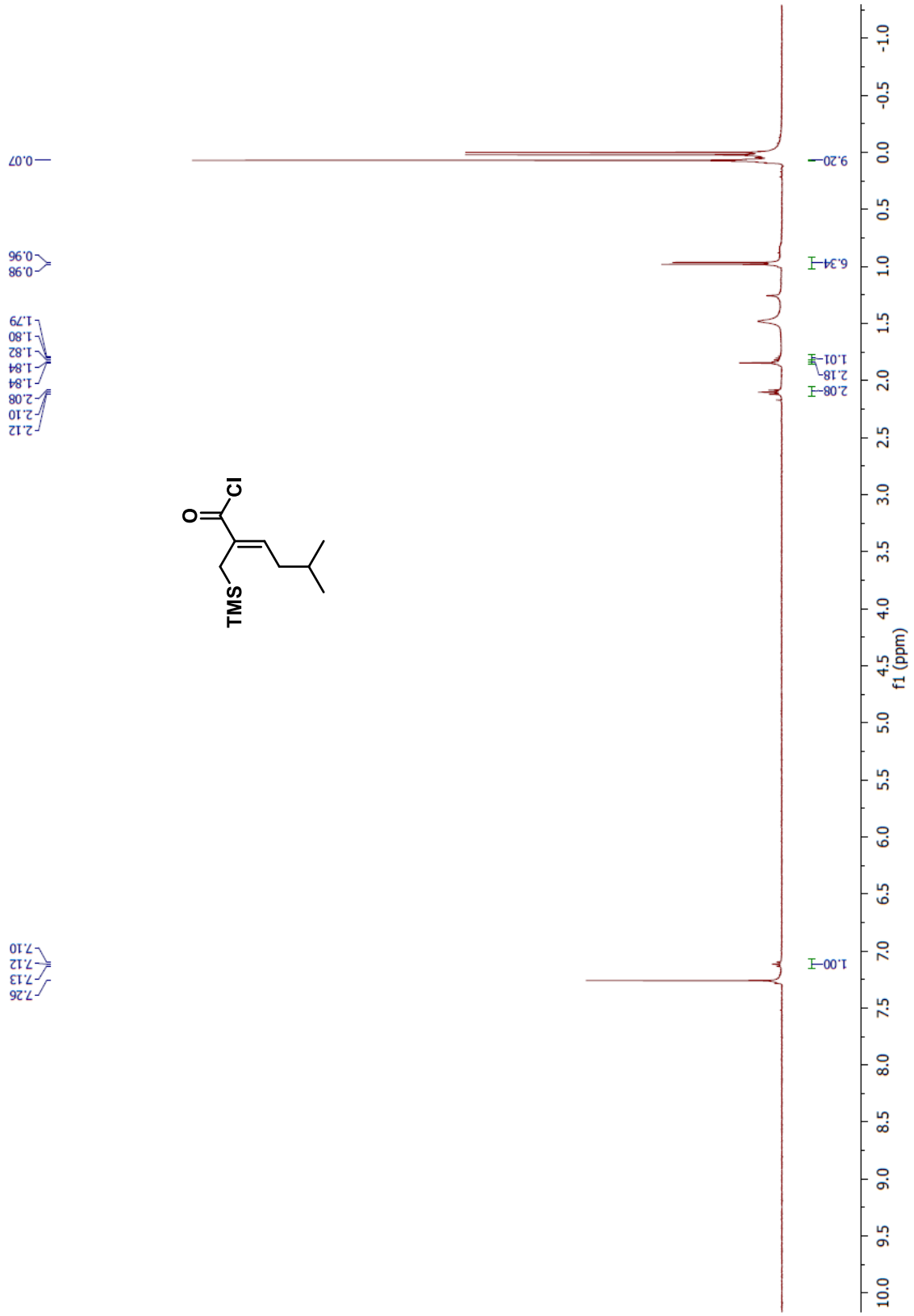

Figure 22. ^{1}H-NMR spectrum of **15a** in $CDCl_3$.

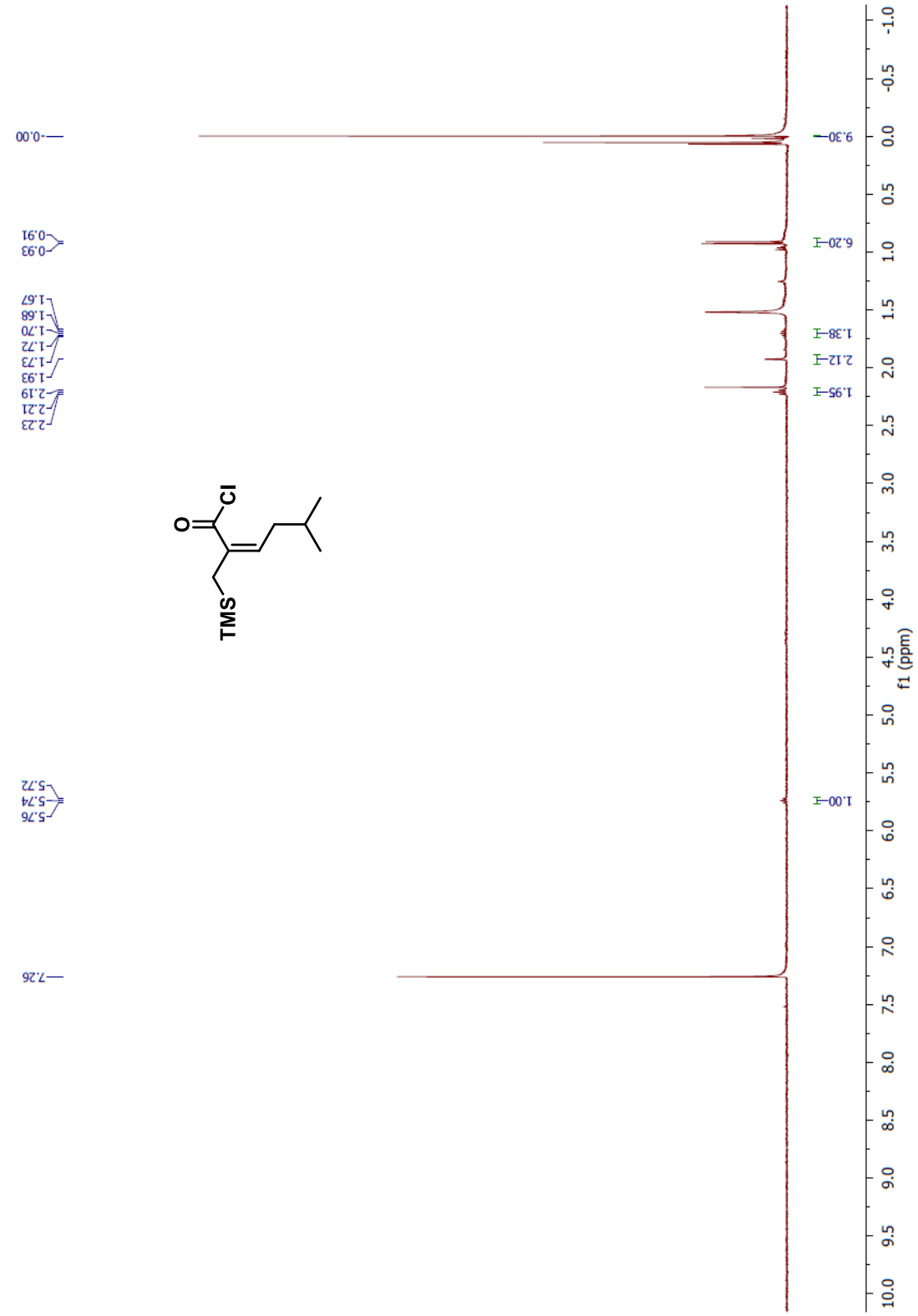

Figure 23. ^{1}H-NMR spectrum of **15b** in $CDCl_3$.

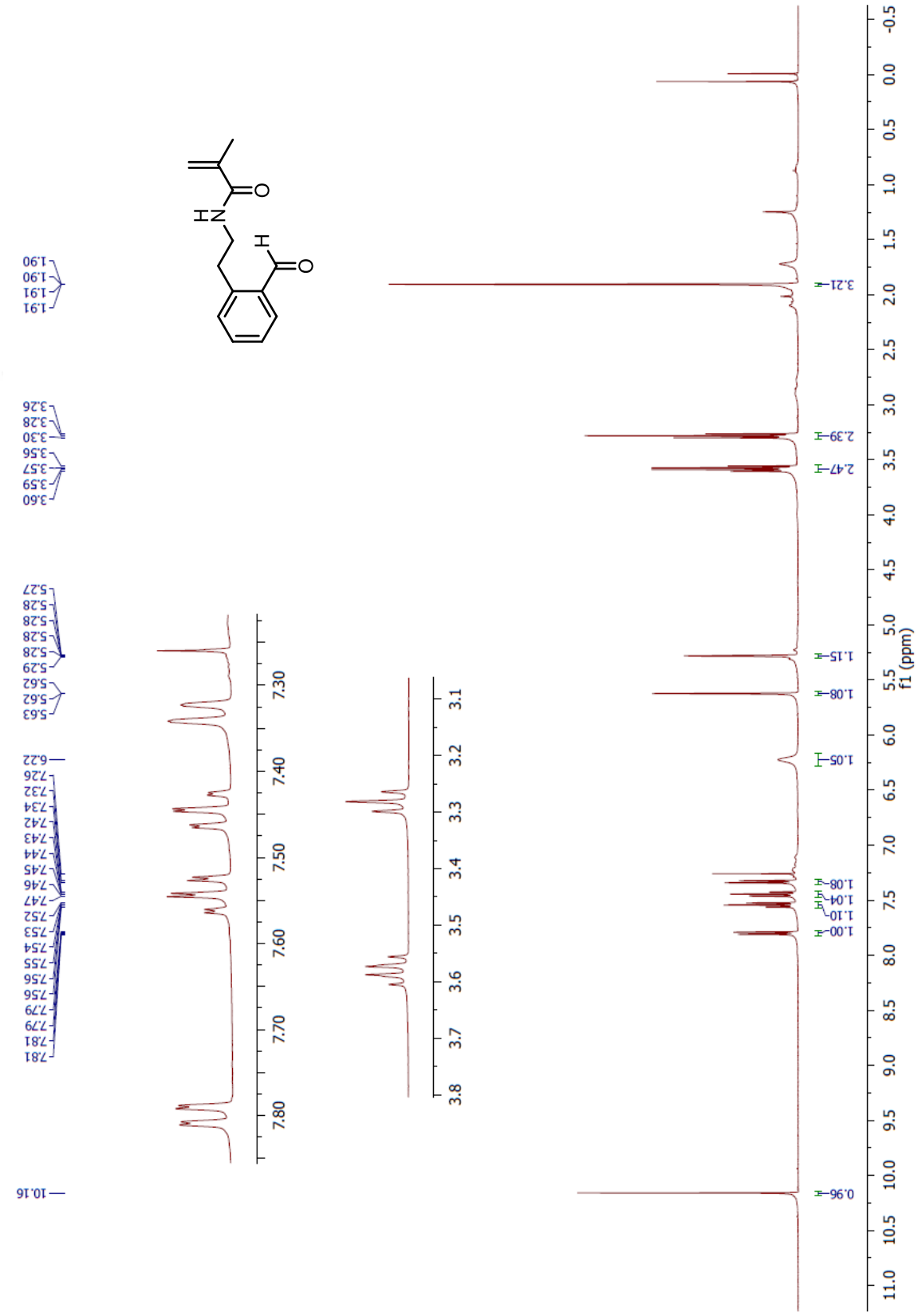

Figure 24. ^{1}H-NMR spectrum of **20** in $CDCl_3$.

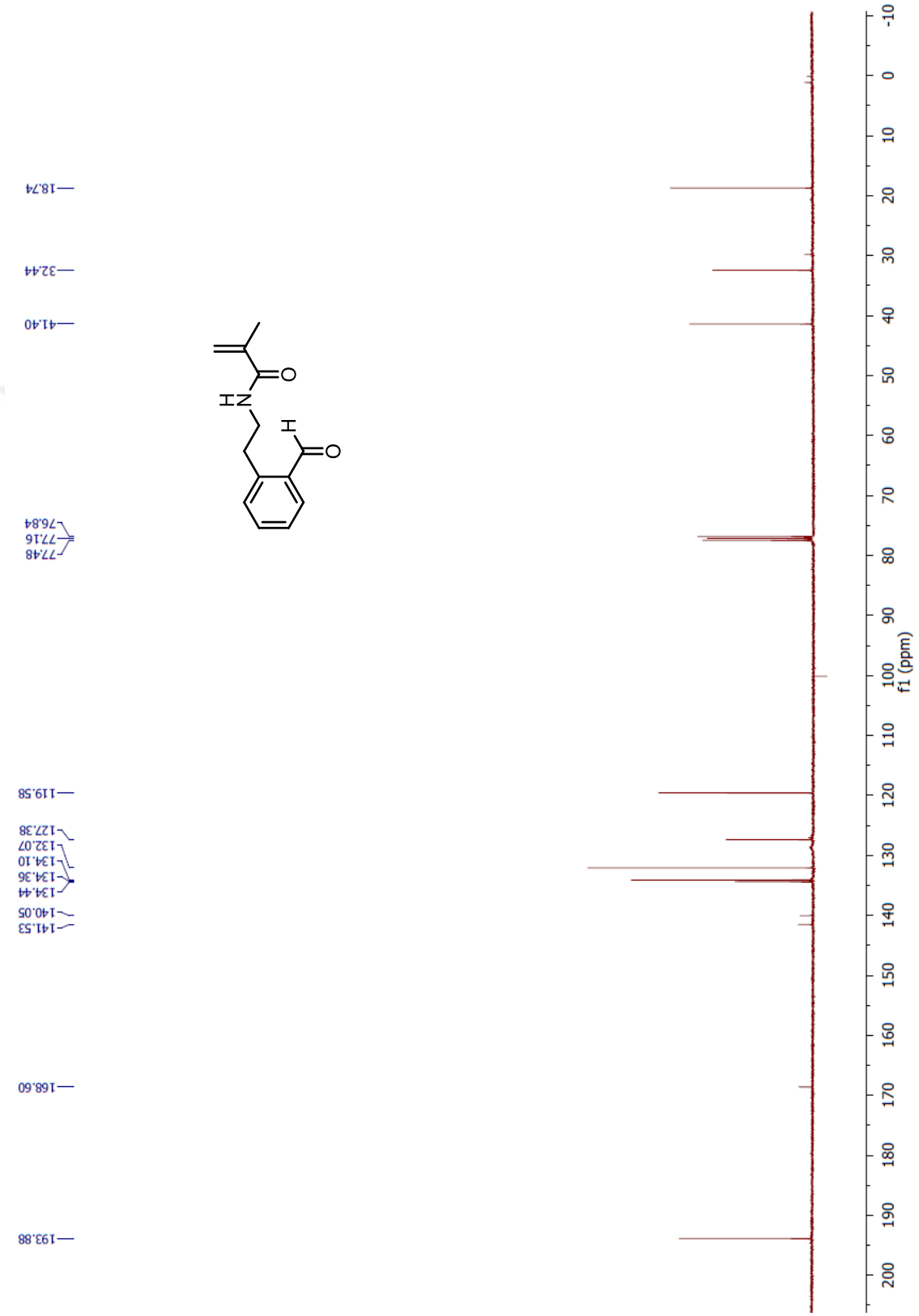

Figure 25. ^{13}C-NMR spectrum of **20** in $CDCl_3$.

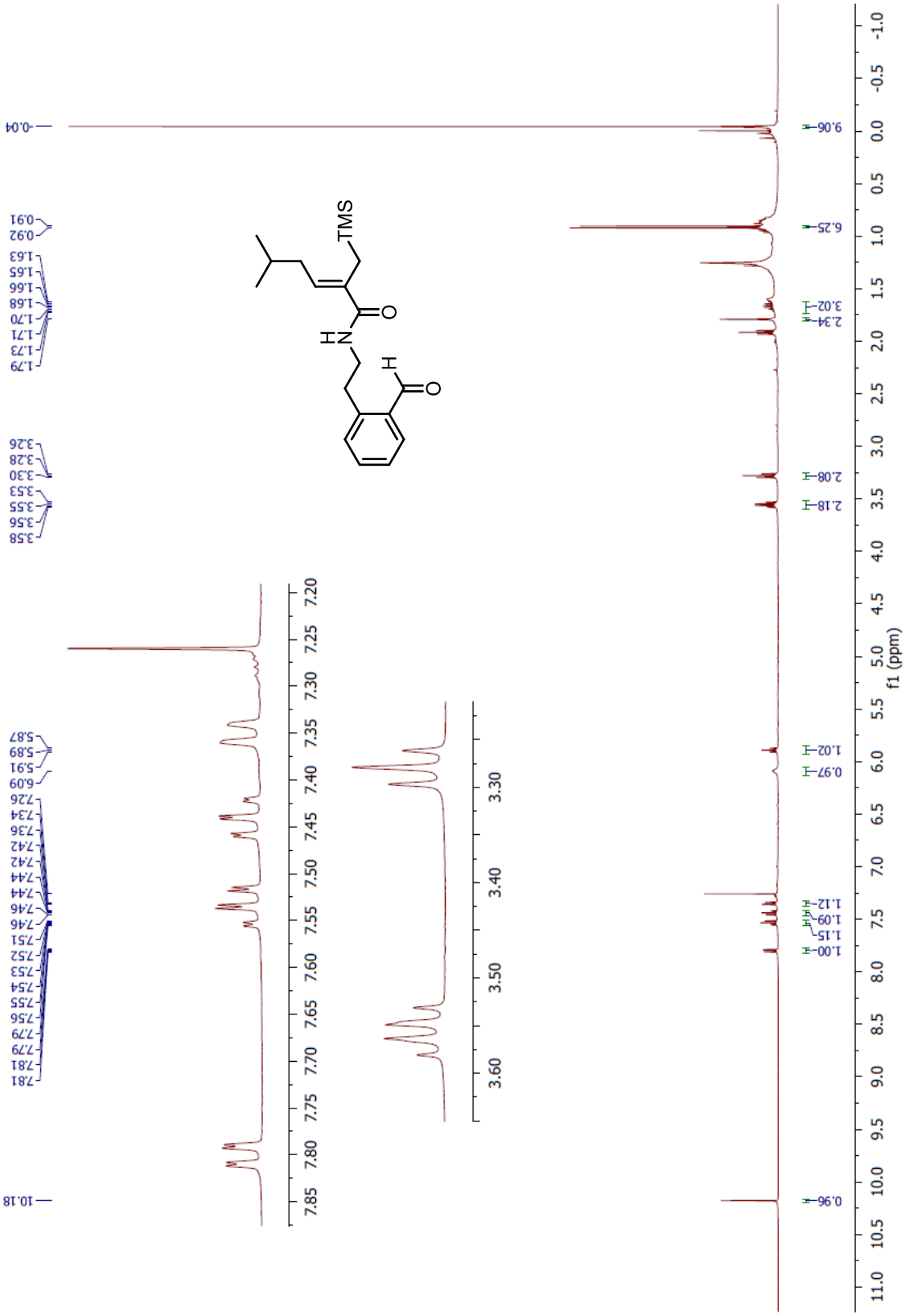

Figure 26. ^{1}H-NMR spectrum of **18** in $CDCl_3$.

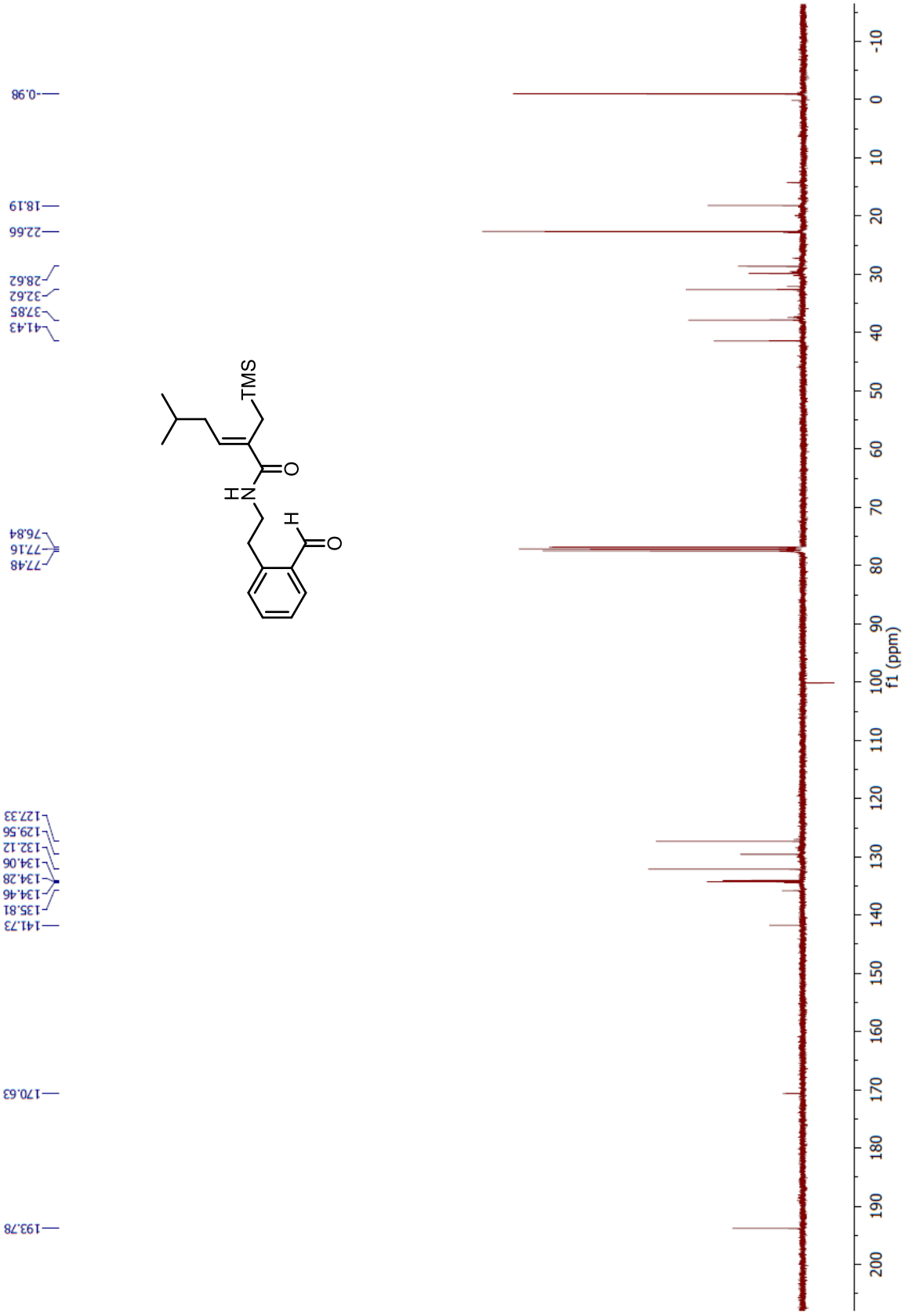

Figure 27. ^{13}C-NMR spectrum of **18** in $CDCl_3$.

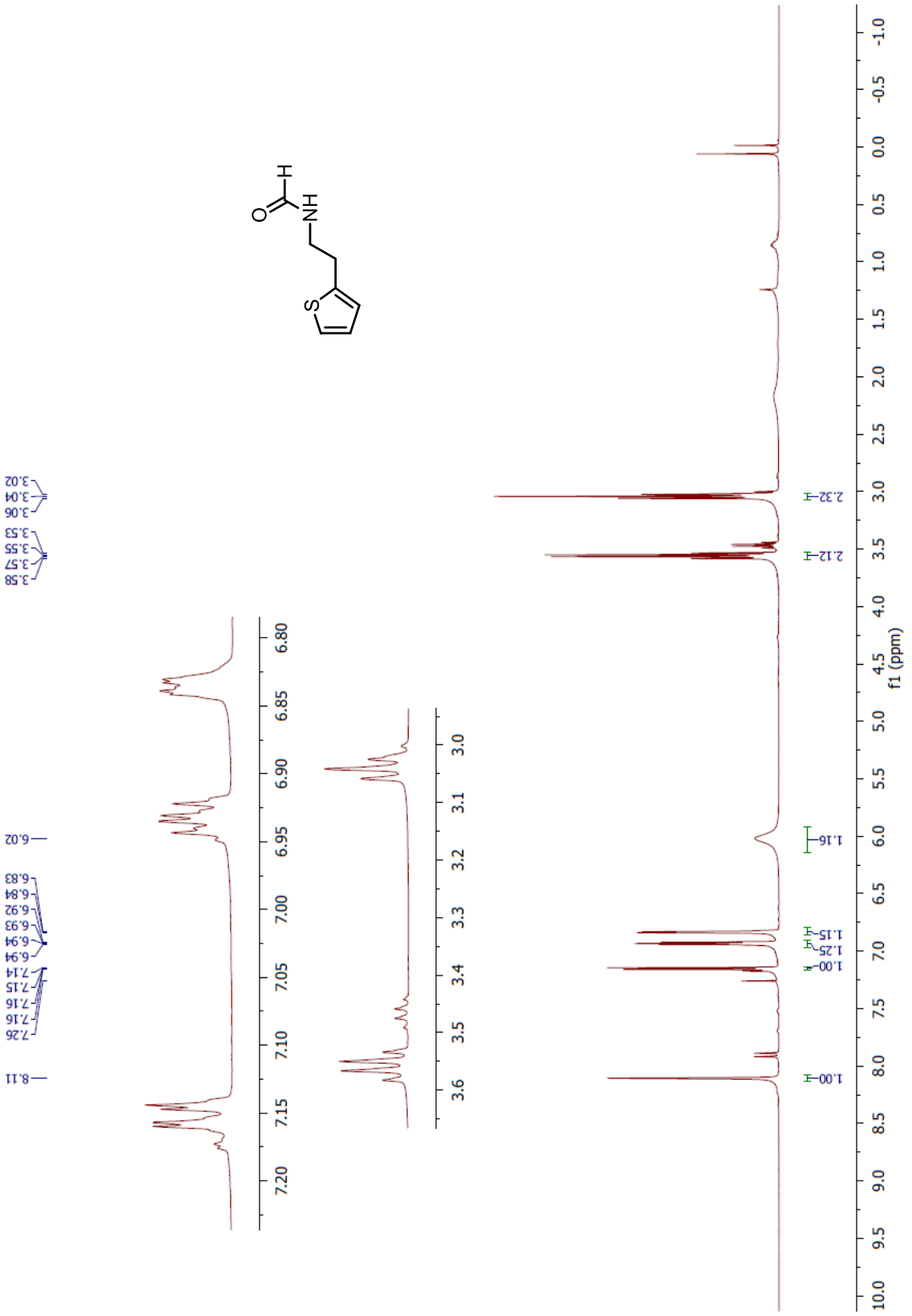

Figure 28. ^{1}H-NMR spectrum of **31** in $CDCl_3$.

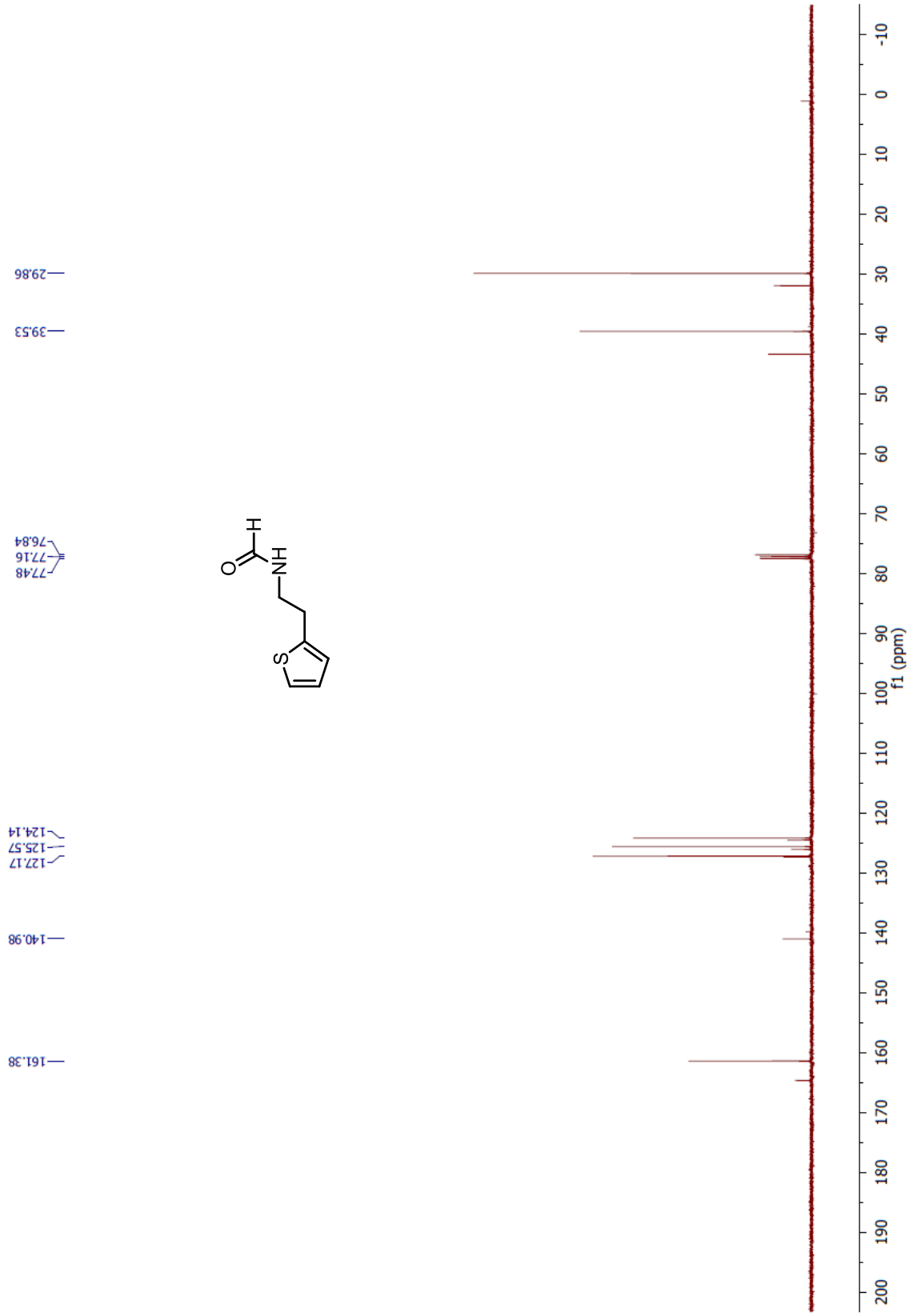

Figure 29. ^{13}C-NMR spectrum of **31** in $CDCl_3$.

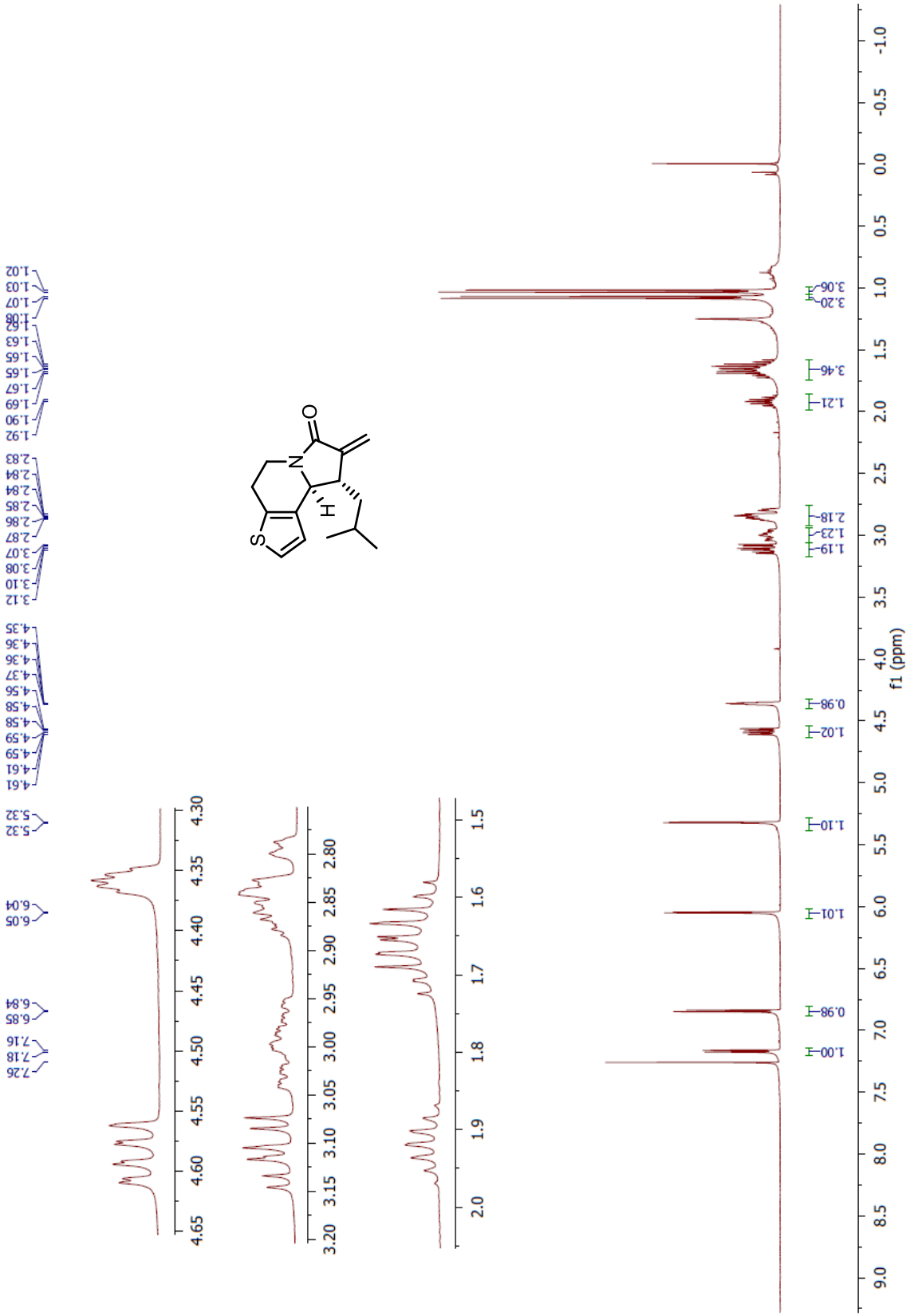

Figure 30. ^{1}H-NMR spectrum of **33** in $CDCl_3$.

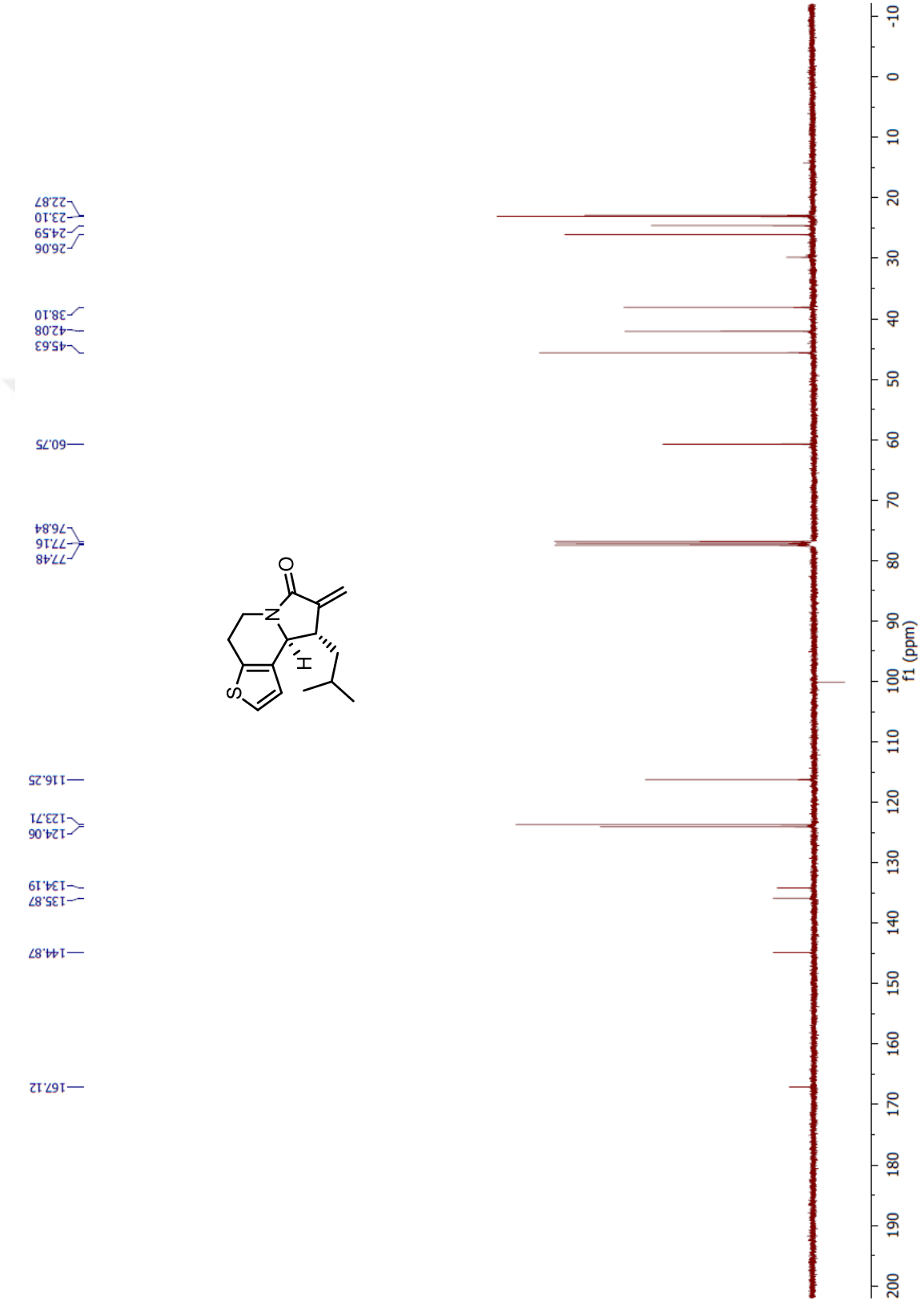

Figure 31. ^{13}C-NMR spectrum of **33** in $CDCl_3$.

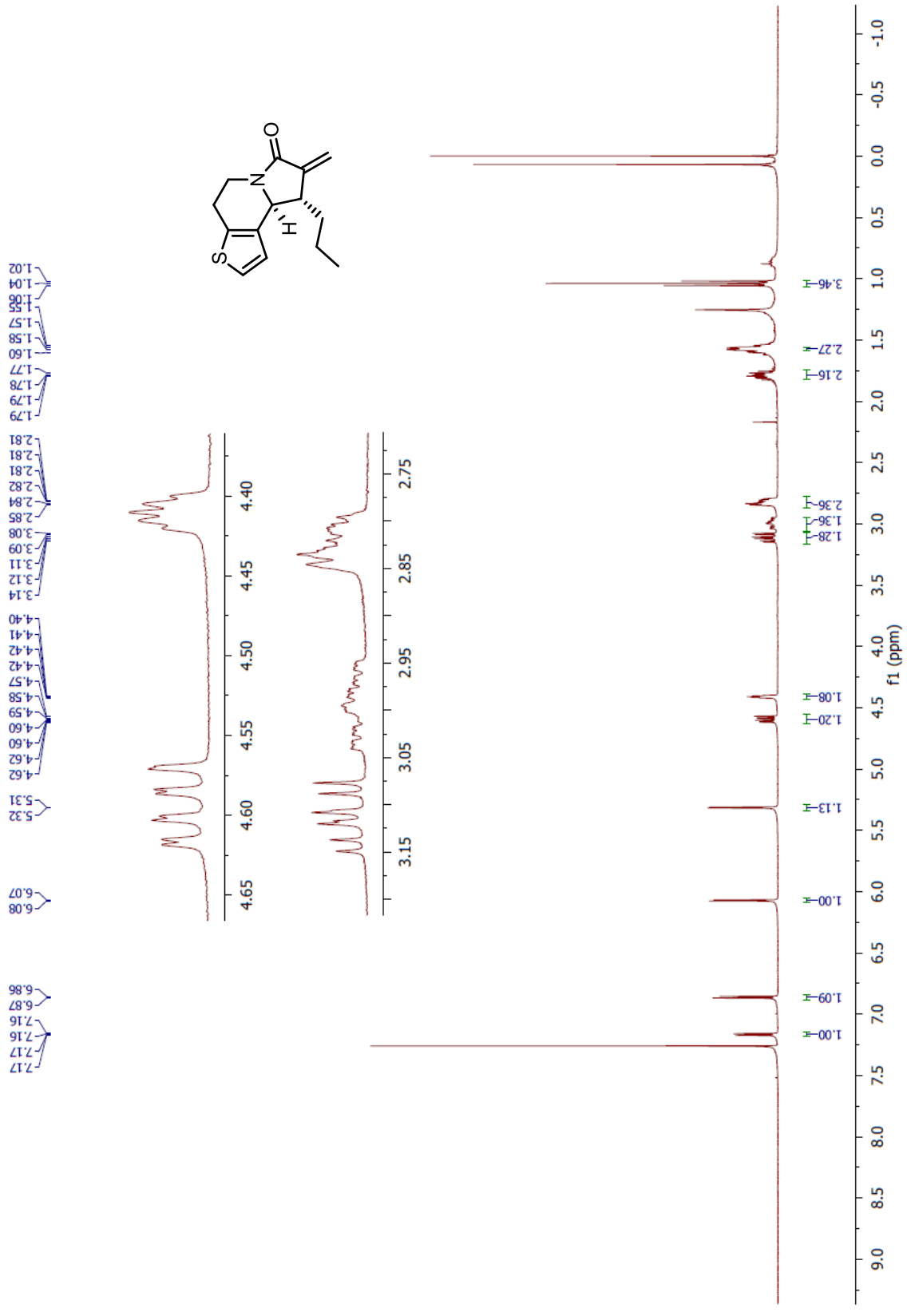

Figure 32. ^{1}H-NMR spectrum of **34** in $CDCl_3$.

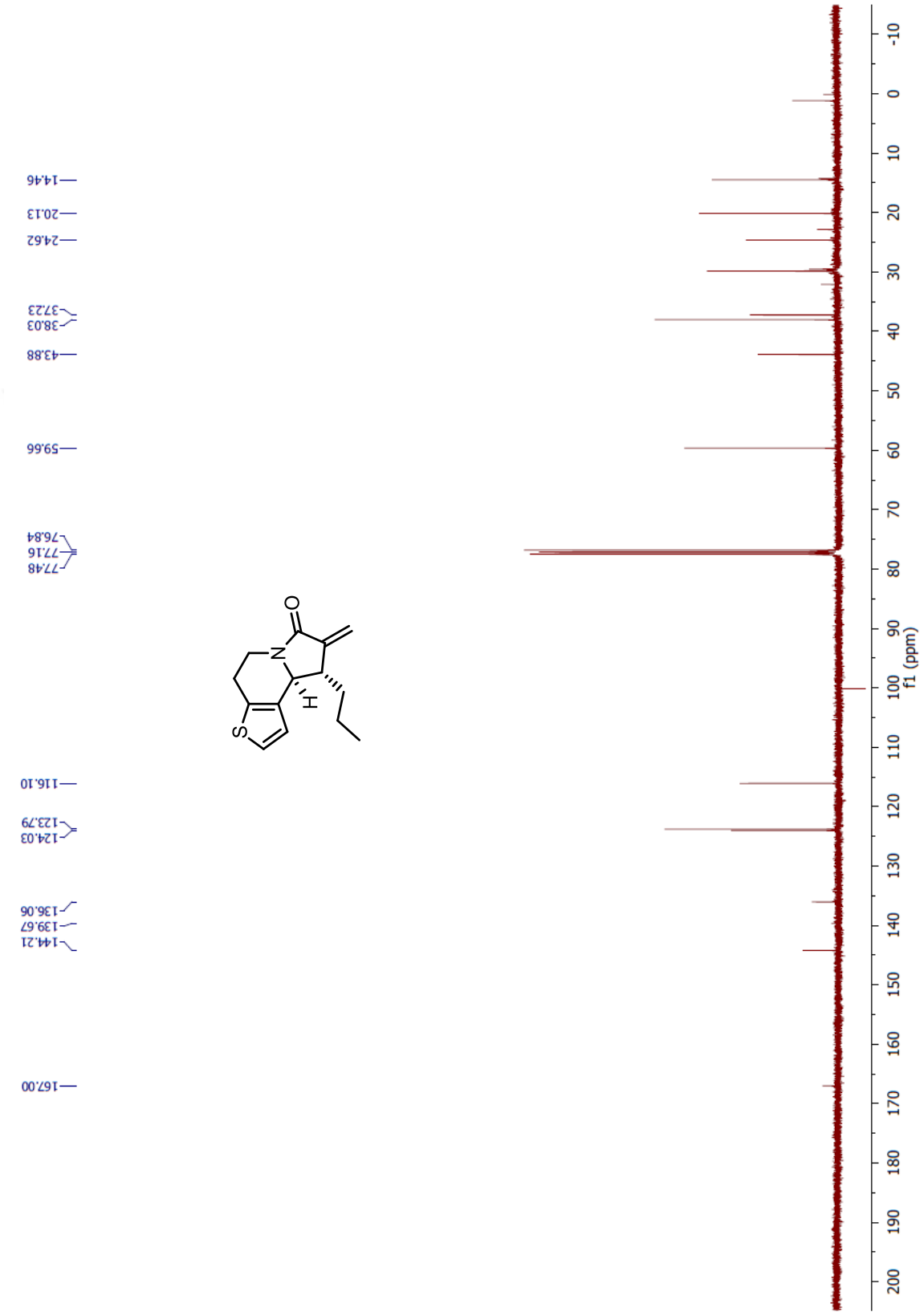

Figure 33. ^{13}C-NMR spectrum of **34** in $CDCl_3$.

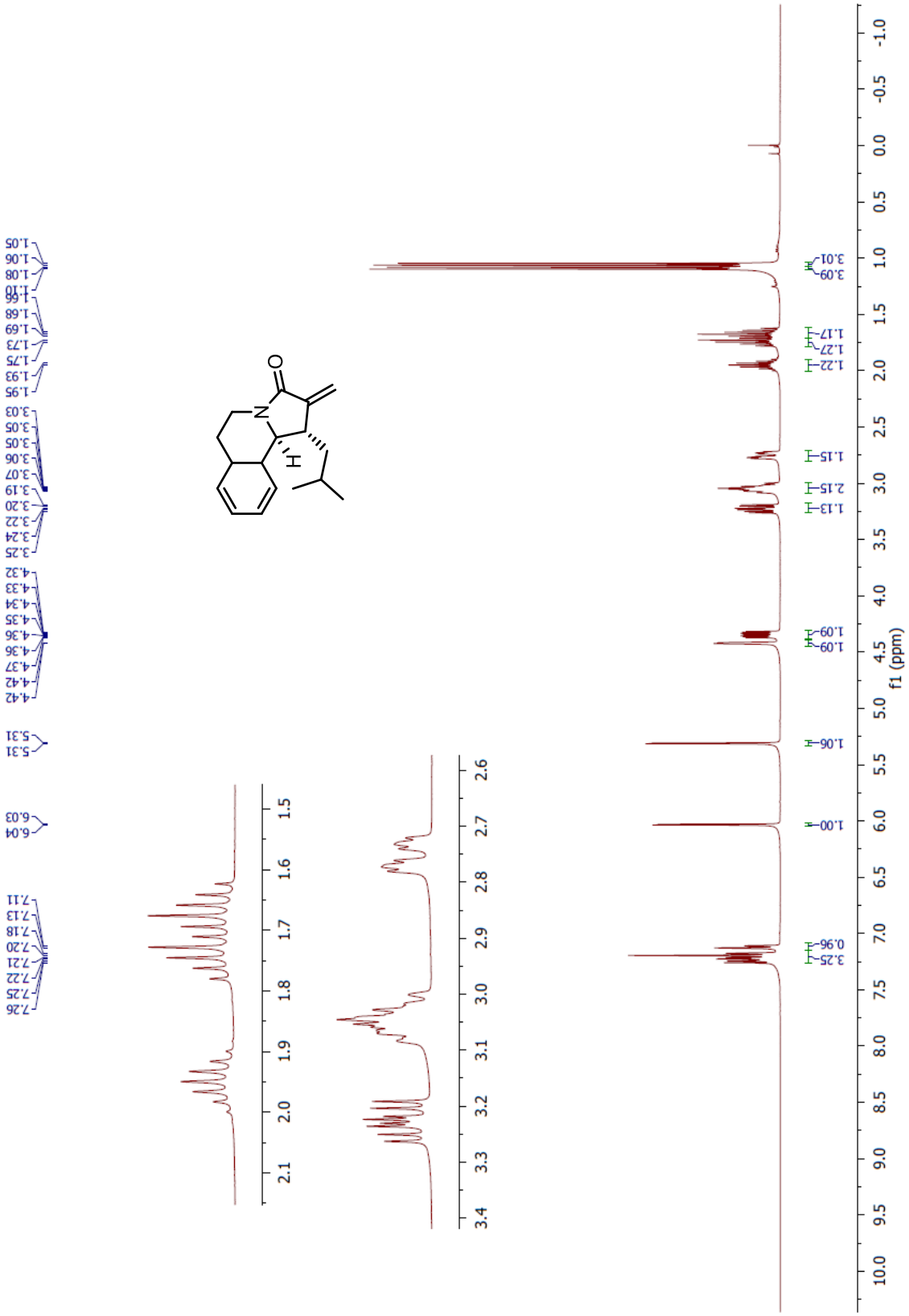

Figure 34. ^{1}H-NMR spectrum of **24** in $CDCl_3$.

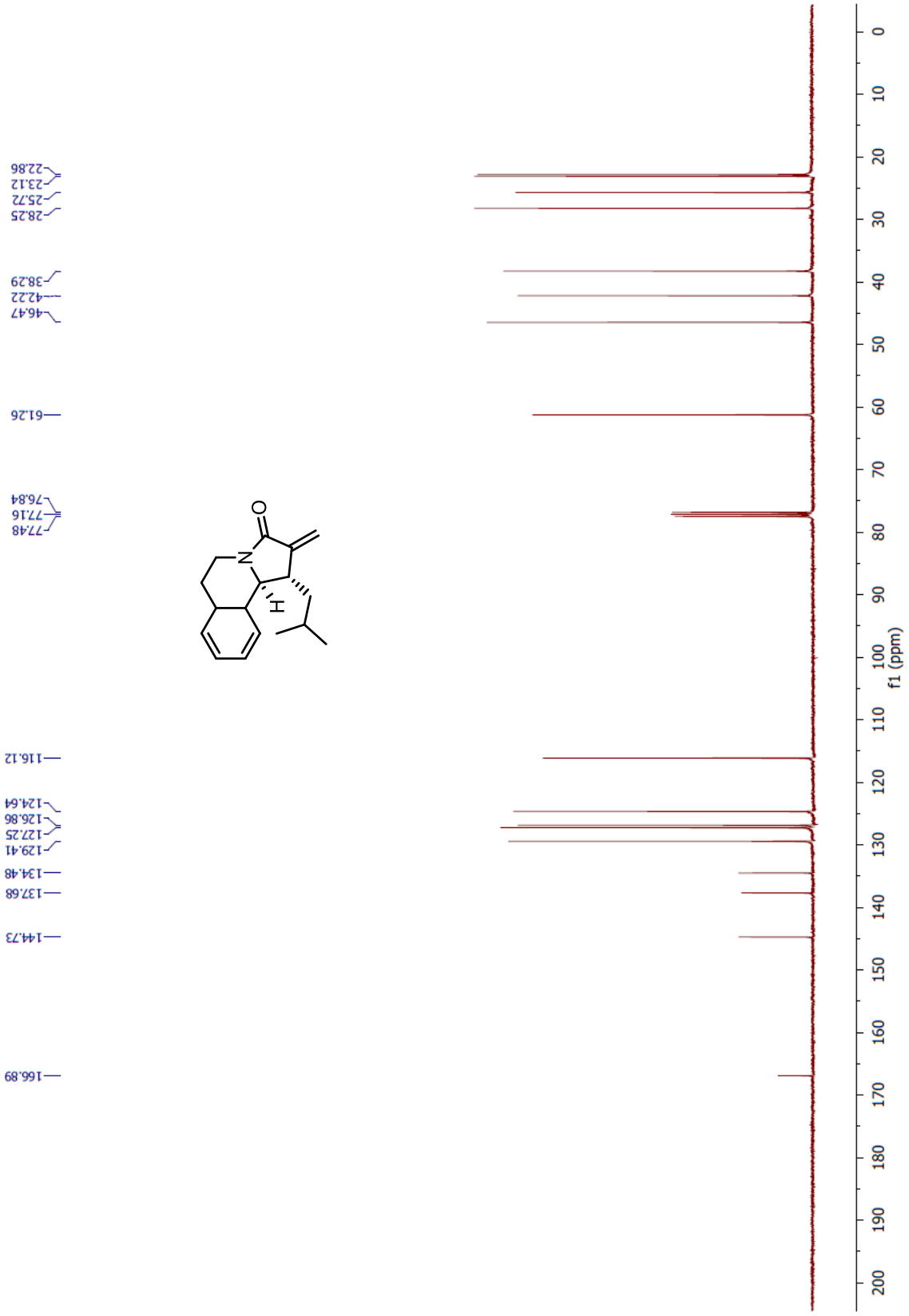

Figure 35. ^{13}C-NMR spectrum of **24** in $CDCl_3$.

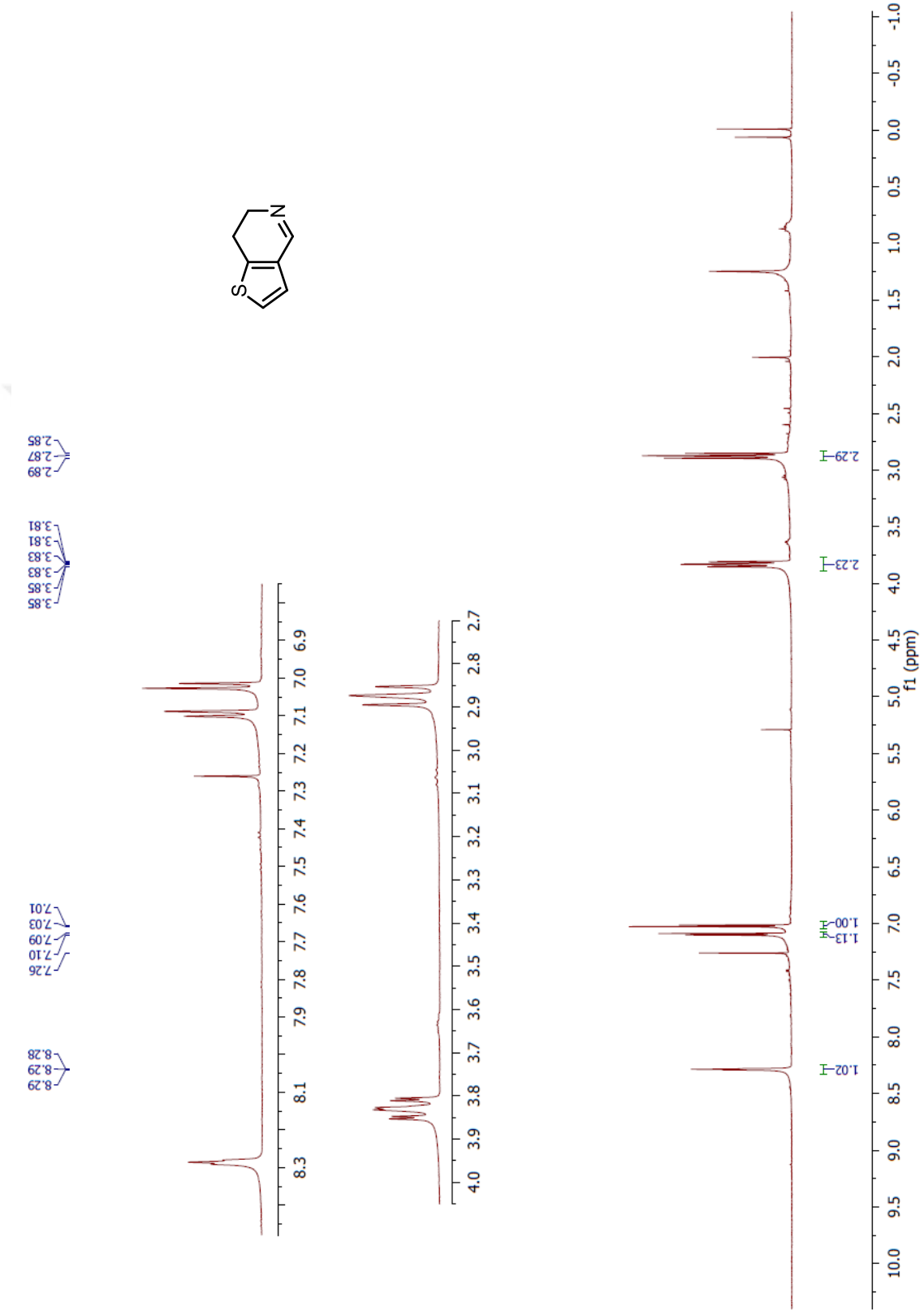

Figure 36. ^{1}H-NMR spectrum of **32** in $CDCl_3$.

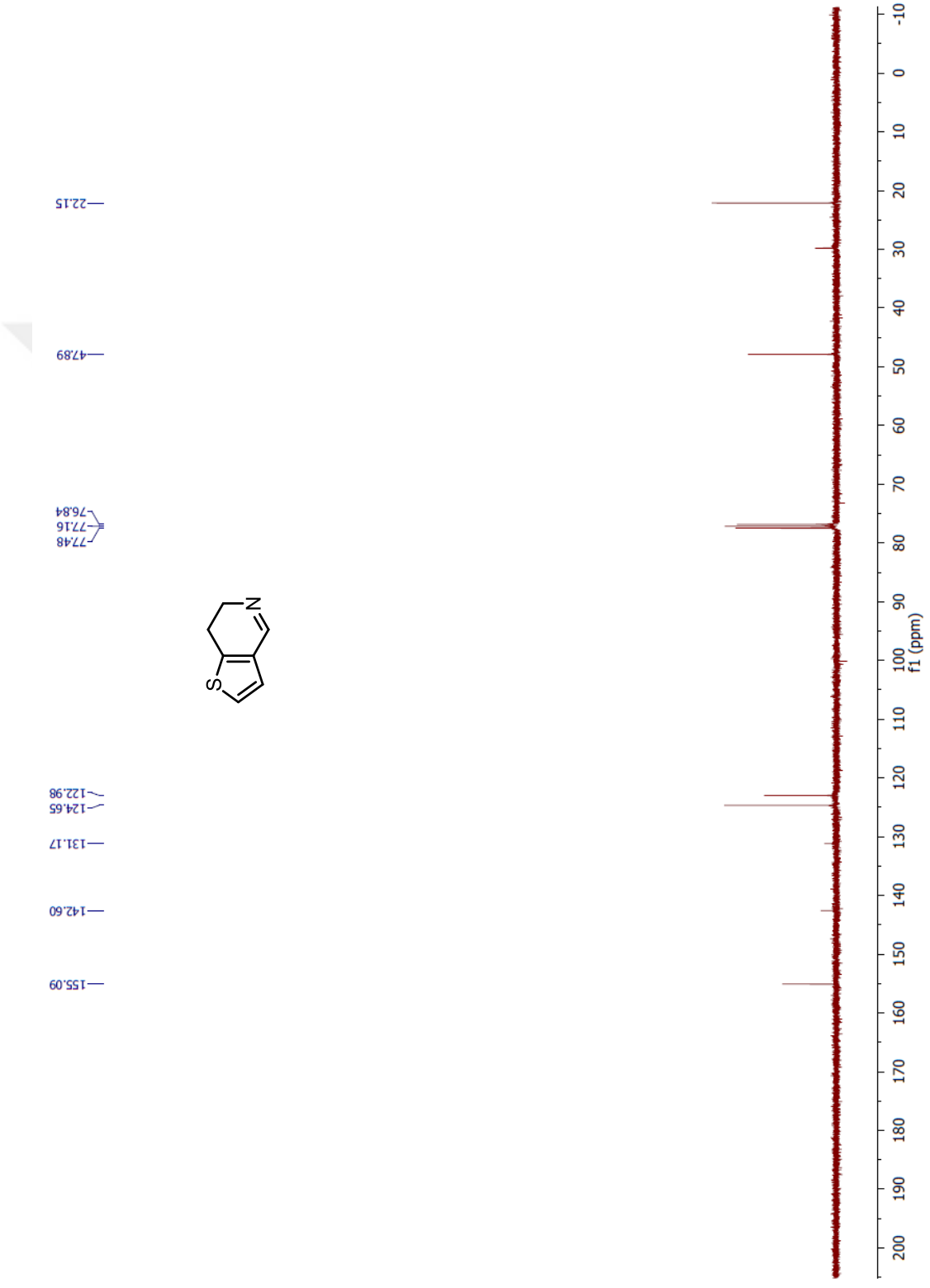

Figure 37. ^{13}C-NMR spectrum of **32** in $CDCl_3$.

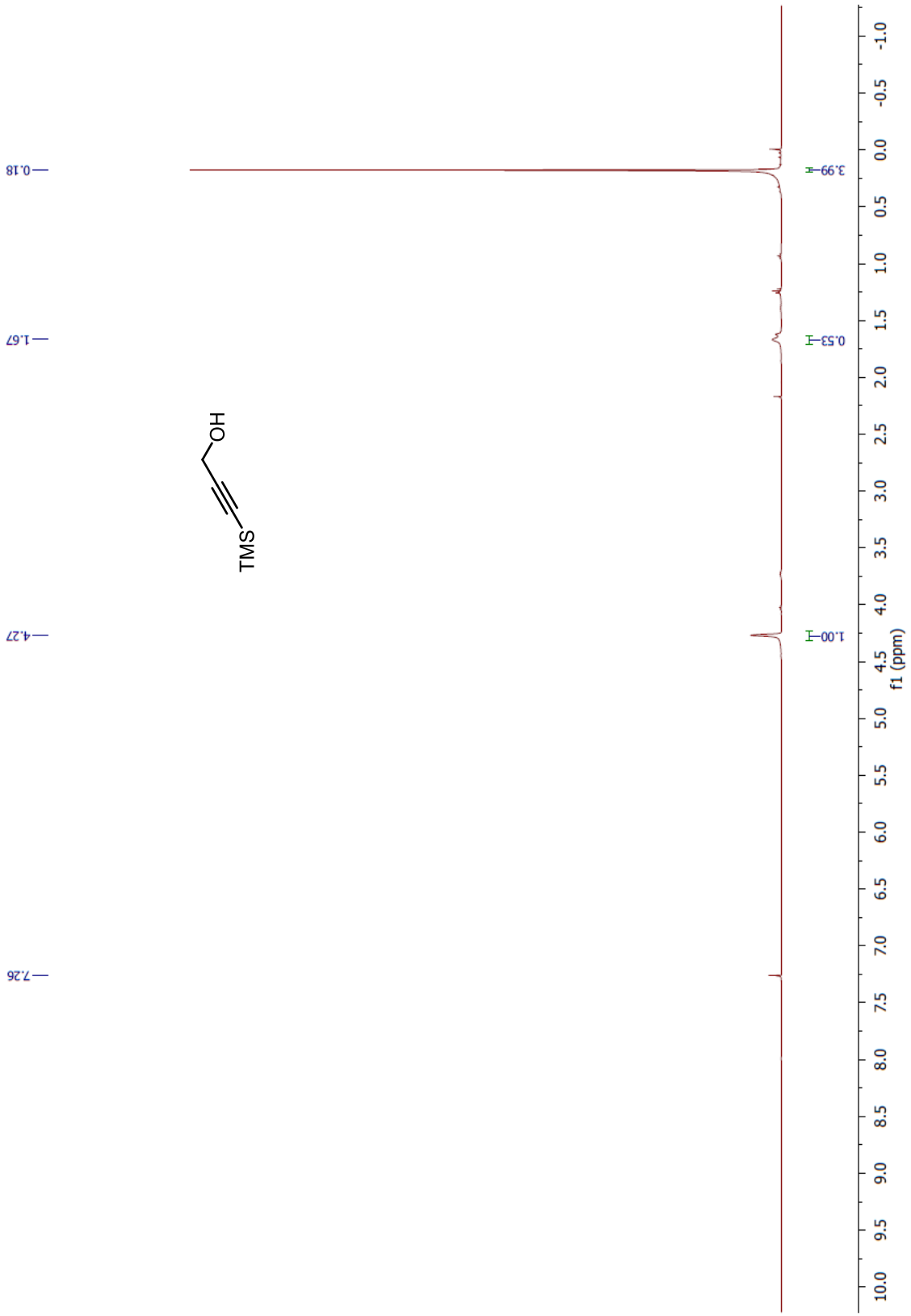

Figure 38. ^{1}H-NMR spectrum of **38** in $CDCl_3$.

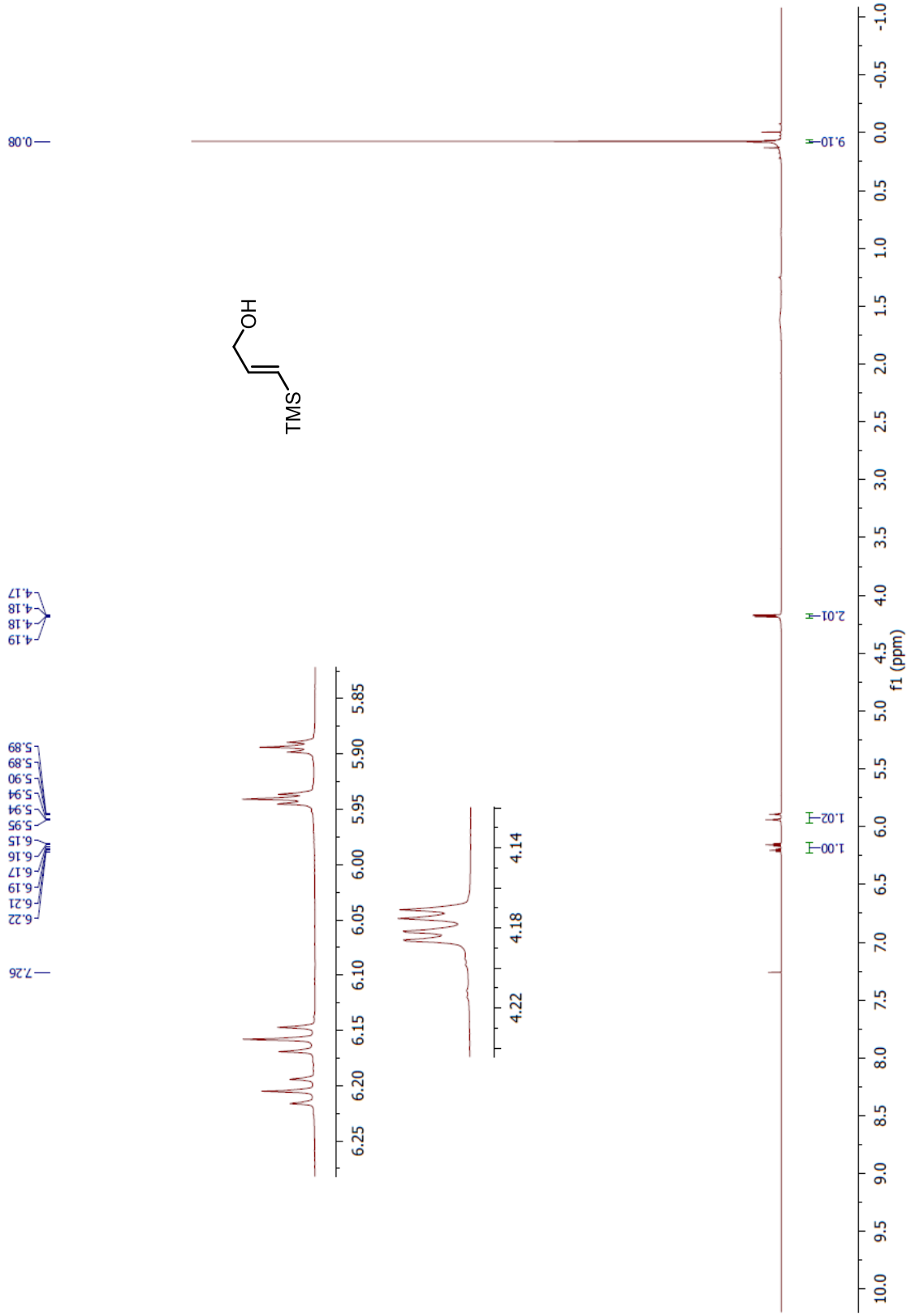

Figure 39. ^{1}H-NMR spectrum of **39** in $CDCl_3$.

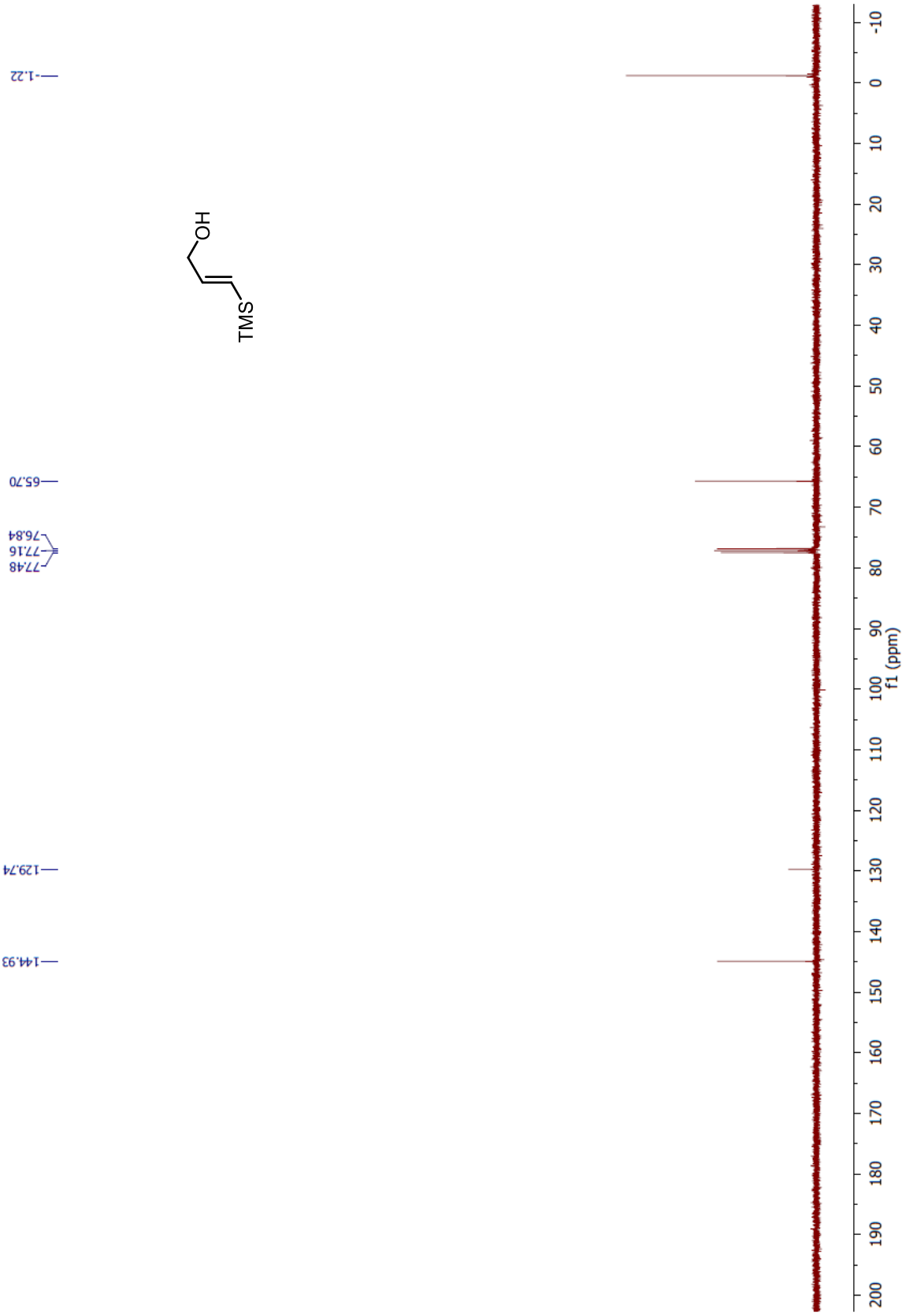

Figure 40. ^{13}C-NMR spectrum of **39** in $CDCl_3$.

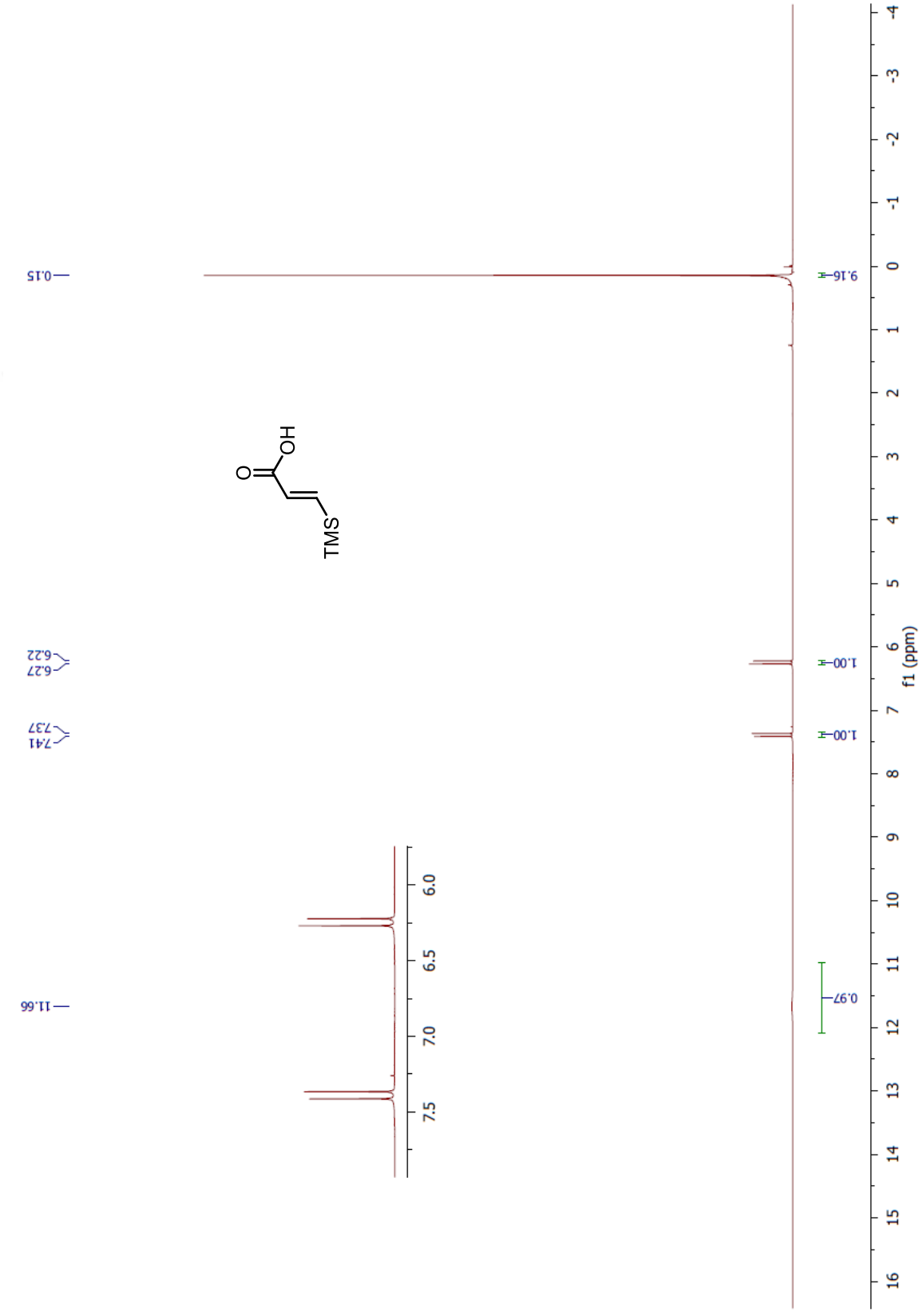

Figure 41. ^{1}H-NMR spectrum of **40** in $CDCl_3$.

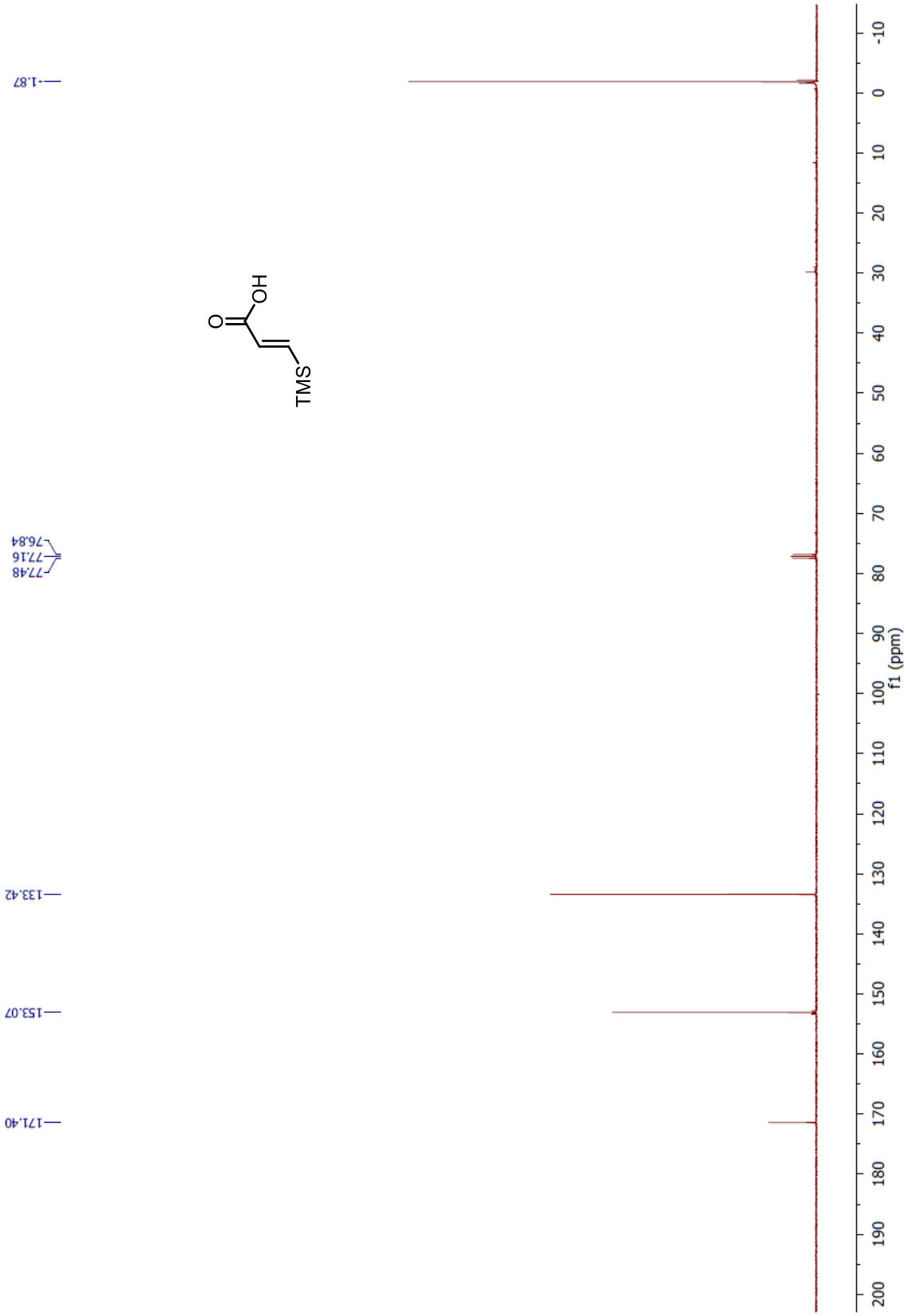

Figure 42. ^{13}C-NMR spectrum of **40** in $CDCl_3$.

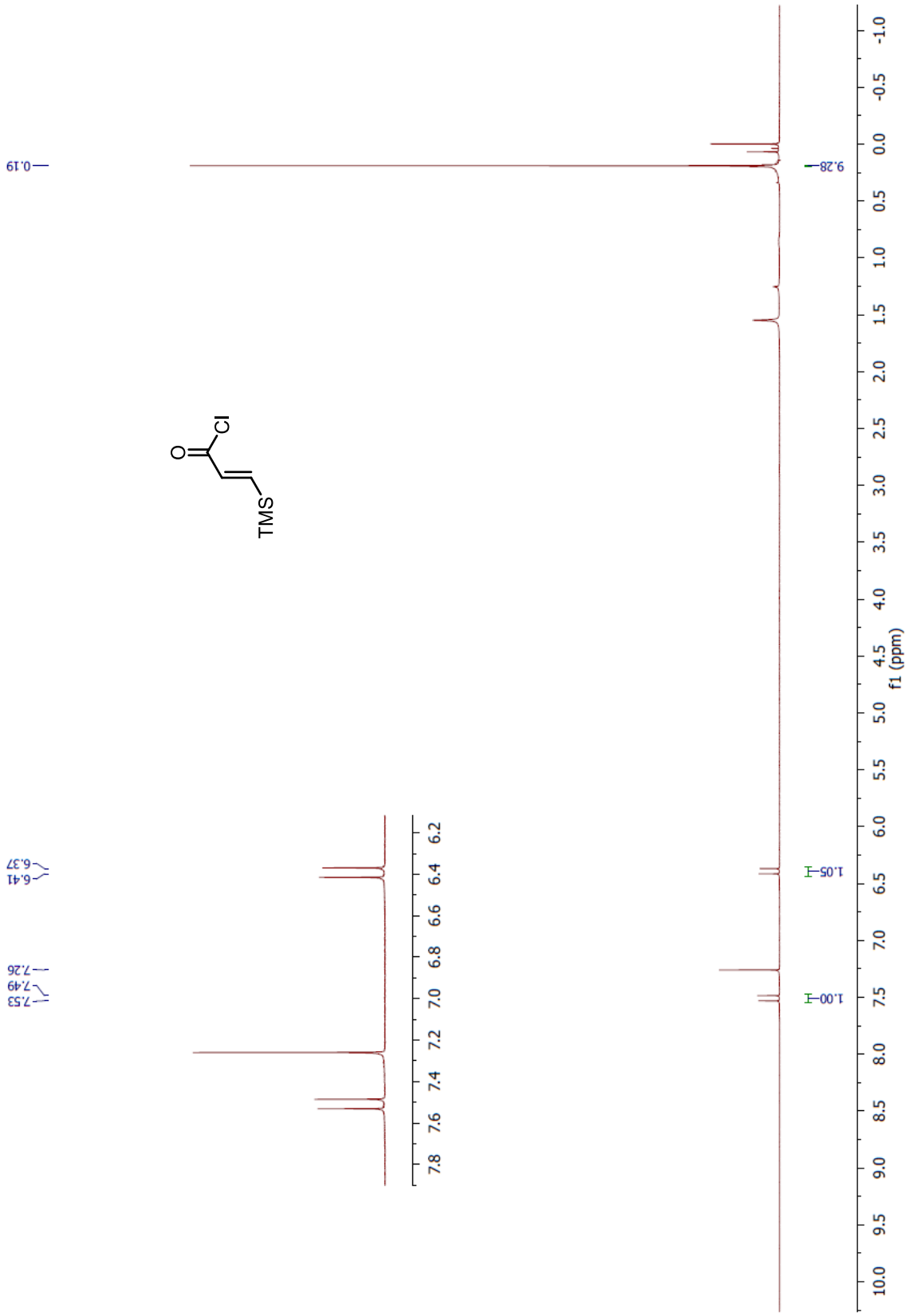

Figure 43. ^{1}H-NMR spectrum of **41** in $CDCl_3$.

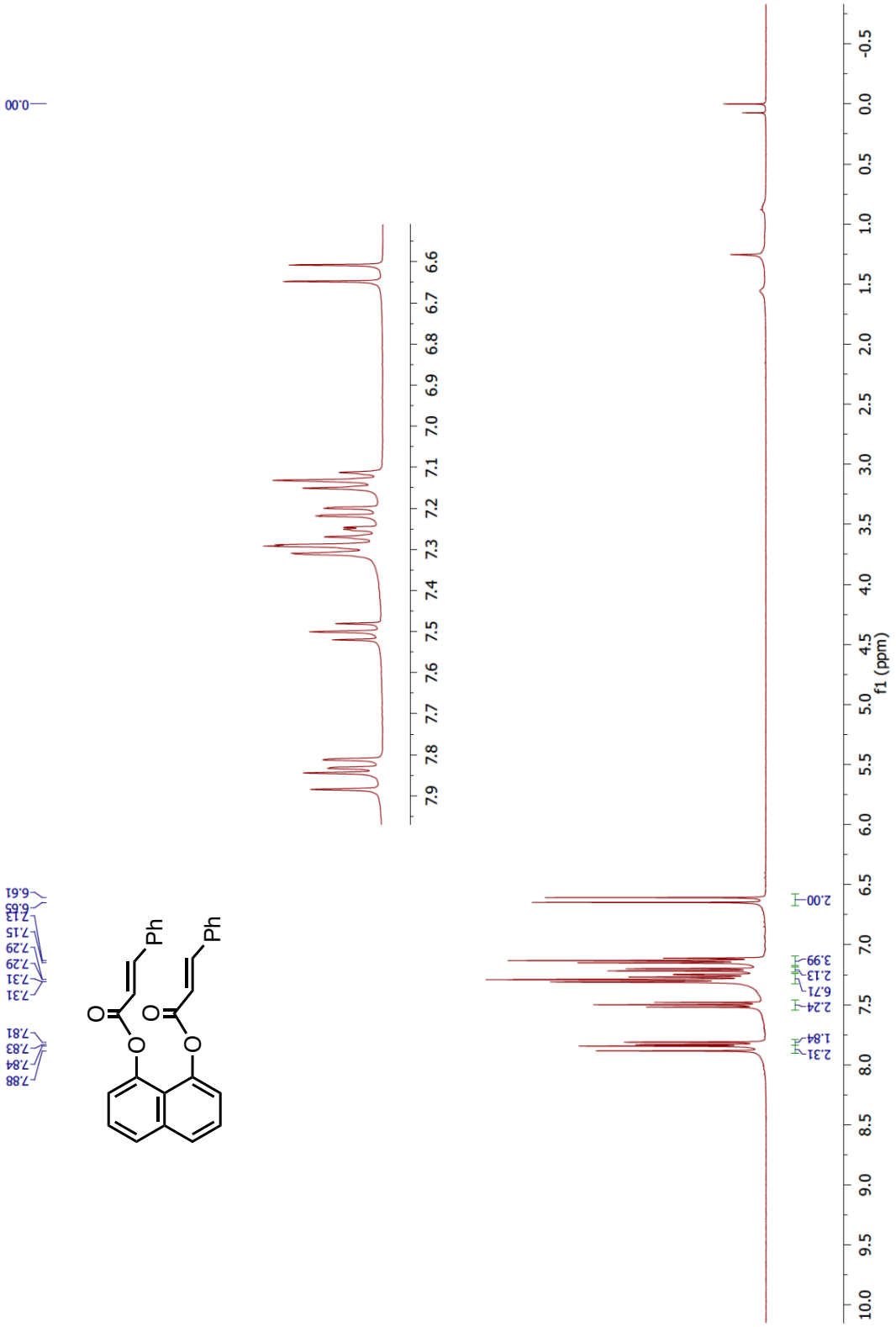

Figure 44. ^{1}H-NMR spectrum of **44** in $CDCl_3$.

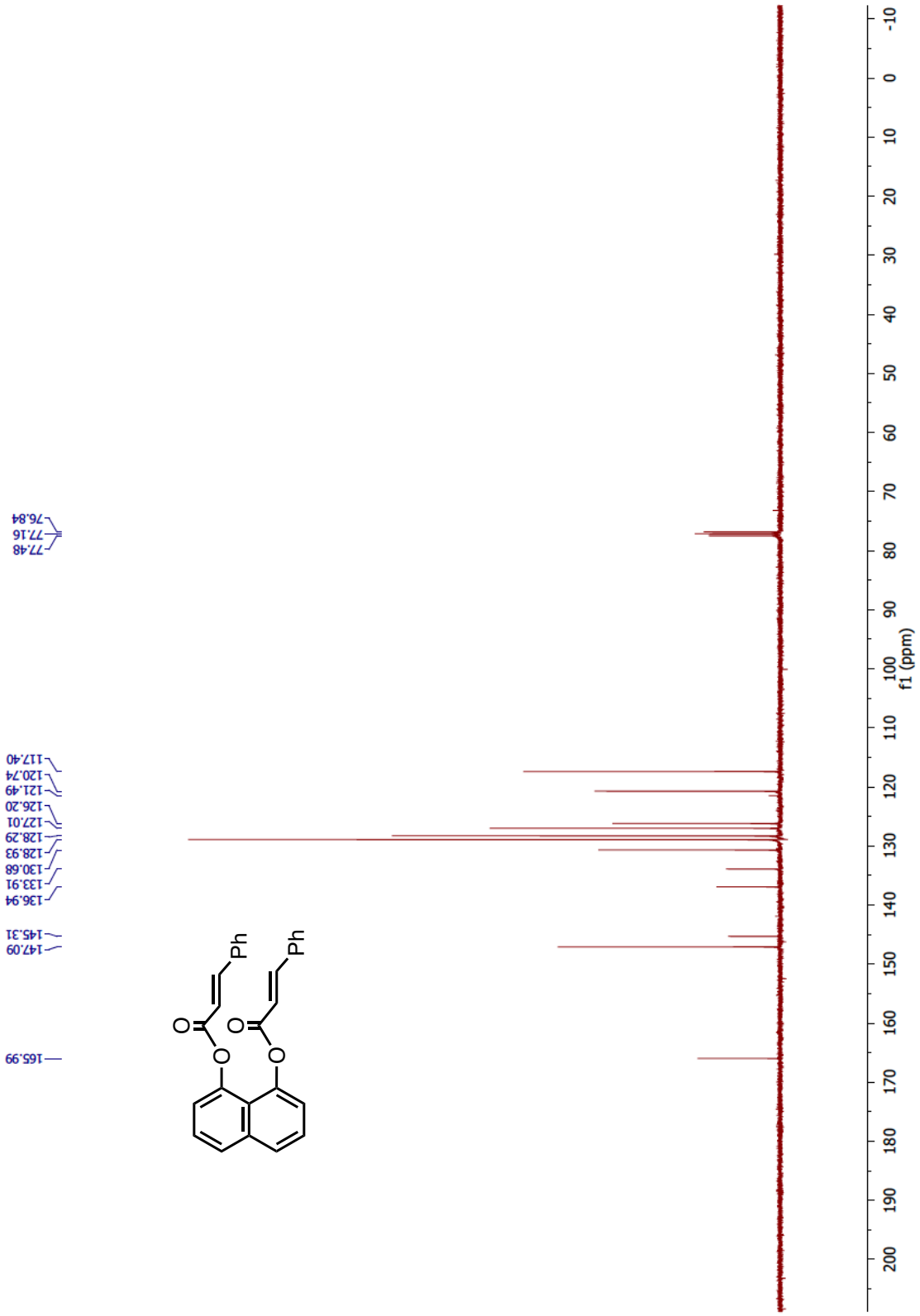

Figure 45. ^{13}C-NMR spectrum of **44** in $CDCl_3$.

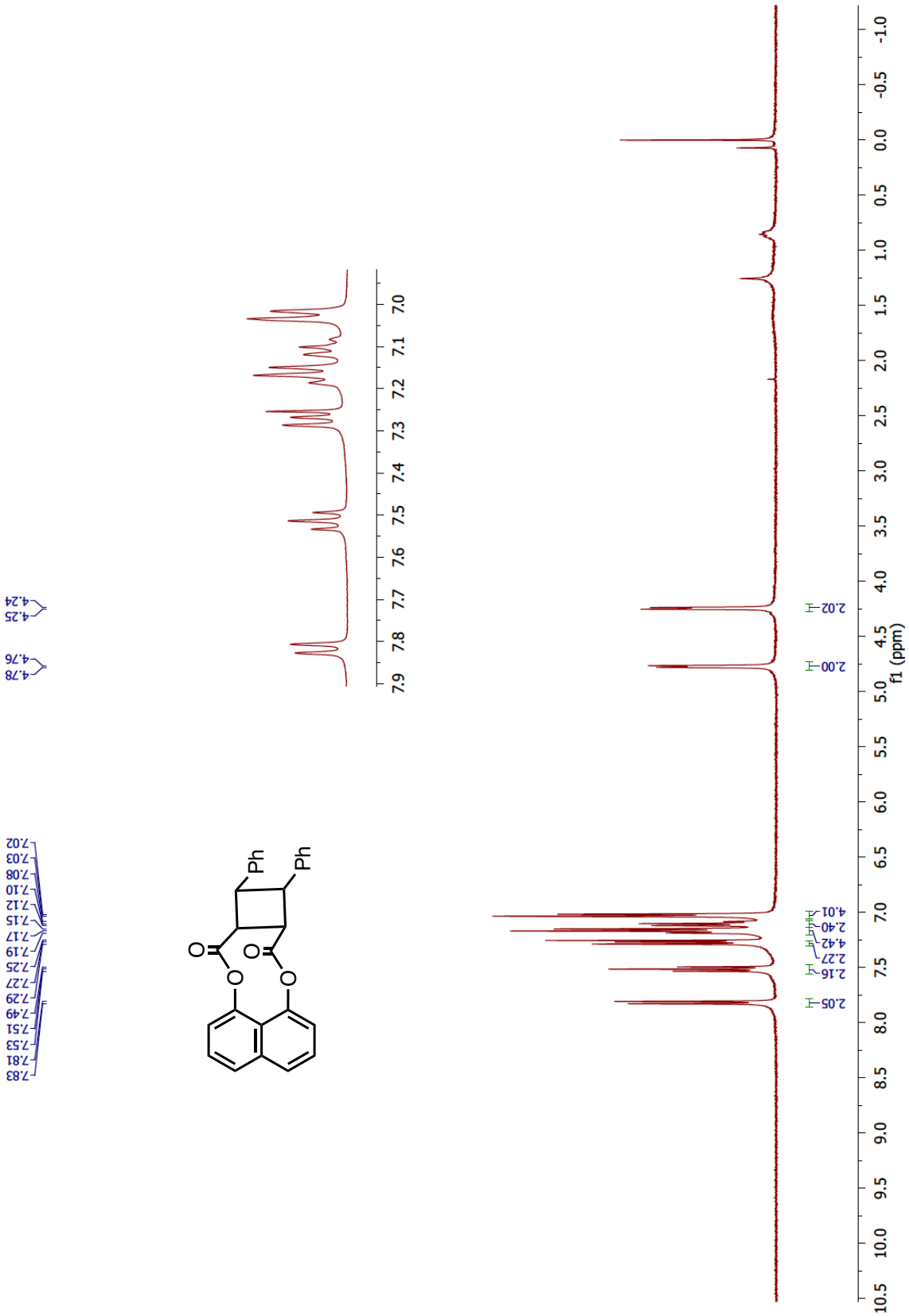

Figure 46. ^{1}H-NMR spectrum of **50** in $CDCl_3$.

Figure 47. ^{13}C-NMR spectrum of **50** in $CDCl_3$.

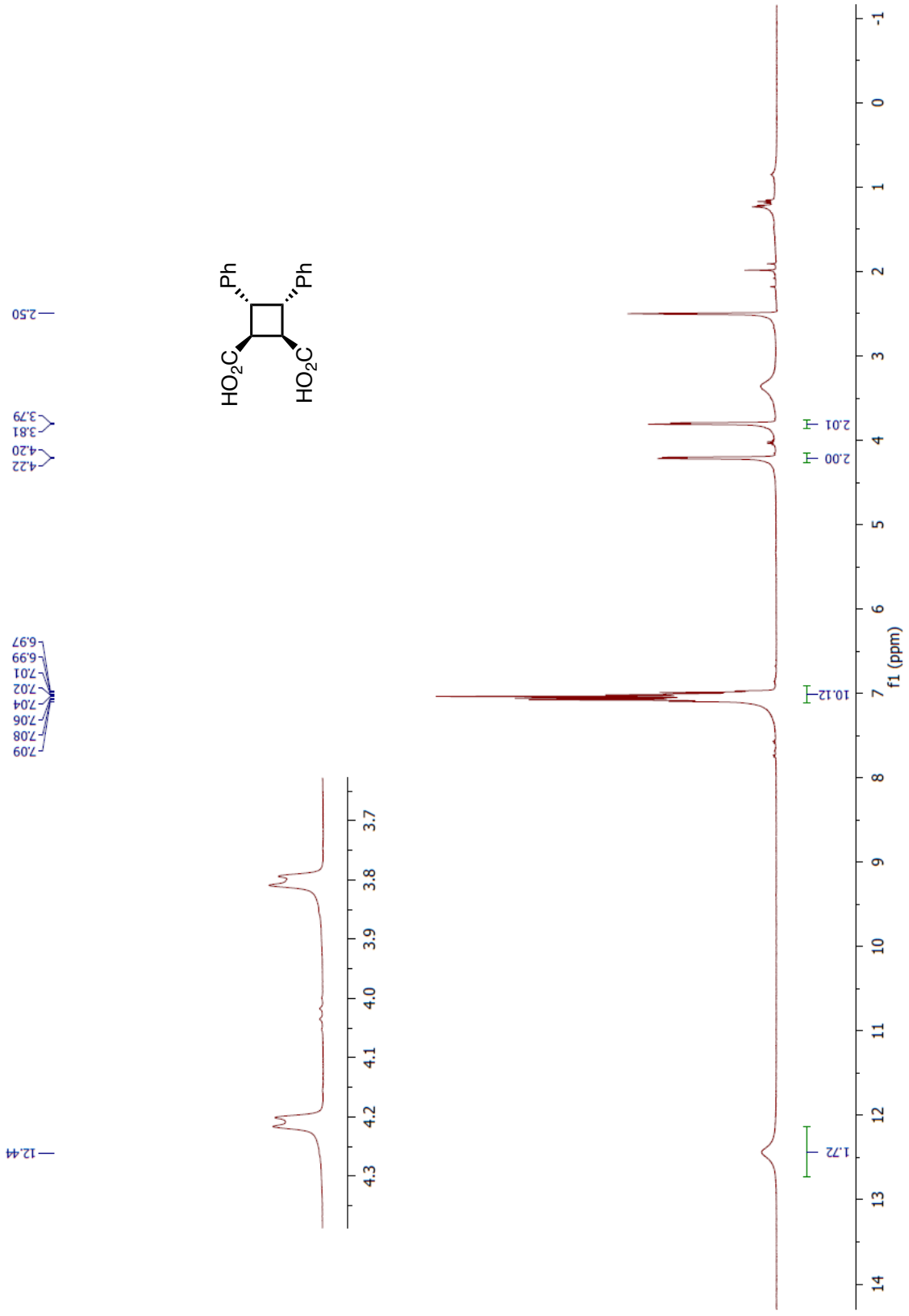

Figure 48. ^{1}H-NMR spectrum of **54** in DMSO-d^{6}.

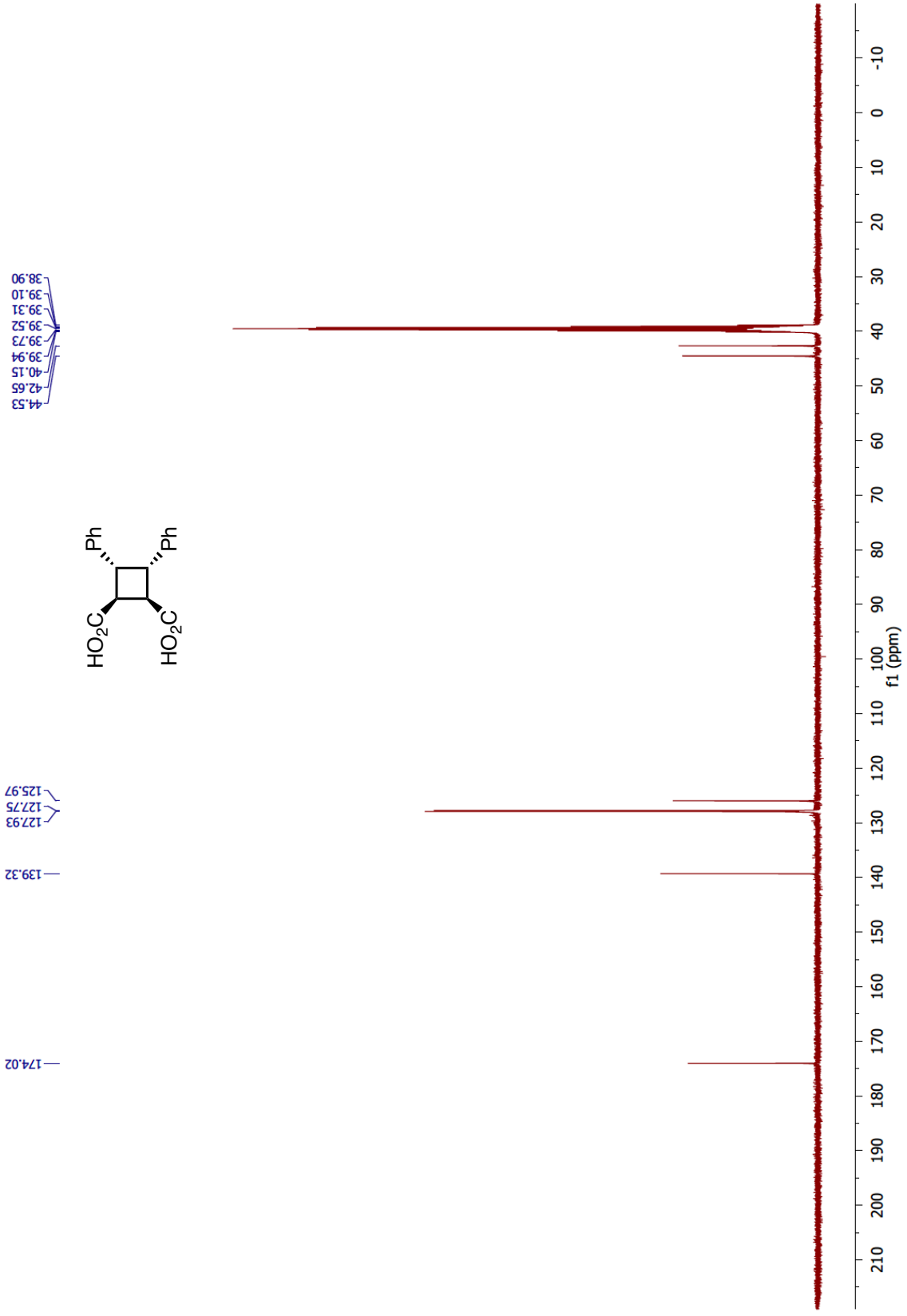

Figure 49. ^{13}C-NMR spectrum of **54** in DMSO-*d*^{6}.

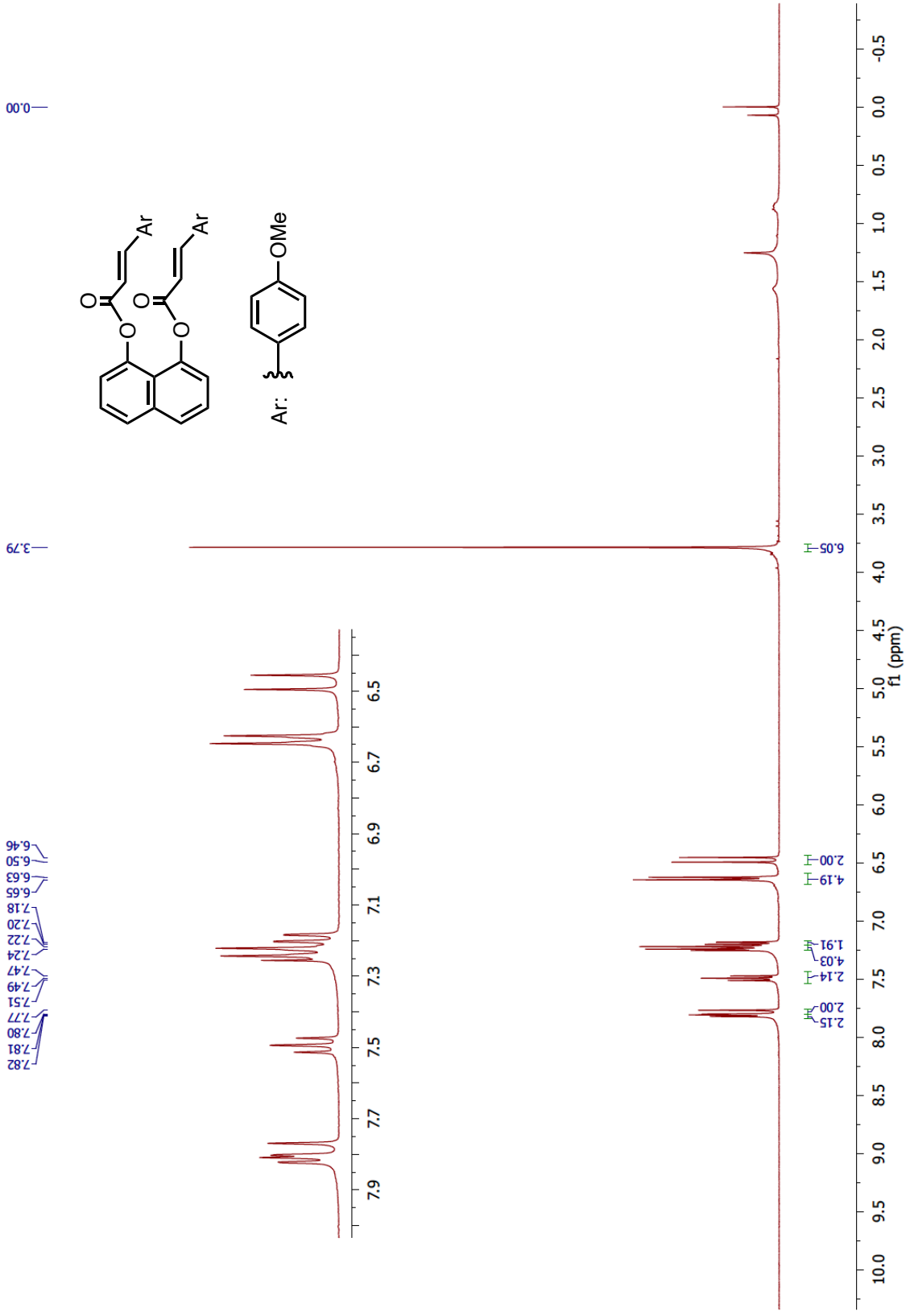

Figure 50. ^{1}H-NMR spectrum of **45** in $CDCl_3$.

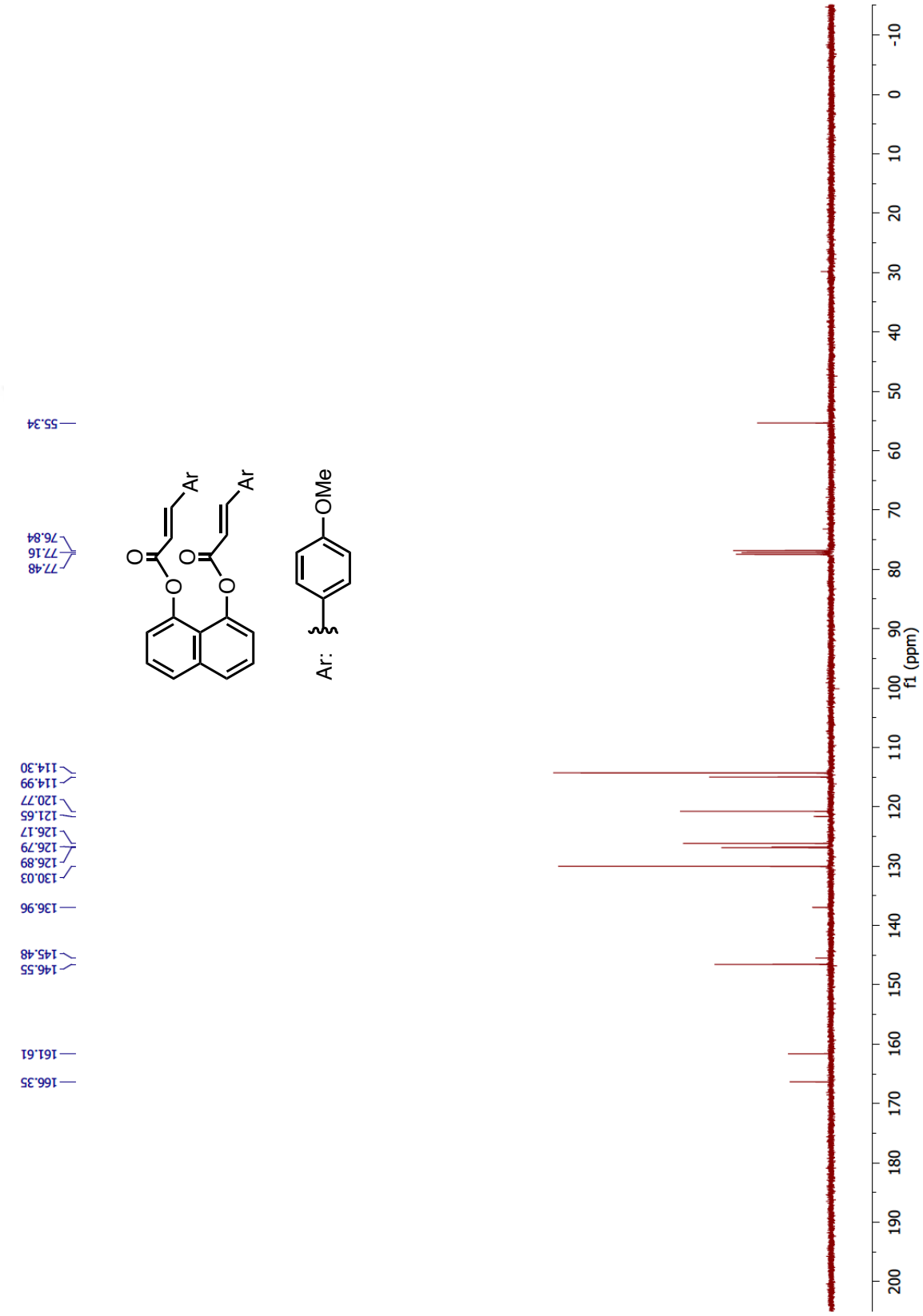

Figure 51. ^{13}C-NMR spectrum of **45** in $CDCl_3$.

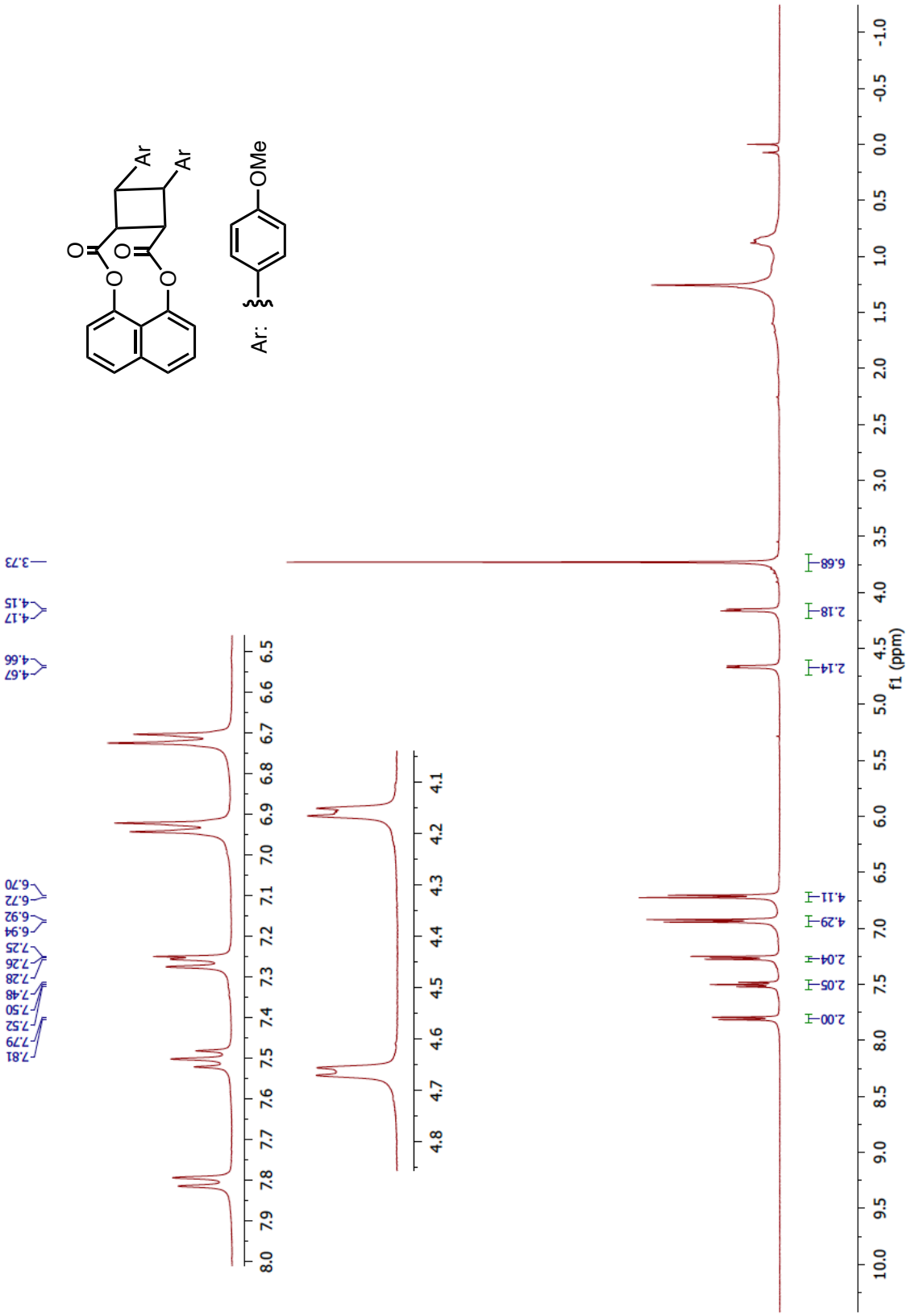

Figure 52. ^{1}H-NMR spectrum of **51** in $CDCl_3$.

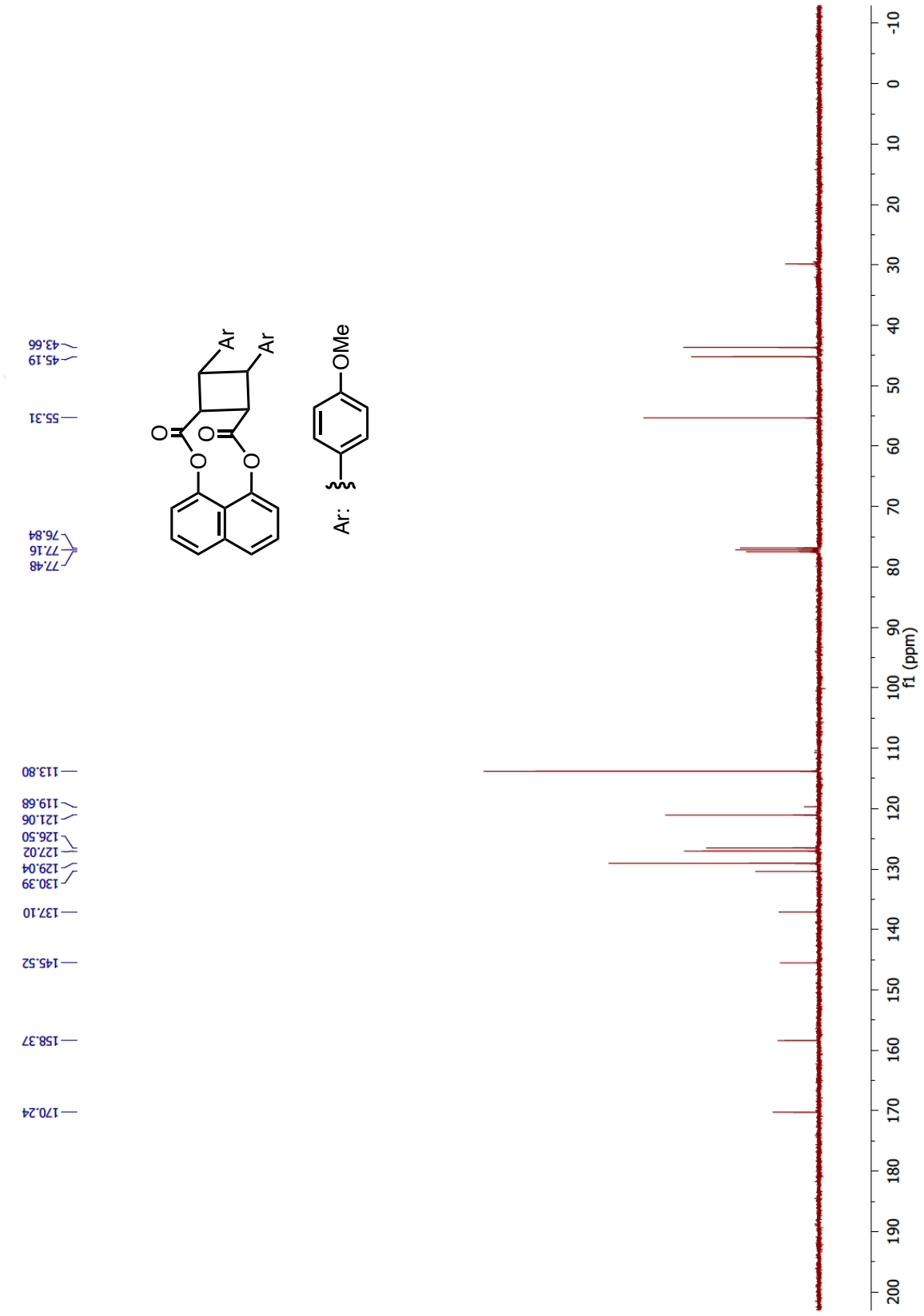

Figure 53. ^{13}C-NMR spectrum of **51** in $CDCl_3$.

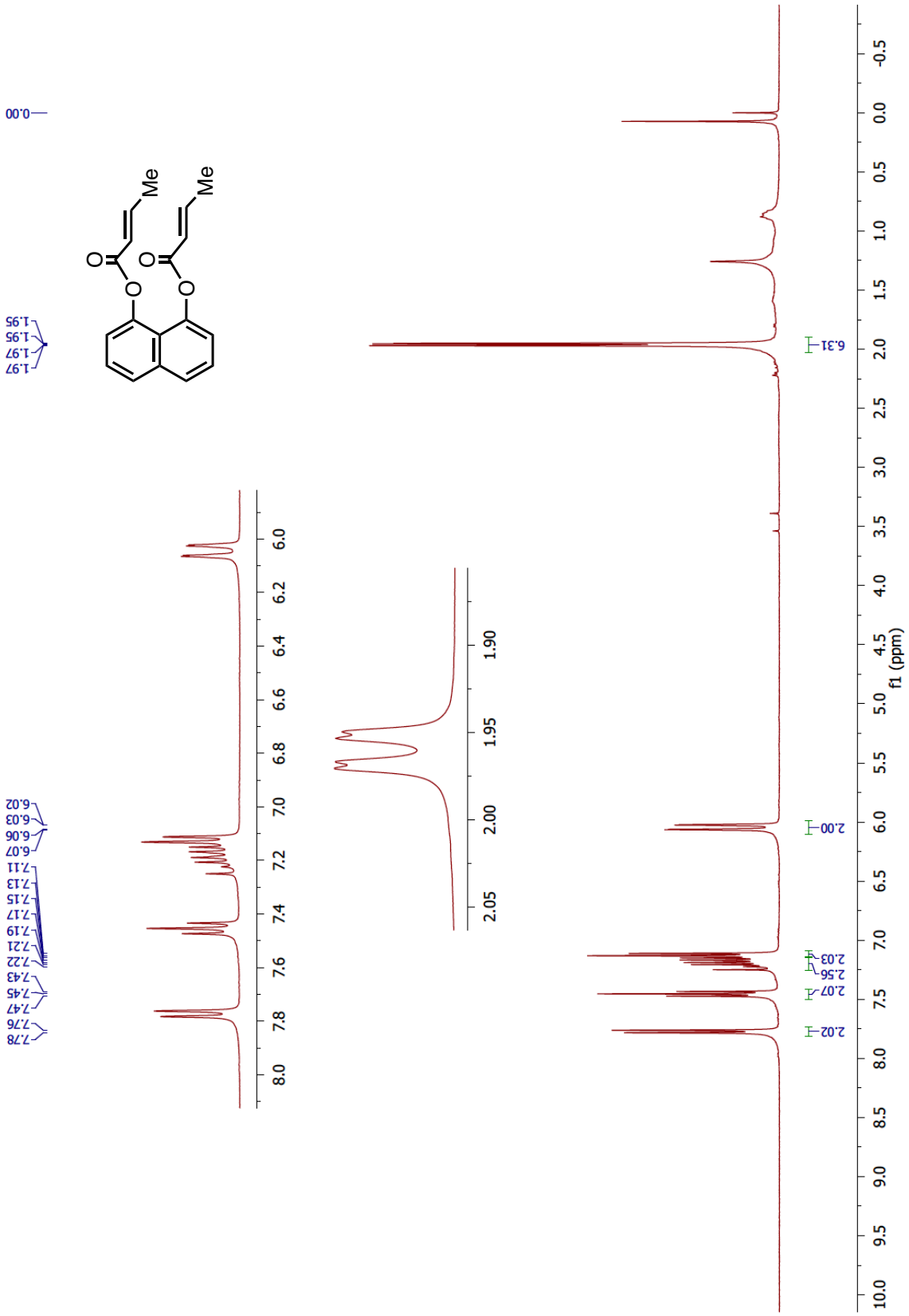

Figure 54. ^{1}H-NMR spectrum of **46** in $CDCl_3$.

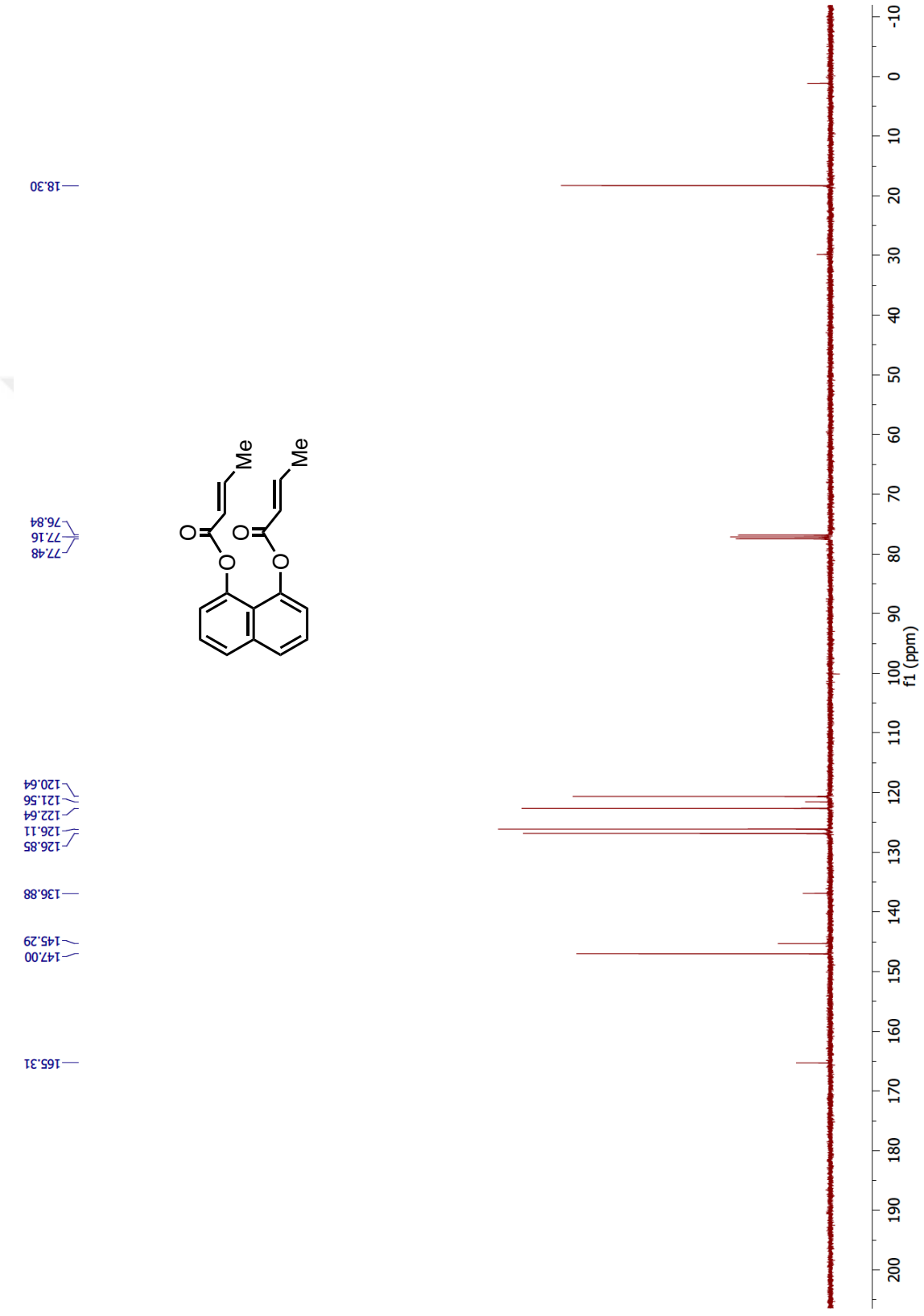

Figure 55. ^{13}C-NMR spectrum of **46** in $CDCl_3$.

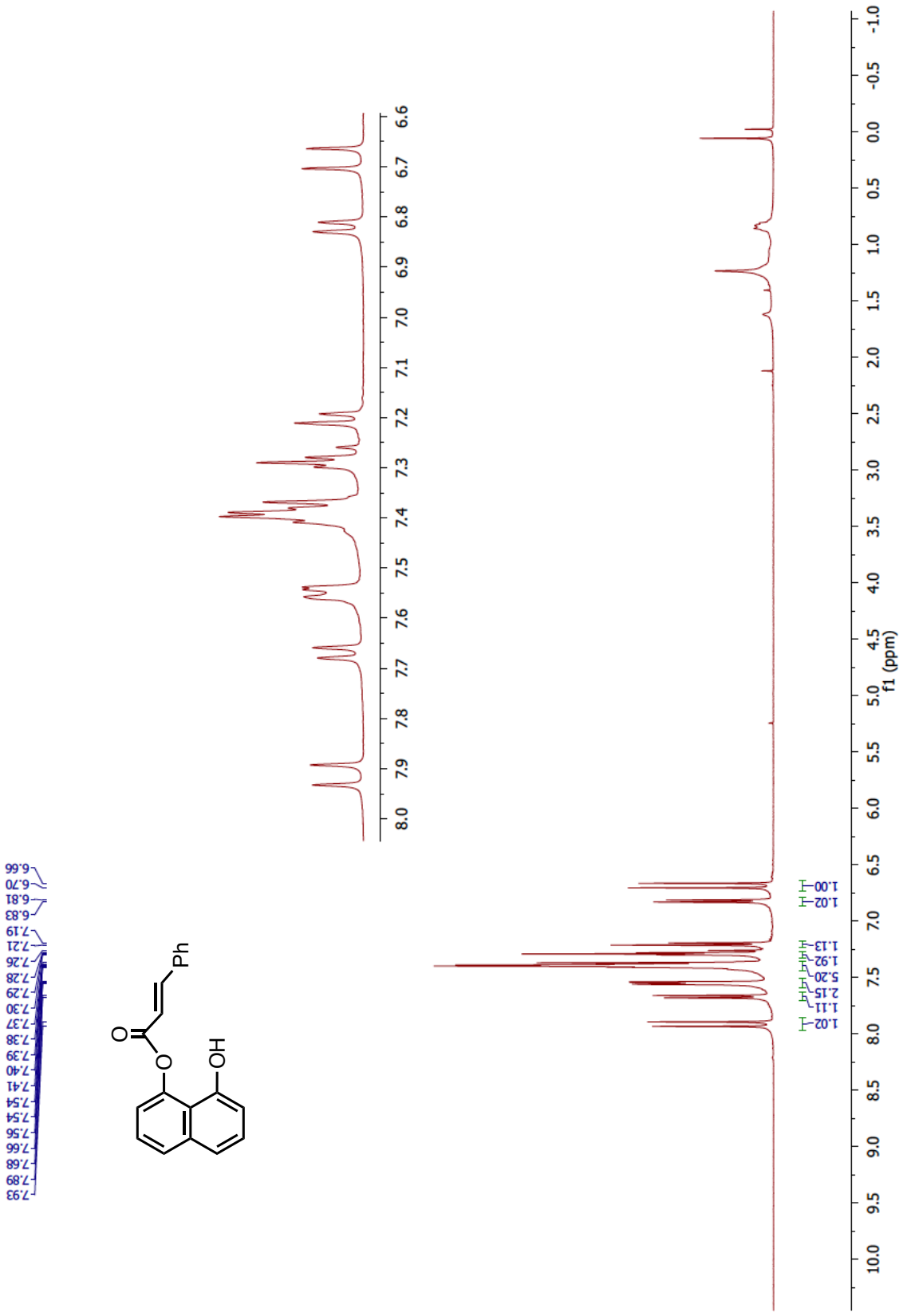

Figure 56. ^{1}H-NMR spectrum of **48** in $CDCl_3$.

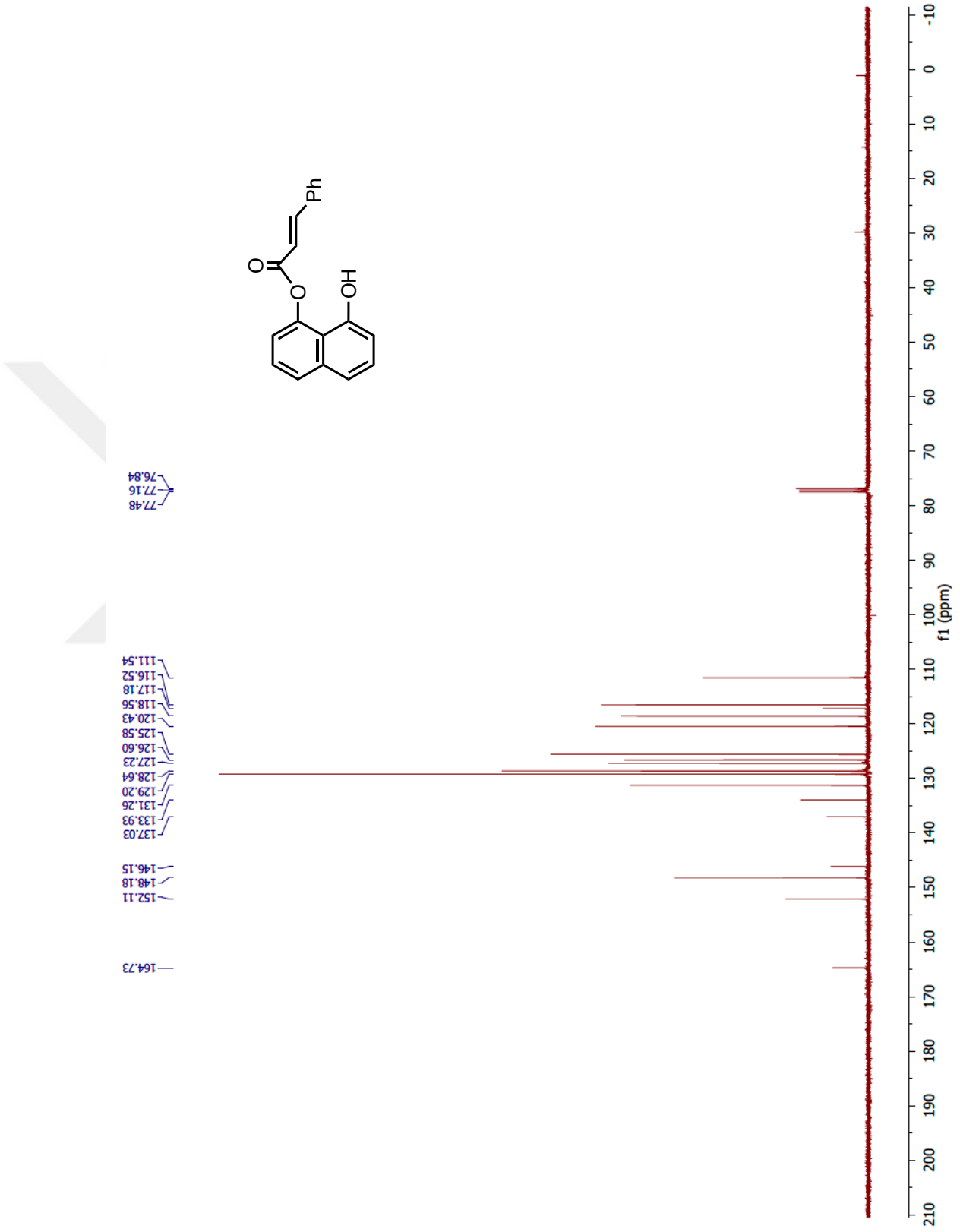

Figure 57. ^{13}C-NMR spectrum of **48** in $CDCl_3$.

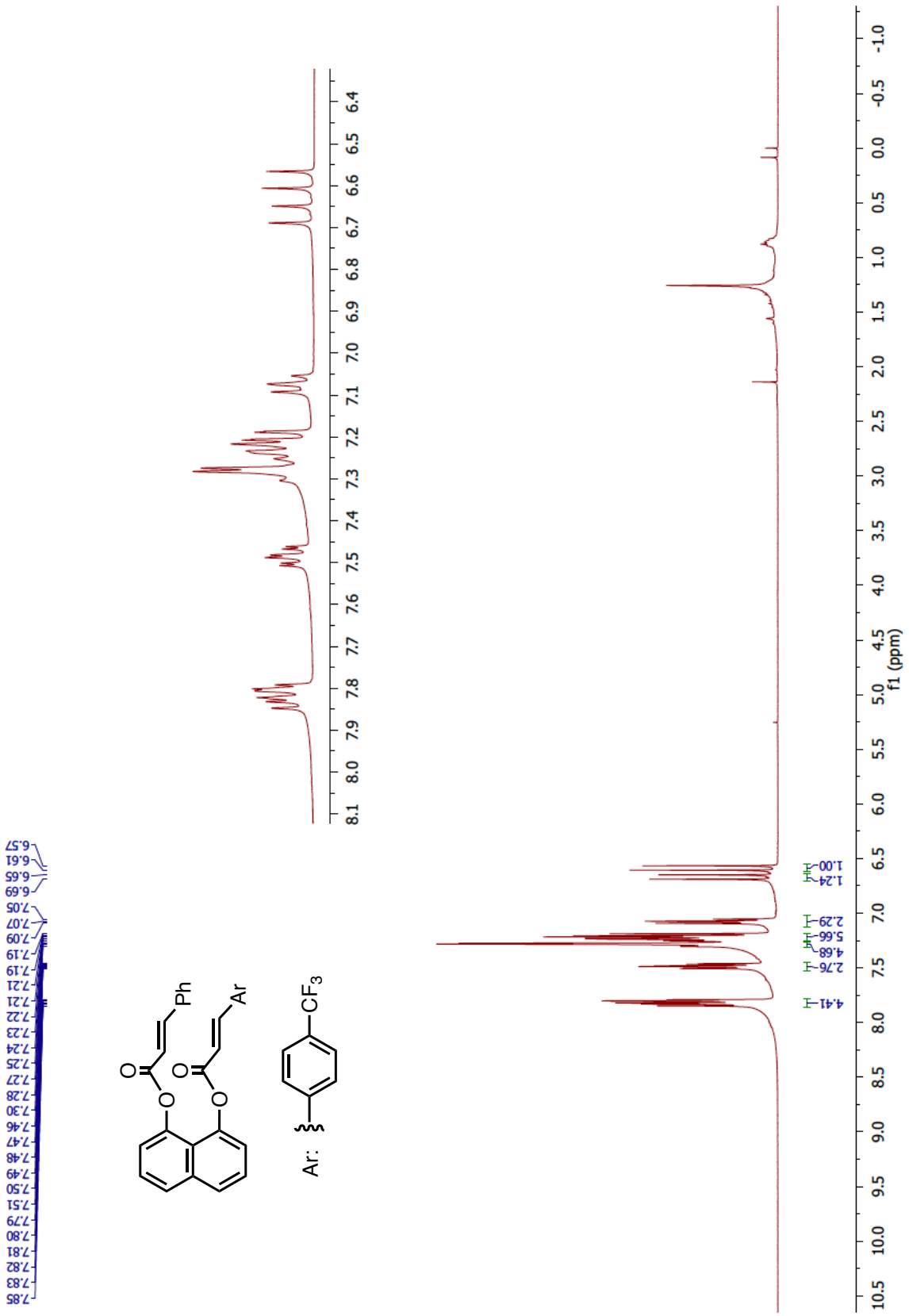

Figure 58. ^{1}H-NMR spectrum of **49** in $CDCl_3$.

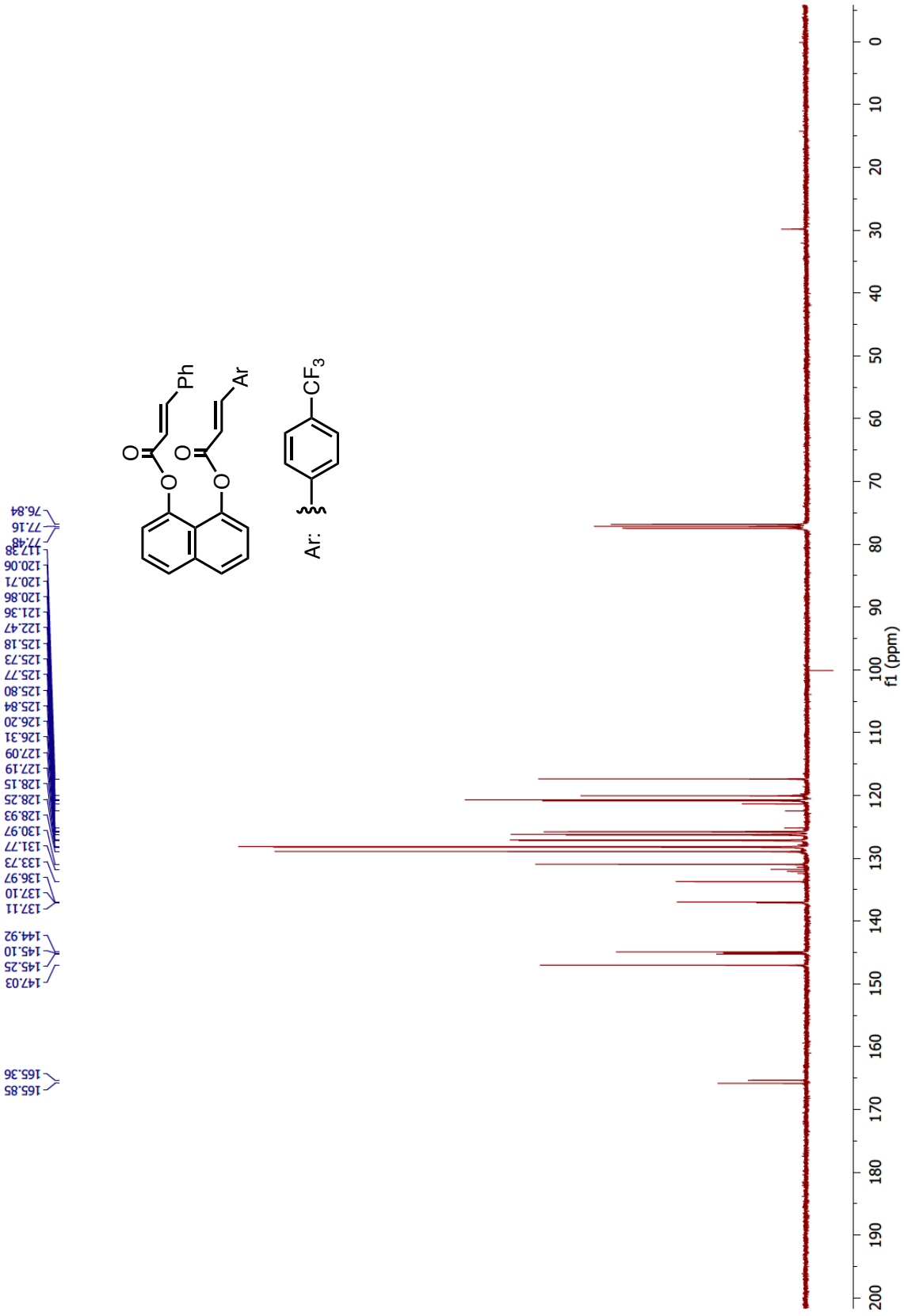

Figure 59. ^{13}C-NMR spectrum of **49** in $CDCl_3$.

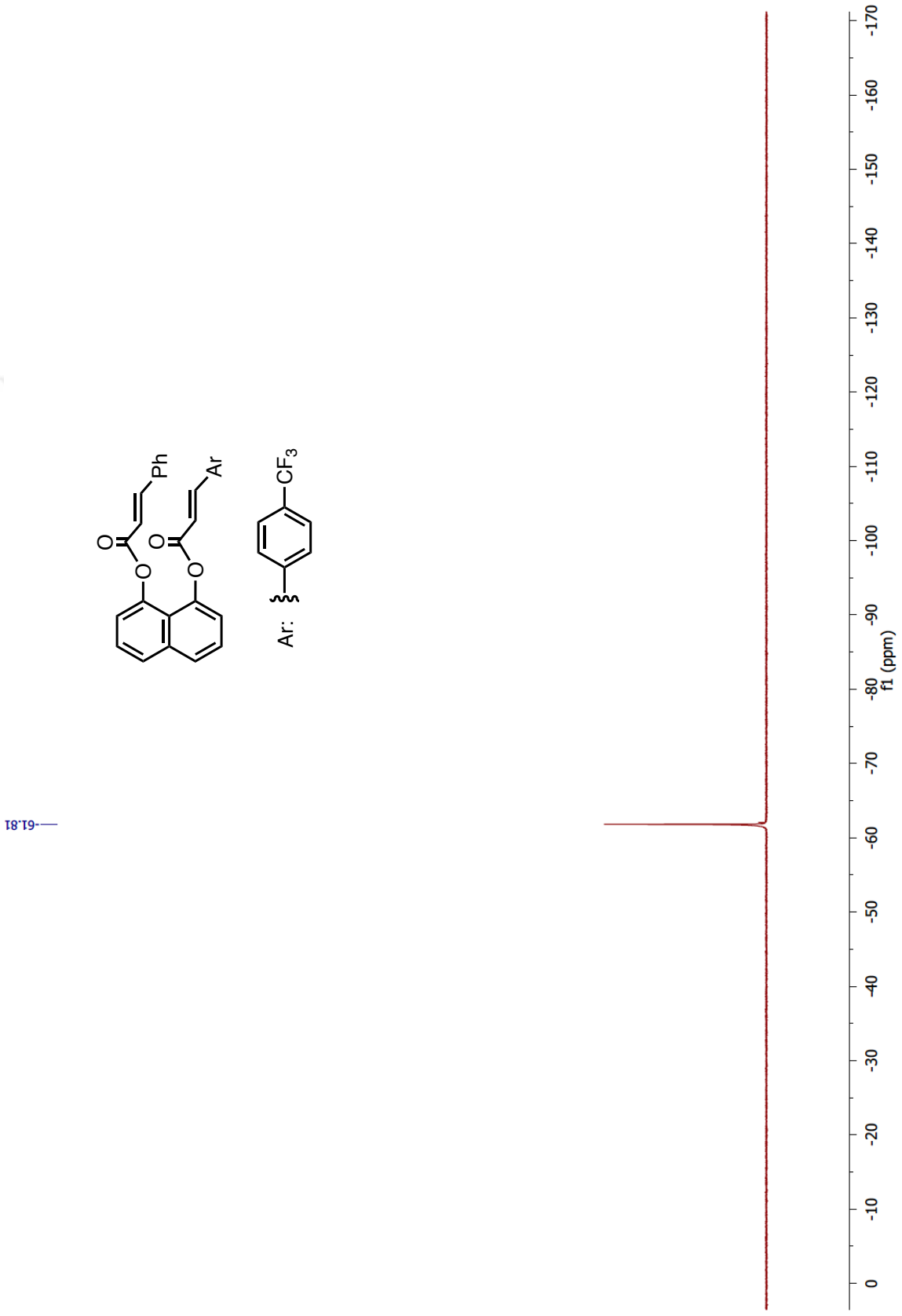

Figure 60. ^{19}F-NMR spectrum of **49** in $CDCl_3$.

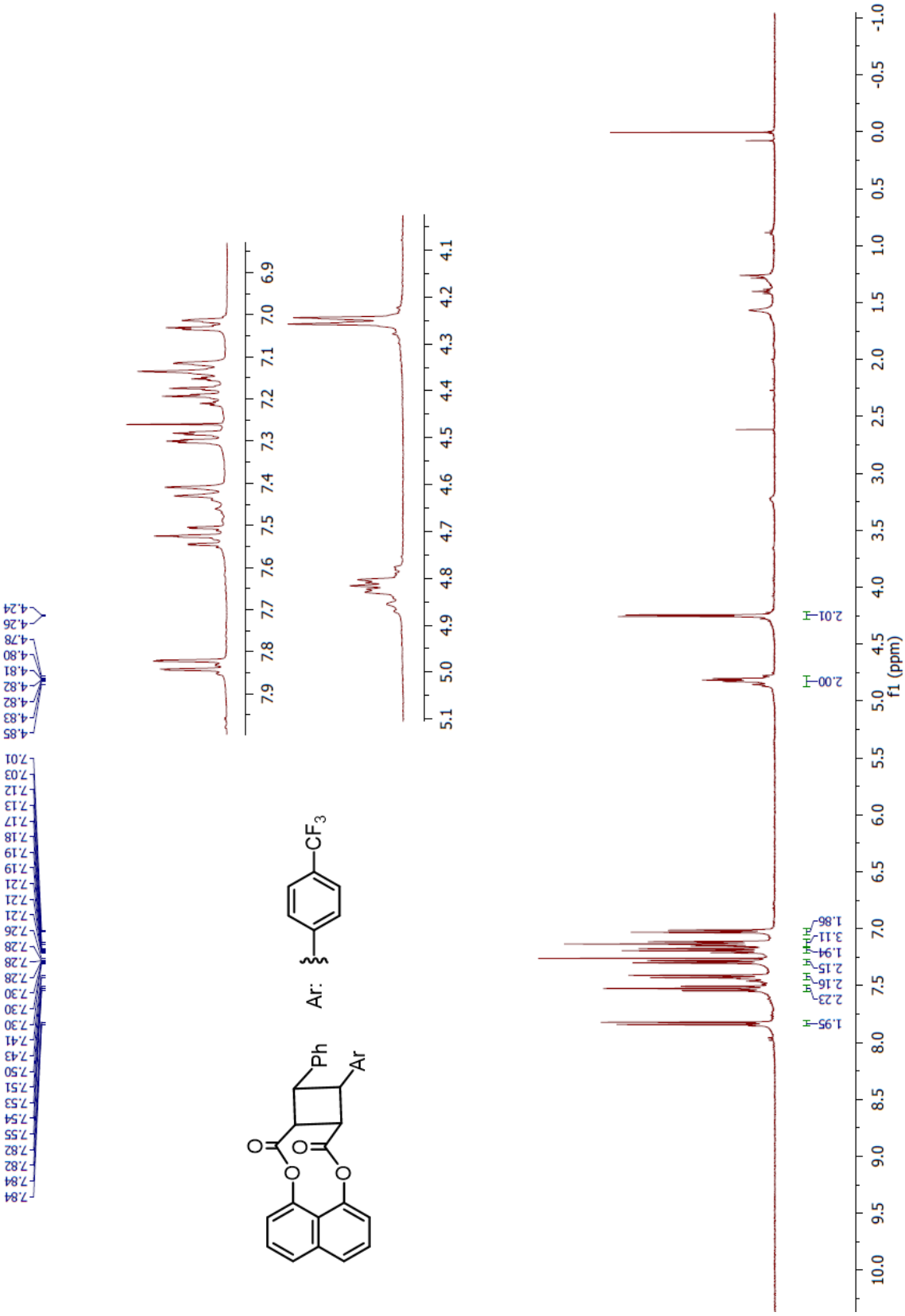

Figure 61. ^{1}H-NMR spectrum of **53** in $CDCl_3$.

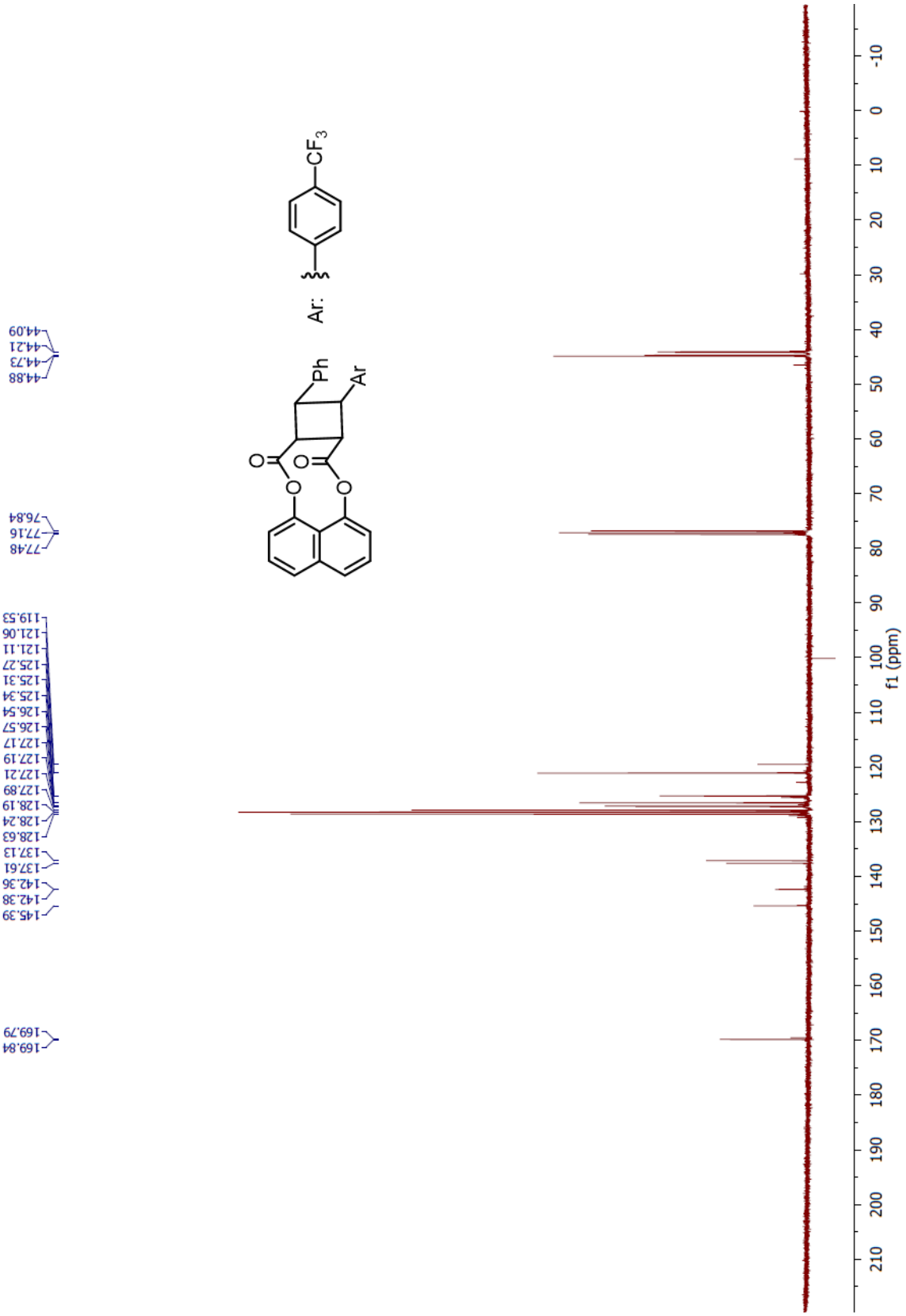

Figure 62. ^{13}C-NMR spectrum of **53** in $CDCl_3$.

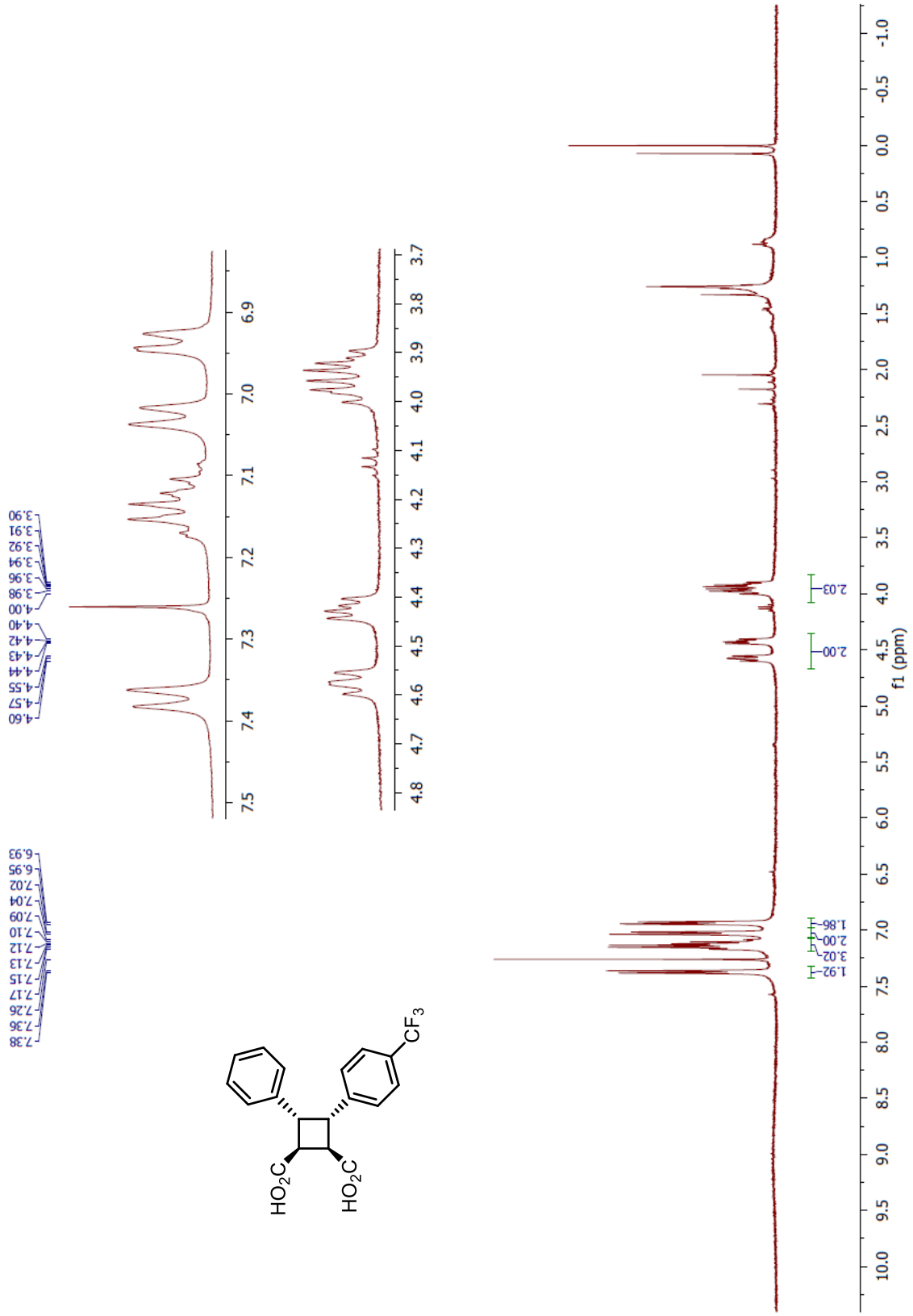

Figure 63. ^{1}H-NMR spectrum of **56** in $CDCl_3$.